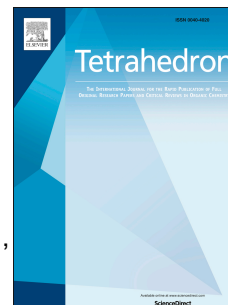


Accepted Manuscript

Synthesis and studies of symmetric dibenzothienylcyclopentenes

Vasily A. Migulin , Michael M. Krayushkin , Valery A. Barachevsky , Olga I. Kobeleva ,
Valentin V. Novikov , Konstantin A. Lyssenko



PII: S0040-4020(14)01726-8

DOI: [10.1016/j.tet.2014.12.036](https://doi.org/10.1016/j.tet.2014.12.036)

Reference: TET 26257

To appear in: *Tetrahedron*

Received Date: 29 September 2014

Revised Date: 25 November 2014

Accepted Date: 9 December 2014

Please cite this article as: Migulin VA, Krayushkin MM, Barachevsky VA, Kobeleva OI, Novikov VV, Lyssenko KA, Synthesis and studies of symmetric dibenzothienylcyclopentenes, *Tetrahedron* (2015), doi: 10.1016/j.tet.2014.12.036.

This is a PDF file of an unedited manuscript that has been accepted for publication. As a service to our customers we are providing this early version of the manuscript. The manuscript will undergo copyediting, typesetting, and review of the resulting proof before it is published in its final form. Please note that during the production process errors may be discovered which could affect the content, and all legal disclaimers that apply to the journal pertain.

Graphical Abstract

Synthesis and studies of symmetric dibenzothiienylcyclopentenenes

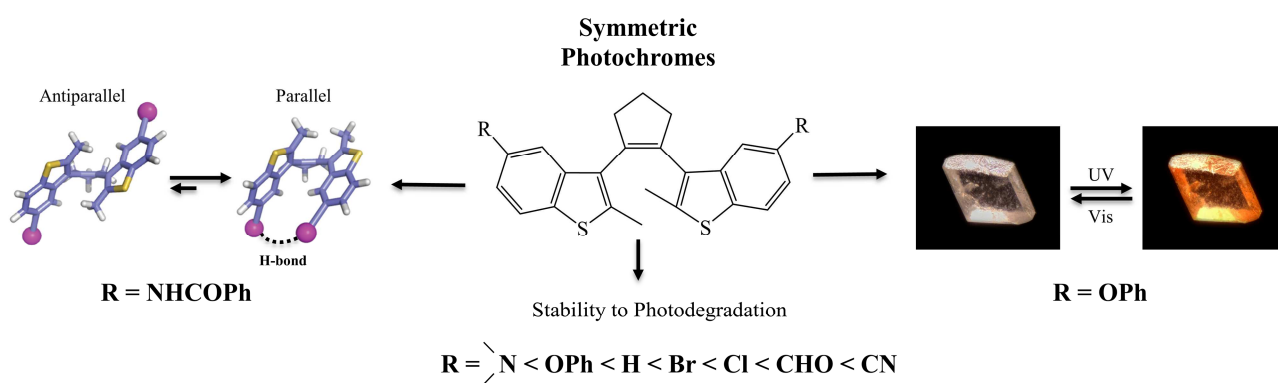
Leave this area blank for abstract info.

Vasily A. Migulin ^{a,*}, Michael M. Krayushkin ^a, Valery A. Barachevsky ^b, Olga I. Kobeleva ^b, Valentin V. Novikov ^c, Konstantin A. Lyssenko ^c

^a N. D. Zelinsky Institute of Organic Chemistry, Russian Academy of Sciences, Leninsky prospect, 47, 119991 Moscow, Russian Federation

^b Photochemistry Center, Russian Academy of Sciences, Novatorov Str., 7a, 119421 Moscow, Russian Federation

^c A. N. Nesmeyanov Institute of Organoelement Compounds, Russian Academy of Sciences, Vavilov Str., 28, 119991 Moscow, Russian Federation





Tetrahedron
journal homepage: www.elsevier.com



Synthesis and studies of symmetric dibenzothiénylcyclopentenes

Vasily A. Migulin ^{a,*}, Michael M. Krayushkin ^a, Valery A. Barachevsky ^b, Olga I. Kobeleva ^b, Valentin V. Novikov ^c, Konstantin A. Lyssenko ^c

^a N. D. Zelinsky Institute of Organic Chemistry, Russian Academy of Sciences, Leninsky prospect, 47, 119991 Moscow, Russian Federation

^b Photochemistry Center, Russian Academy of Sciences, Novatorov Str., 7a, 119421 Moscow, Russian Federation

^c A. N. Nesmeyanov Institute of Organoelement Compounds, Russian Academy of Sciences, Vavilov Str., 28, 119991 Moscow, Russian Federation

ARTICLE INFO

Article history:

Received

Received in revised form

Accepted

Available online

Keywords:

Photochromism

UV/Vis spectroscopy

NMR spectroscopy

Conformation analysis

Density functional calculations

X-ray diffraction

ABSTRACT

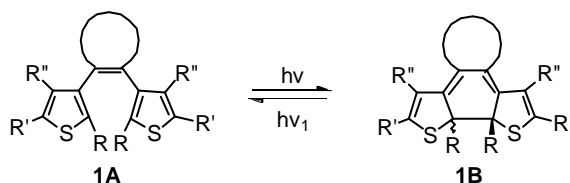
Various symmetric 5,5'-substituted dibenzo[b]thienylcyclopentenes were synthesized from the corresponding dibromide with a formation of new C-C, C-N, C-O, C-Si, and C-I bonds. The influence of the introduced substituent on the photochromic properties of the obtained compounds was systematically researched in both solution and solid state. The ratio of antiparallel and parallel conformers in solution was determined by NMR spectroscopy. Only one compound of the series – 5,5'-diphenoxy-substituted – has displayed photochromism in the single crystal. High resolution X-ray diffraction showed that intermolecular S... π and S...H contacts kept two benzothiophene rings together in the molecule, hence decreasing the distance between the two reactive centers responsible for the photocyclization reaction. DFT calculations of the isolated molecules appeared to be in good agreement with the obtained XRD data, and therefore could also essentially assist a researcher in the design of photochromic molecules.

2009 Elsevier Ltd. All rights reserved.

* Corresponding author. Tel.: +7-916-319-9665; fax: +7-499-135-5328; e-mail: vmiguli@mail.ru

1. Introduction

In recent years much attention has been drawn to the fields of optoelectronics^{1,2} and photo switching,³ where organic compounds are being widely used as photoresponsive functional materials. Most promising results in this area have been achieved by exploiting an extensive class of dihetarylethenes^{4,5} and dithienylethenes of general formula **1**, in particular.^{1,6} Under photo irradiation these compounds undergo a reversible interconversion between a colorless open **A** form and a colored cyclic **B** form, as shown in Scheme 1, thus allowing a controllable change of distinct physical properties within a material under light as an external trigger. Dithienylethenes are also characterized by thermal irreversibility, high fatigue resistance and rapid response time to the radiation^{1,4} – features that are indispensable for modeling and construction of practical photoresponsive objects.



Scheme 1. Photochromic interconversion of dithienylethenes under irradiation.

To date, the best results in this field are achieved with dithienylethenes having a perfluorocyclopentene bridge: numerous compounds of this subclass, both symmetric and nonsymmetric, have been synthesized and thoroughly studied in solution and solid state for their photochromic properties.^{4,7} However, the described syntheses are limited by one general strategy of either concurrent or sequential anionic substitution of fluorides^{5,8} in rather expensive and volatile octafluorocyclopentene. At the same time, alternative dithienylethenes with a cyclopentene bridge could be easily assembled by McMurry reaction from available corresponding diketones.⁹ The comparison of physical properties in various solutions of dithienylethenes linked by either perfluoro- or perhydrocyclopentene showed no major dissimilarities in their photochromic behavior,¹⁰ thus, promoting further search and exploration of perspective cyclopentene-based photochromes nowadays.

In 1998 Feringa et al. reported a synthesis of dithienylethene **2**,¹¹ which later became one of the most commonly used intermediates for further modification. Introduction of various functionalized substituents into both thienyl moieties in this molecule allowed construction of numerous photochromic systems with applications as metal ion complexes,¹² photoresponsive organogels,¹³ gold nanoparticle binders,¹⁴ silicon atom-connected two-component molecular photo switches,¹⁵ living cells imaging,¹⁶ peptidomimetics,¹⁷ etc. Considering that inclusion of benzothiophene units in perfluorocyclopentene-bridged analogs led to high quantum yield, rapid response, remarkable fatigue resistance and excellent thermal stability of the photochromic molecules,^{6,18} it would be logical to investigate benzothiophene-substituted cyclopentenones, in turn. However, despite the synthesis of the first symmetric unsubstituted analog described years ago,¹⁹ only a handful of functionalized molecules of this type were reported since, which comprised compounds of both symmetric²⁰⁻²² and nonsymmetric^{23,24} structures. Recent review on synthetic methods used for construction of dithienylcyclopentenones nicely summarized known approaches.²⁵

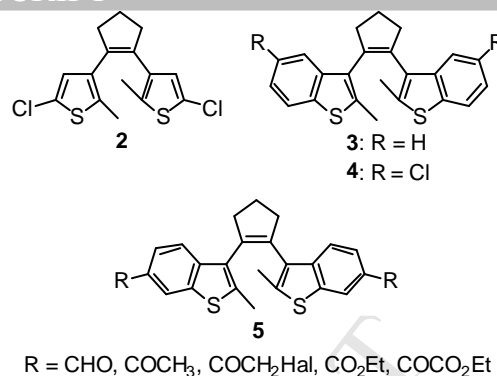


Fig. 1. Known symmetric cyclopentene-based dithienylethenes.

As can be seen from Fig. 1 representatives, both 5,5'- and 6,6'- disubstituted symmetric benzothiencylcyclopentenones are known. Two general strategies were developed towards these compounds. The first one was based on acylation of easily accessed **3** by various acylating reagents to give **5**, while the second one included the final construction of the molecule based on already functionalized benzothiophene. However, both methods have their limitations with restrained availability of suitable electrophiles in the synthesis of **5**, and a necessity for substituted 2-methylbenzo[b]thiophenes as starting materials for **4**, which resulted in rather scarce representation of this subclass of photochromes. As a result, only isolated individual descriptions of physical properties like UV-vis absorption spectra or X-ray analysis could be found in the literature for these compounds.²⁰⁻²² In our previous work, we have compared the physical properties of 5,5'-dichlorosubstituted photochrome **4** and its perfluorocyclopentene analog in both solution and crystal.²⁰ However, the influence of the substituent itself in the core of the molecule on the photochromic properties of the corresponding compound was never performed for this class of dithienylethenes. Thus, a profound systematic research of various symmetric functionalized benzothiencylcyclopentenones has become required in order to find a relation between the nature of the substituent and the photochromic properties of the molecule.

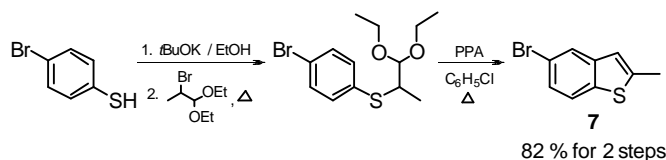
In this article, we demonstrate that dibromide **6** could be easily prepared in multigram quantities and could serve as an important precursor to diverse symmetric 5,5'- disubstituted dibenzothiencylcyclopentenones with formation of either C-C, C-N, C-O, C-Si or C-I chemical bonds. All novel compounds reported here were obtained with yields varying from good to excellent and could participate in further modification according to the needs of the target molecule due to the different nature of the introduced functional groups. Physical properties of the synthesized compounds were studied both in solution and solid state in comparison mode to see all possible relations between the original structure of the photochrome and its physical and chemical behavior.

2. Results and discussion

2.1. Synthesis

Recently we reported a synthesis of symmetric dichloride **4** starting from 5-chloro-2-methylbenzothiophene via McMurry condensation of the corresponding diketone.²⁰ Unfortunately, chlorides in **4** remained inert both under standard catalytic conditions and via anion formation synthetic procedures, thus, prompting us to switch attention to the analogous 5-bromo-2-methylbenzothiophene **7** which could be easily accessed in any quantities from 4-bromothiophenol in 82 % yield by slight modification of the published procedure²⁶ (Scheme 2). It is worth

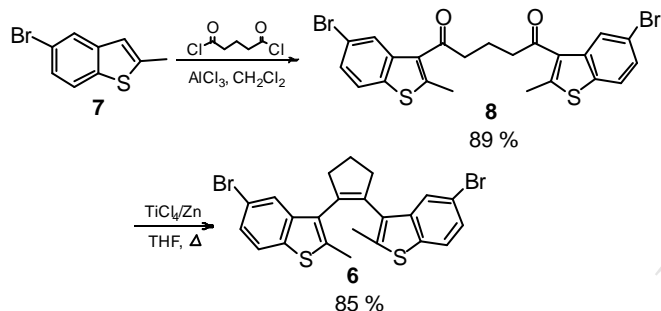
mentioning that this optimized protocol is the most practical one to date for synthesis of **7** in bulk.



Scheme 2. Optimized synthesis of 5-bromo-2-methylbenzo[b]thiophene.

The main consideration was that substitution of the bromides in the benzothiophene moiety must proceed much easier as compared to the chlorides as it was attested for catalytic amination reactions for nonsymmetric photochromic dithienylcyclopentenes.²³ Besides, as was shown, bromides in dithienylethenes remained intact under McMurry conditions.

Acylation of benzothiophene **7** with glutaryl dichloride was rather straightforward and afforded diketone **8**, which was subsequently converted to the target dibromide **6** by McMurry reaction in excellent overall yield. The synthesis was repeated several times with different loads showing high reproducibility for either small amounts of starting materials or on the multigram scale.



Scheme 3. Synthetic route to symmetric dibromide **6**.

In the course of our research, synthesis of dibromide **6** was also performed by Wagenknecht group.²⁷ However, despite the fact that the general synthetic route appeared to be analogous, the reported yields turned out to be inferior to ours. Further substitution of either one or both bromides by connecting the benzothiophene units to the chosen nucleoside allowed authors to introduce a photochromic moiety into a DNA chain. Thus, the published work gave another justification for the necessity and the great potential of synthetically available photochromic dibenzothienylcyclopentene capable of various further transformations.

Substitution of bromides in **6** could be performed by either dianion formation or under catalytic conditions. Lithiation was accomplished by *n*-BuLi in THF at -80 °C with formation of a dianionic intermediate, which subsequently reacted with various electrophiles as shown in Table 1.

Table 1. Coupling of dibromide **6** with various electrophiles via dianion formation.

Entry		Electrophile	R	Product	Yield
1		I ₂	-I	9	81 %
2		TMSCl	-TMS	10	90 %
3		DMF	-CHO	11	83 %
4		Acetamide	-COCH ₃	12	52 %

5	Acetaldehyde	-CH(OH)CH ₃	13	81 %
---	--------------	------------------------	-----------	------

As can be seen, the reaction proceeded smoothly with electrophiles of a different nature providing target materials in good yields. As a result, several important symmetric precursors with essential functionalities, such as aldehyde or iodide, were accessed by this method.

Diiodide **9** was synthesized in excellent yield as well by catalytic halogen exchange under Buchwald conditions.²⁸ It also appeared to serve as an *in situ* intermediate in other copper (I) iodide catalyzed substitution of bromides in **6** (Table 2).

Table 2. Copper (I) iodide catalyzed coupling of dibromide **6**.

Entry		Reagent	T °C / Time	R	Product	Yield
1		NaI	115 °C / 24 h	-I	9	93 %
2 ^a		NaCN, KI	120 °C / 20 h	-CN	14	88 %
3		Benzamide, K ₂ CO ₃	115 °C / 24 h		15	60 %
4 ^b		Phenol, <i>t</i> -BuOK	135 °C / days		16	82 %

^a Toluene was used as a solvent.

^b No ligand was added.

While the cyano-substituted²⁹ product **14** and the amide derivative³⁰ **15** could be obtained under standard conditions without complications, the synthesis of **16** turned out to be the most laborious. Employing *N,N'*-dimethylethylenediamine led to the undesired amination, while other suggested ligands for copper (I) catalyzed coupling,³¹ switching to CuO or Pd (0), addition of a crown ether or cesium iodide for better solubility of the phenolate did not furnish the target compound as a major product. As a result of our search, the best conditions for coupling of **6** with potassium phenolate, obtained *in situ* from phenol and *t*-BuOK, were observed after prolonged stirring in dioxane at 135 °C without input of any ligand. However, in order to force the reaction to completion, addition of the reagents and CuI as solids was required each time TLC analysis showed no further progress of the reaction. This procedure allowed us to finally obtain diphenoxy-substituted **16** in 82 % yield, thus demonstrating the universality of CuI as a catalyst for various couplings of **6** with the formation of a C-C, C-N, C-O, or C-I bonds.

Palladium (0) catalyzed coupling³² of 5-bromobenzothiophene containing a nonsymmetric photochrome with functional amines was reported earlier.²³ This time we decided to show applicability of Pd (0) catalysis to the coupling of symmetric dibromide **6** with simple amines: *n*-amylamine and pyrrolidine, as primary and secondary amines, correspondingly (Table 3).

Table 3. Palladium (0) catalyzed amination of dibromide **6**.

Entry		Amine	R	Product	Yield
1		<i>n</i> -Amylamine		17	93 %



Both reactions proceeded smoothly providing symmetric diamines after 7 h of stirring at 85 °C. Lower yield of **18** could be explained by the visually observed air sensitivity of the product, besides, to minimize its decomposition Al₂O₃ was used during the purification of **18** instead of the traditionally employed silica gel.

Thus, symmetric dibromide **6** was synthetically converted to various disubstituted molecules. Both dilithiation of **6**, followed by addition of miscellaneous electrophiles, and catalytic coupling on either CuI or Pd₂(acac)₃ appeared to be reliable and effective methods for symmetric functionalization of dithienylcyclopentenes at the 5 and 5' positions in the benzothiophene units.

2.2. Spectral and kinetic characteristics

Synthesized symmetric dibenzothiencylcyclopentenes **6**, **9-18** together with known unsubstituted compound **3**¹⁹ and previously reported dichloride **4**²⁰ were subjected for spectral and kinetic studies at C = 2 × 10⁻⁴ M in both toluene (ε = 2.4) and acetonitrile (ε = 36.1), as two chosen solvents of dissimilar polarities. Typical photoinduced spectral changes in toluene solution are presented for “unsubstituted” **3** and compounds **14**, **16**, **17** with diverse functional groups (Fig. 2).

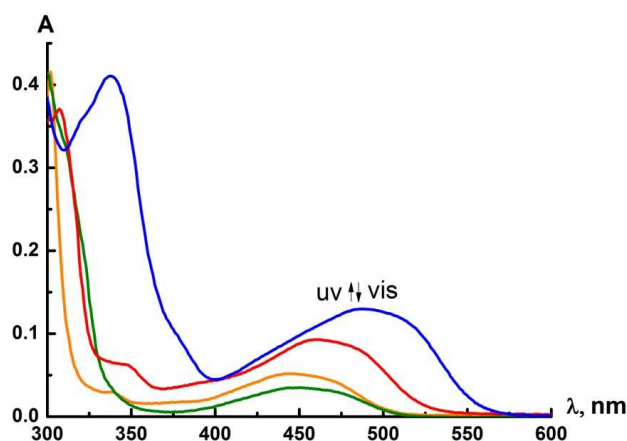


Fig. 2. Absorption spectra of dibenzothiencylcyclopentenes **3** (orange), **14** (green), **16** (red), and **17** (blue) in toluene after UV irradiation.

Table 4. Spectral and kinetic characteristics for symmetric dibenzothiencylcyclopentenes in solution

Compound	Solvent	λ_A , nm	ϵ_A , M ⁻¹ cm ⁻¹	λ_B , nm	$\Delta D_B^{ph}/D_A$	k_{A-B}/k_{B-A}	$\tau_{1/2}^{deg}$, s
3 (H)	PhCH ₃ CH ₃ CN	301	9250	445	0.2	2.8	215
		289	16750	438	0.1	3.4	70
		300	15250				
4 (Cl)	PhCH ₃ CH ₃ CN	306	7500	455	0.2	3.7	375
		296	8250	450	0.1	5.3	100
		308	7000				
6 (Br)	PhCH ₃ CH ₃ CN	312	6250	457	0.2	4.1	260
		296	6500	450	0.1	4.3	90
		308	6250				
9 (I)	PhCH ₃ CH ₃ CN	312	6750	460	0.2	-	225
		298	10500	360	-	-	-
		313	9500				
10 (TMS)	PhCH ₃ CH ₃ CN	302	8000	448	0.1	0.3	400
		295	6000	442	0.1	3.7	60
		306	5500				
11 (CHO)	PhCH ₃ CH ₃ CN	317 sh	8000	444	0.1	5.9	800
		282	5750	442	0.1	9.9	115
		324	2750				
12 (COCH ₃)	PhCH ₃	320 sh	6250	442	0.2	5.0	700

	CH ₃ CN	324	4500	440	0.2	6.9	120
13 (CHOHCH ₃)	PhCH ₃	306	7500	450	0.03	2.8	835
	CH ₃ CN	291	6750	445	0.1	3.3	40
		303	6500				
14 (CN)	PhCH ₃	<300	-	445	0.1 ^a	5.0	900
	CH ₃ CN	286	12500	445	0.1	5.5	180
15 (NHCOPh)	PhCH ₃	301 sh	4750	457	0.05	7.0	300
	CH ₃ CN	301	14500	460	0.02	8.3	110
16 (OPh)	PhCH ₃	306	8500	460	0.3	3.8	145
	CH ₃ CN	306	5750	455	0.2	4.4	55
17 (NHC ₅ H ₁₁)	PhCH ₃	330	10250	490	0.3	8.5	110
	CH ₃ CN	334	9500	480	0.3	8.7	195
18 (NC ₄ H ₈)	PhCH ₃	346	6750	496	0.6	16.4	25
	CH ₃ CN	350	5500	490	0.4	11.8	145

^a $\Delta D_B^{ph}/D_{300}$ value was calculated.

Note: λ_A and λ_B are wavelengths of absorption band maxima for open and cyclic forms, respectively; ϵ_A is a molar extinction coefficient at the maximum of the absorption band for the open form; D_{300} is a value of optical density of the absorption band at 300 nm for the open form; D_A is a value of optical density at the long-waved absorption band maximum for the open form; ΔD_B^{ph} is a value of the photoinduced optical density at the maximum of the long-waved absorption band for the cyclic form in the photoequilibrium state; $k_{A \rightarrow B}$ and $k_{B \rightarrow A}$ are rate constants for photocoloration and photobleaching reactions, respectively; $\tau_{1/2}^{deg}$ is the time required for a 50% decrease of a maximum value of photoinduced optical density at the maximum of the long-wave absorption band for the cyclic form under unfiltered light; sh stands for absorption shoulder.

As can be seen from Table 4, the absorption maximum of the cyclic form **B** for “unsubstituted” **3** is located at 440–445 nm (depending on the solvent) and remained practically unchanged with introduction of substituents of electron-withdrawing nature at 5- and 5'- positions. On the contrary, any electron-donating character of the introduced functional groups at these positions immediately resulted in significant bathochromic shift by up to 50 nm. Apparently, the electron-donating effect was responsible as well for higher light-sensitivity values observed for compounds **16–18**.

In addition, this conclusion was confirmed by the absorption spectra of these compounds recorded in acetonitrile. Despite the fact that absolute values of ΔD_B^{ph} in this solvent appeared to be slightly lower than in toluene, all general observations recorded earlier were also valid for the more polar media.

The described photochromes were subjected to reversible photoinduced transformations between open **A** and cyclic **B** forms, at first conducting the intramolecular cyclization under UV light, followed by the converse photobleaching procedure with rate constants being calculated for each process. Typical of other previously studied dithienylethenes, the dibenzothienylethenes displayed an immediate increase in absorption density to a certain constant level under UV irradiation, after which the formed solution was subjected to visible light. Photobleaching of the formed colored solutions was also rather prompt, usually taking seconds until total loss of color. Thus, the rate constant ratio $k_{A \rightarrow B}/k_{B \rightarrow A}$ for all compounds appeared to be in the range of one order of magnitude (Table 4).

The only exception from the typical photochromic behavior was observed for diiodide **9**. In fact, in the toluene solution of this compound an intensity of photocoloration was distinctly dependant on the time of the exposure to the UV irradiation with no complete decoloration after its exposure to the visible light even for a prolonged period of time. At the same time, practically no coloration was observed under UV irradiation in the acetonitrile solution with absorption spectra revealing several growing peaks, all located in the UV region. Such deviation from the regular photochromic behavior for **9** should be explained by chemical decomposition of the labile C-I bond under UV and

visible light irradiation, thus discarding the photochromic potential of this compound.

We also found it important to study photodegradation of the obtained compounds. For this purpose, the prepared solutions in either toluene or acetonitrile were subjected to a prolonged exposure to high intensity unfiltered light (simultaneous UV and visible light). The measured $\tau_{1/2}^{deg}$ value was recorded when the absorption density at the maximum of the long-waved absorption band for the cyclic form of the studied solution reached its 50% decrease of the starting maximum value (Table 4). Normalized photodegradation curves are presented in Fig. 3:

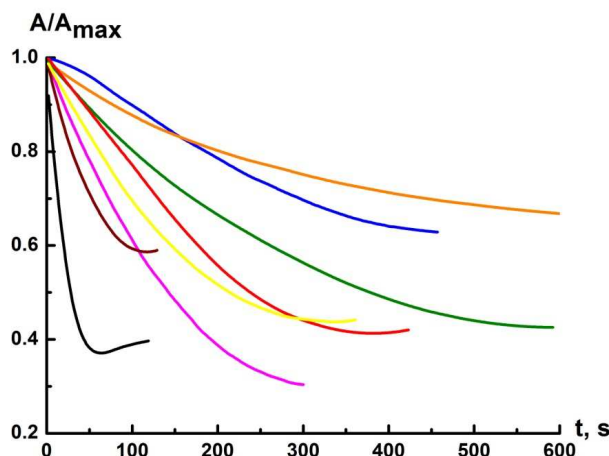


Fig. 3. Normalized photodegradation kinetic curves for dibenzothienylcyclopentenes **3** (yellow), **4** (green), **6** (red), **11** (blue), **14** (orange), **16** (pink), **17** (brown), and **18** (black) in toluene.

One general assumption that could be made from the obtained data was that the presence of electron-withdrawing groups in the body of the molecule noticeably increased the resistance to photodegradation of the compound. Indeed, while “unsubstituted” **3** displayed an intermediary behavior pattern in toluene solution under unfiltered light, amino- and phenoxy-substituted compounds underwent a considerably quicker drop in absorption density. On the other hand, with an increase of electron withdrawing ability of the substituent in the row: $H < Br < Cl < CHO < CN$, the same tendency was observed while

comparing the stability to photodegradation for the corresponding compounds. This important observation should definitely be considered while designing various photochromic systems based on dithienylethenes.

At the same time, in acetonitrile solutions the photodegradation of the researched compounds took place at higher rates than in toluene, usually reaching the 50% absorption density drop within a minute or two. This might be explained by the higher efficiency of UV irradiation in acetonitrile due to the absence of any absorption in the UV region for this solvent, as compared to toluene.

To study the photochromic properties of dibenzothienylethenes in the solid state we chose compounds **11** and **17** bearing formyl- and amino- groups, respectively. As can be seen from Table 5, both compounds retained photochromic properties in either polymeric film (PMMA, C = 10 mass. %) or straightforwardly accessed by evaporation solid film.

Table 5. Spectral and kinetic characteristics for dibenzothienylcyclopentenes **11** and **17** in the solid state.

Compound	Media	λ_A , nm	λ_B , nm	$\Delta D_B^{ph}/D_A$	$k_{A \rightarrow B}/k_{B \rightarrow A}$
11 (CHO)	PMMA film	325	440	0.2	15
	Solid-phase	336	451	0.2	*
17 (NHC ₅ H ₁₁)	PMMA film	338	500	0.3	69
	Solid-phase	338	496	0.4	80

* – data could not be obtained.

While UV light sensitivity (characterized by $\Delta D_B^{ph}/D_A$ values) for these compounds proved to be similar to values recorded in the solution, rate constants for the process of photobleaching for both compounds appeared to be much lower in the solid state.

It is worth mentioning that dibenzothienylethenes displayed thermal irreversibility in solution, polymer, or solid film. The value of the photoinduced optical density in the photoequilibrium state remained unchanged within 24 hours in the dark at room temperature.

Finally, we decided to explore the influence of the position of a substituent in benzothienylethenes on photochromic properties in a comparison mode. For this purpose, two acetyl substituted compounds were chosen with this functional groups in either 5,5'- (**12**) or 6,6'- (**5**, R = COCH₃)²² positions (Table 6).

Table 6. Spectral and kinetic characteristics for dibenzothienylcyclopentenes **12** and **5** (R = COCH₃) in solution.

Compound	Solvent	λ_A , nm	λ_B , nm	$\Delta D_B^{ph}/D_A$	$k_{A \rightarrow B}/k_{B \rightarrow A}$	$\tau_{1/2}^{deg}$, s
12 (5,5'-COCH ₃)	PhCH ₃	320	442	0.2	5.0	700
	CH ₃ CN	324	440	0.2	6.9	120
5 (6,6'-COCH ₃)	PhCH ₃	332	489	0.6	9.9	300
	CH ₃ CN	286	480	0.6	11	60

Switching the position of the acetyl groups from 5,5'- to 6,6'-disubstitution led to a significant bathochromic shift of an absorption band maxima for the cyclic form. Also, this modification resulted in higher UV sensitivity of **5** (R = COCH₃) in both toluene and acetonitrile solutions. At the same time, the stability to photodegradation dropped with its value becoming two times less, as compared to 5,5'-disubstituted **12**. Thus, the particular location of the same functional group in the benzothiophene ring could noticeably influence the photochemical characteristics of the studied compound.³³ However, more specific generalizations on the overall influence of various substituents in other than 5,5'-symmetric positions in

dibenzothienylethenes could be done only after additional research on this subject.

2.3. NMR studies

Synthesized symmetric dibenzothienylcyclopentenes were characterized using ¹H and ¹³C NMR spectroscopy. While solving the ¹H spectra taken at room temperature we have observed a significant broadening of proton peaks for all studied compounds. Such behavior generally indicates the intermediate time-scale dynamic exchange of various protons in the molecule. Indeed, due to the relatively hindered rotation around the C-C bond that connects the thienyl and cyclopentene moieties, two distinct conformers with antiparallel and parallel orientation³⁴ of two benzothienyl fragments could be stable at the same time, as shown on Fig. 4, with the existence of an individual set of NMR peaks for each rotamer. Room temperature, however, appeared high enough allowing the mixture of two conformers to reach its fast exchange limit in solution, therefore leading to an evident fusion of most signals of both rotamers into broad peaks. On the contrary, cooling the sample to -50 °C allowed us to obtain two well-resolved sets of signals, corresponding to individual antiparallel and parallel conformers (Fig. 5). The dynamic exchange between these signals was additionally confirmed using 2D EXSY NMR spectra³⁵ (Fig. 6).

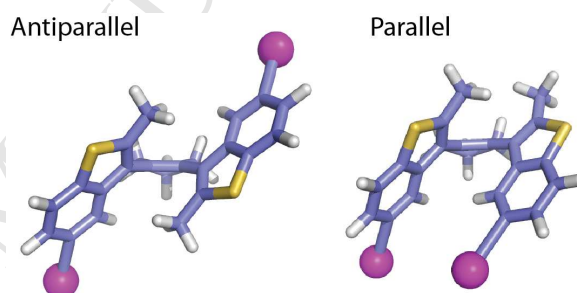


Fig. 4. Sketch of two conformers of symmetric dibenzothienylcyclopentenes with antiparallel and parallel orientation of benzothienyl fragments.

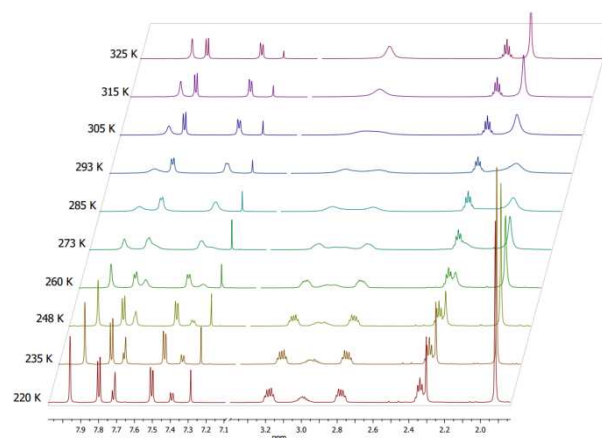


Fig. 5. Temperature dependence of ¹H NMR spectrum at 600 MHz of dinitrile **14** in CDCl₃.

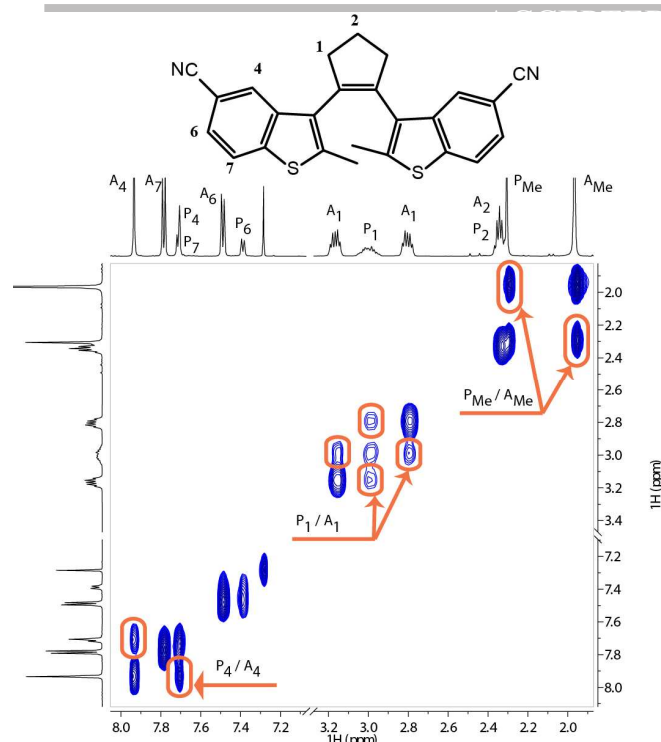


Fig. 6. EXSY NMR spectrum at 600 MHz of dinitrile **14** in CDCl_3 at 235 K. The off-diagonal signals (cross-peaks) are indicated by arrows and demonstrate dynamical exchange between the corresponding protons of antiparallel (A) and parallel (P) conformers.

The ^1H NMR signals of antiparallel and parallel rotamers were distinguished using the remarkable difference in the shielding of the nuclei by aromatic benzothienyl moieties. Thus, in the antiparallel conformer the methyl groups are located in the region above the opposite aromatic rings (Fig. 4), leading to a significant shielding of its nuclei that resulted in an upfield shift of its signals.³⁶ For example, in ^1H NMR spectra of **14** in CDCl_3 at 220 K such a shift occurred from 2.30 ppm for methyl signals in the parallel conformer (P_{Me}) where no shielding of methyl groups was possible to 1.92 ppm for the antiparallel position (A_{Me}). Similarly, due to symmetric orientation of the benzothiophene fragments over each other in the parallel conformer, they also shielded the nuclei of each ring, leading to an analogous upfield shift of their signals (P_4 , P_6 , P_7) (Fig. 6). Accordingly, in the spectra of dibenzothienylethenes **3**, **4**, **6**, **9** – **18** the signals of antiparallel rotamers were distinguished by up- and downfield shifts of its methyl group and aromatic group signals, respectively (see Supplementary data). However, the low-temperature NMR spectrum of dialcohol **13** with two chiral substituents was too complicated to decipher (owing to the abundance of signals of diastereomerically and conformationally non-equivalent species) and was, therefore, excluded from further discussion.

It is worth mentioning that despite the fact that substantial structure identification (based on the obtained NMR data) remained theoretically possible,³⁶ such analysis should be of major complexity due to the dynamic nature of the equilibrium between the two conformers, temperature dependence of the observed chemical shifts, different values of the rotation barrier in the molecule, and other possible complications.

The integration of the corresponding signals of each rotamer allowed us to roughly estimate the fraction of both states in the equilibrium in the solution. It was found that the proportion of two conformers was directly dependant on the nature of the substituent in the benzothienyl moiety (Table 7). Besides, since

the difference in free Gibbs energy between two rotamers of one molecule was of the same order as the solvation enthalpies of their solutes in most cases,³⁷ it was expected that the choice of the solvent should also influence the relative ratio of rotamers. Indeed, as could be seen from Table 7, the proportion of the conformers varied over a wide range, depending both on the substituent in the core and the solvent.

Table 7. Ratio dependence of antiparallel (A) and parallel (P) rotamers on the substituent (R) at 5,5'-positions of symmetric dibenzothienylcyclopentenes in both CDCl_3 and CD_3CN at 235 K.

Compound	R	CDCl_3 (A), %	CDCl_3 (P), %	CD_3CN (A), %	CD_3CN (P), %
3	H	71	29	50	50
4	Cl	67	33	43	57
6	Br	59	41	39	61
9	I	46	54	37	63
10	TMS	48	52	32	68
11	CHO	53	47	43	57
12	COCH_3	47	53	41	59
14	CN	75	25	37	63
15	NHCOPh	7	93	19	81
16	OPh	60	40	38	62
17	$\text{NHC}_5\text{H}_{11}$	54	46	28	72
18	NC_4H_8	50	50	22	78

The influence of the substituent in the benzothiophene ring on the preferred conformation of the molecule in solution is best seen on the halide-substituted compounds. Thus, in the row $\text{R} = \text{H}$, Cl, Br, I with an increase of the size of the halogen atom the proportion of the parallel conformation had also been increasing in either solvent, with diiodide **9** displaying a majority of its parallel-oriented rotamer even in non-polar chloroform at 235 K. However, the molecules with other functional groups did not demonstrate any general regularities in the observed distribution of antiparallel and parallel conformers with the only notable exception of dibenzamide **15**. Indeed, the parallel conformation for this compound was totally dominating in chloroform and prevailing in more polar acetonitrile, as could be calculated from the ^1H NMR spectra. Apparently, the most logical explanation for this phenomenon should include the formation of intramolecular hydrogen bonds, which connected two amide moieties within a molecule. Such connection, therefore, would strengthen in less polar solvents, like chloroform, and slightly weaken in polar media, however, still governing the orientation of the molecule – the fact that was in accordance with the observed ratio for **15**.

At the same time, the proportion of an antiparallel conformation for all other benzothienylethenes had invariably dropped by switching to more polar acetonitrile. We explain this observation by formation of a higher dipolar moment in the parallel orientation, as compared to the opposite position of benzothiophene rings in the antiparallel conformation, where such a dipolar moment will be of less value due to its partial quenching. As acetonitrile has its dielectric constant of much higher value, this solvent stabilized the conformers with larger dipolar moment much more efficiently than chloroform.³⁷ Thus, one should expect a general raise of a parallel fraction of a corresponding symmetric benzothienylcyclopentene in solution with an increase of the dielectric constant of the solvent.

For this purpose we have performed the measurements of dibromide **6** in various deuterated solvents with either known or calculated dielectric constants (Table 8). To our delight the expectations were totally confirmed with an evident trend of a smooth decrease of an amount of the antiparallel conformer in the equilibrium between two rotamers as less stabilized in more polar media.

Table 8. Ratio dependence of antiparallel and parallel rotamers of dibromide **6** at 235 K on the dielectric constant of the solvent.

Solvent	Antiparallel, %	Parallel, %	ϵ , 235 K ^a	ϵ , RT
Toluene- <i>d</i> ₈	60	40	2.5	2.4
CDCl ₃	59	41	6.1	4.8
CD ₂ Cl ₂	50	50	12.0	8.9
Pyridine- <i>d</i> ₅	48	52	17.2 ^b	12.4
Acetone- <i>d</i> ₆	45	55	29.1 ^b	20.7
DMF- <i>d</i> ₇	44	56	51.3	38.3
CD ₃ CN	39	61	57.6 ^b	37.5

^a Dielectric constants at 235 K were obtained using published equations.³⁸

^b Values were obtained by interpolation of the published equations³⁸ to the temperatures, outside of the recommended interval.

This experiment had finally explained the observed lower values of absorbance in acetonitrile as compared to chloroform for the same compounds at the identical concentrations, as was mentioned earlier. Indeed, since dithienylethenes are being photoactive only in antiparallel conformation while the parallel rotamer could not photocyclize as a result of symmetry forbiddance,³⁹ low interconversion between two conformers (due to lower temperatures, or structural characteristics) should inevitably lead to a decrease in light-sensitivity of a researched benzothienylethene with an increase of a dielectric constant value of the used solvent. Moreover, additional strong intramolecular association in the molecule will certainly lead to domination of one of the conformers in solution, thus significantly influencing the photochromic properties of the corresponding compound. Indeed, as was shown before, light-sensitivity of dibenzamide **15** appeared it be inferior to any other analogous value of the researched dibenzothienylethenes (Table 4). At the same time, with the help of NMR studies we have learned that parallel conformation stabilized by intramolecular hydrogen bonds was by far dominating in this case in either chloroform or acetonitrile, as compared to other compounds, thus also explaining such inadequacy in the observed absorbance for **15**.

Hence, low temperature NMR spectroscopy has shown that the position of conformational equilibrium between antiparallel and parallel orientation can easily be influenced by both nature of the chemical substituent in the molecular core and a choice of a solvent. These variable factors should enable a researcher to optimize the design of a potential dithienylethene in order to increase the chances for certain needed physicochemical properties including its photochromic assets.

2.4. Molecular and crystal structure

Photochromism in the crystalline phase is a favorable characteristic of dithienylethenes, which is not commonly found. Indeed, for realization of this phenomenon two factors should combine accordingly: the molecule must acquire the antiparallel conformation and the distance between two reactive centers should not exceed an allowed limit of ~ 4.2 Å.⁴⁰ Only two examples of benzothienyl-containing substituted perhydrocyclopentenes that are photochromic in the crystal are known to date including both symmetric²² and nonsymmetric²³ examples. As we showed above, polarity of a solvent turned out to play a crucial role in a conformer ratio increasing the percentage of the antiparallel orientation of two benzothiophene moieties in the molecule in less polar solvents. Therefore, we decided to enhance our chances in acquiring desired single-

crystalline photochromism by using a non-polar crystallization system such as hexane diffusion into a chloroform solution for most compounds. The importance of a specific crystallization system was neatly demonstrated with 4,4'-dinitro-dibenzothienylperfluorocyclopentene which formed two polymorphic modifications with either photochromic antiparallel or UV-inactive parallel orientation of benzothiophene rings in the molecule depending on the used solvent.⁴¹

Ultimately, crystallization of the researched symmetric dibenzothienylcyclopentenes furnished single crystals that were subjected to X-ray analysis for a total of 10 compounds. It was found that antiparallel (A) orientation of benzothiophene rings was observed for dibenzothienylethenes **4** (Cl), **6** (Br), **9** (I), **14** (CN), **11** (CHO), and **16** (OPh) (Fig. 7) with similar molecular structures for these compounds, while the parallel (P) arrangement was established for dibenzothienylethenes **3** (H), **12** (COCH₃), **15** (NHCOPh), and **18** (NC₄H₈).

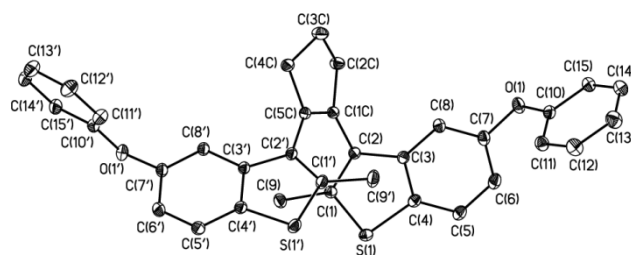


Fig. 7. General view of diphenoxy-substituted **16** in representation of atoms by thermal ellipsoids ($p = 50\%$).

In order to resolve the question of whether an appearance of the specific conformation of the molecule has been a result of the crystal packing for each compound or its occurrence has been dictated by inherent features (as a consequence of the nature of the substituent in the core), we have performed DFT calculations (PBE1PBE/6-311*G) for these compounds including both antiparallel and parallel orientation.

The obtained results of the DFT optimization for the isolated molecules appeared to be in apparent agreement with the observed arrangement of the corresponding molecules in the solid state. Indeed, according to our estimations, only for dibenzamide **15** the parallel position of benzothienyl fragments was more stable by 6 kJ/mol, while other compounds tended to prefer the antiparallel orientation (Table 9). However, the calculated differences in energy (ΔE) between two conformers turned out to be moderate in general, varying from 0.3 to 7.2 kJ/mol with a negligible value of 0.3 kJ/mol for “parallel” diketone **12**. Another compound that preferred the parallel conformation in the crystal – dipyrrolidine **18** – also had a low calculated value of $\Delta E_{A-P} = -2.6$ kJ/mol. In fact, the highest calculated difference in energy was observed for halide-substituted benzothienylcyclopentenes (5.88 - 6.21 kJ/mol), dinitrile **14** (6.4 kJ/mol) and diphenoxy **16** (7.2 kJ/mol) – compounds with an established antiparallel orientation of benzothiophenes in the crystalline state. At the same time, “unsubstituted” **3** had retained the parallel orientation in the crystal despite calculated $\Delta E_{A-P} = -5.3$ kJ/mol which appeared slightly higher than the analogous value for “antiparallel” dialdehyde **11** (-3.9 kJ/mol).

Table 9. The difference in energy and dipole moments of antiparallel and parallel conformations of dibenzothiienylcyclopentenones according to PBE1PBE/6-311G* calculations.

	3 (H)	4 (Cl)	6 (Br)	9 (I)	11 (CHO)	12 (COCH ₃)	14 (CN)	15 (NHCOPh)	16 (OPh)	18 (NC ₄ H ₈)
ΔE_{A-P} , kJ/mol	-5.3	-6.1	-6.2	-5.9	-3.9	-0.3	-6.4	6.0	-7.2	-2.6
D (A), D	1.1	0.8	0.7	0.8	0.3	3.7	3.5	5.8	0.9	3.2
D (P), D	1.5	4.3	4.2	4.3	8.0	6.1	9.6	7.7	2.3	4.5

However, in general, the defined ΔE values should be considered only as a rough way of estimation that helps in assessing the presence of various substituents. In fact, ΔE depends not only on various external factors (like the used functional and the basis set) but also on the polarity of the media – especially for dibenzothiienylethenes with high difference of dipole moments for two conformers like **11** or **14**. Indeed, such difference calculated for two conformations for these two compounds turned out to be the largest in the whole series with $\Delta D_{P-A} = 7.7$ D for **11** and $\Delta D_{P-A} = 6.1$ D for **14** (while for “unsubstituted” **3** this value equaled only 0.4 D). To illustrate this point an optimization with the account for a nonspecific solvation (SCRF = PCM, acetonitrile) was carried out for dinitrile **14**. As a result, ΔE value had decreased to -1.6 kJ/mol still favoring the antiparallel arrangement with the dipole moments increasing to 4.6 D and 13.3 D for antiparallel and parallel positions, respectively.

The analysis of calculated differences in energy (Table 9) clearly showed that it cannot be rationalized in terms of inductive or mesomeric effects of the corresponding substituent. Indeed, ΔE values were almost constant for halides and CN-substituted molecule but at the same time it appeared surprisingly different for CHO and COCH₃ substituents, which were both coplanar to the aromatic ring and were characterized by comparable calculated (benzothiophene)C–C(X)=O bond lengths of 1.474 and 1.492 Å for X = H and CH₃, respectively. Also, the lack of either electronic effect was supported by the analysis of geometrical parameters in the isolated molecules in the antiparallel arrangement. The values of the bonds lengths C(1C)–C(5C), C(1C)–C(2) (see Fig. 7 for numeration of atoms) and C(5C)–C(2'), dihedral angle between the benzothiophene rings and the torsion angle C(1)–C(2)–C(1C)–C(5C) were almost identical in this orientation for dialdehyde **11** and diketone **12**, thus clearly showing that the degree of conjugation between the pair of benzothiophene rings and the cyclopentene unit was also equal (Tables S1–S4 in Supplementary data). Furthermore, these geometric parameters remained equivalent for all studied compounds in the antiparallel orientation negating a major influence of a substituent on its values in this conformation. Therefore, the observed variation of ΔE for the isolated molecules can be rationalized only as a consequence of some specific intramolecular interactions, exclusively possible in the parallel arrangement owing to a proximity of the R-substituents to each other (an R...R interaction) and/or a proximity of an R-substituent and the second benzothiophene ring (an R... π interaction).

Given that geometric parameters cannot be considered as an unambiguous indication of bonding interaction, we performed a topological analysis of calculated electron densities function $\rho(\mathbf{r})$ within Bader's quantum theory of “Atoms in Molecules” (QTAIM).⁴² In addition to distinguishing bonding (stabilizing) interactions from all other contacts based on the bond critical points (BCP) (3, -1) search, it also allowed highly accurate

estimation of their energies.^{43,44} The additional benefit of QTAIM is that it could be applied both for $\rho(\mathbf{r})$ functions derived from theoretical and XRD data.

For this purpose, we used “unsubstituted” **3** as a “reference”. For this compound the critical point (CP) search of its antiparallel arrangement showed all expected C–H, C–C and C–S bonds as well as two H...H interactions involving benzothiophene hydrogen atoms C(8), C(8') and –CH₂– atoms C(2C) and C(4C) of the cyclopentene ring (Fig. 8). Such interactions are rather common for various organic compounds and are frequently responsible for conformational stabilization.^{44,45} The formation of these C–H...H–C interactions resulted in the presence of additional ring critical points (RCP) (3,+1) associated with the formed 7-membered rings. It should be noted that the separation between the above BCP for H...H interactions and the RCP appeared to be rather large, indicating that the former represented a “stable fragment” of the molecular graph. These H...H interactions were the only weak interactions being present in the case of the antiparallel position of the benzothiophene rings with an almost equal H...H separation of 2.15 Å and 2.25 Å.

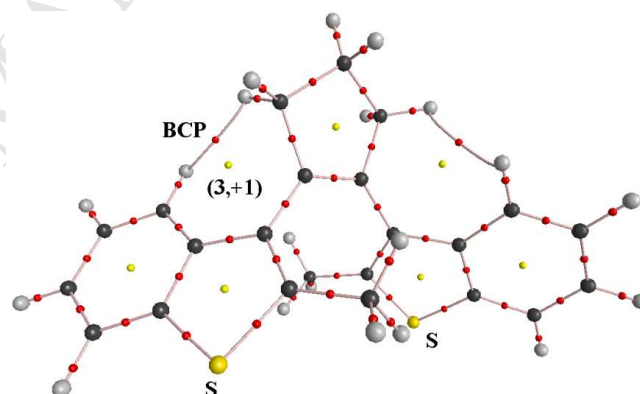


Fig. 8. Molecular graph for “unsubstituted” **3** in the antiparallel conformation according to the DFT calculations. Red and yellow dots correspond to (3,-1) and (3,+1) critical points, respectively.

On the contrary, in the parallel arrangement of **3** the number and type of intramolecular interactions became more diverse (Fig. 9). In addition to the already described H...H interactions between benzothiophenes and a cyclopentene ring, intramolecular H...C and C...C interactions were also established between the –CH₃ group and the spatially opposite benzothiophene ring of the same molecule. In contrast to the antiparallel orientation, the separation between the corresponding BCP and RCP in the parallel position turned out to be rather small (at least for H... π interactions) indicating that even smallest perturbations of the system can cause these bond paths and BCP to disappear.

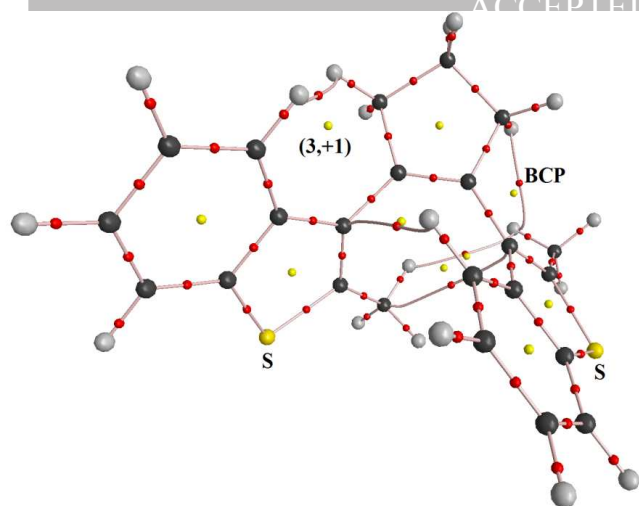


Fig. 9. Molecular graph for “unsubstituted” **3** in the parallel conformation according to the DFT calculations. Red and yellow dots correspond to (3,-1) and (3,+1) critical points, respectively.

Despite the fact that the number of intramolecular interactions in **3** in the parallel conformation notably exceeded those in the antiparallel arrangement, the latter could be additionally stabilized by a “conjugation pass” increase, which is a rather common effect for polyenes.⁴⁶ The same explanation for stabilization of an antiparallel conformation should be retained for other substituents, such as halides, -CN, and -CHO groups since the characteristic sets of CP in both conformations (i.e. the number and the type of intramolecular interactions in the isolated molecule) for all these compounds perfectly coincided with the data obtained for **3**.

However, while in the antiparallel arrangement the characteristic set and the geometry of the molecules remained the same for all dibenzothienylcyclopentenes, the introduction of R = COCH₃, NHCOPh, and NC₄H₈ substituents to the molecule had led to formation of additional interactions in the parallel conformation. Thus, in diketone **12** intramolecular R...R interactions of a C-H...O=C type were discovered (with H...O and C...O distances being equal to 2.48 Å and 3.442 Å, respectively). At the same time, the presence of amide groups in **15** resulted in the expected intramolecular N-H...O hydrogen bond formation (H...O = 2.09 Å; N...O = 3.088 Å), while in dipyrrolidine-substituted **18** the parallel conformation became stabilized by an R...benzothiophene interaction of C-H... π type (H...C = 2.84 Å; C...C = 3.674 Å). The energy values of the above intramolecular interactions were estimated using Espinosa's correlation,⁴⁷ giving 7.0, 16.3, and 4.2 kJ/mol for dibenzothienylethenes **12**, **15**, and **18**, respectively.

At the same time, the independently obtained XRD (Figs. 10-12) data had perfectly confirmed the disclosed DFT calculations for these compounds in the parallel conformation.

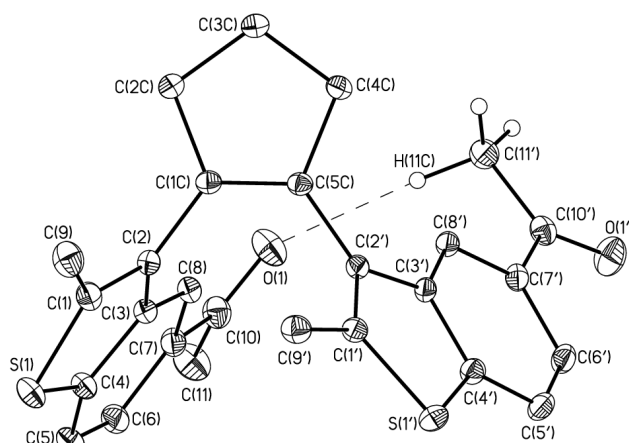


Fig. 10. General view of diketone **12** in representation of atoms by thermal ellipsoids ($p = 50\%$).

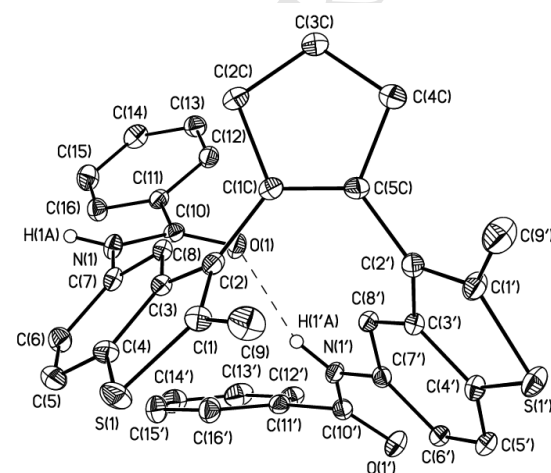


Fig. 11. General view of dibenzamide **15** in representation of atoms by thermal ellipsoids ($p = 50\%$).

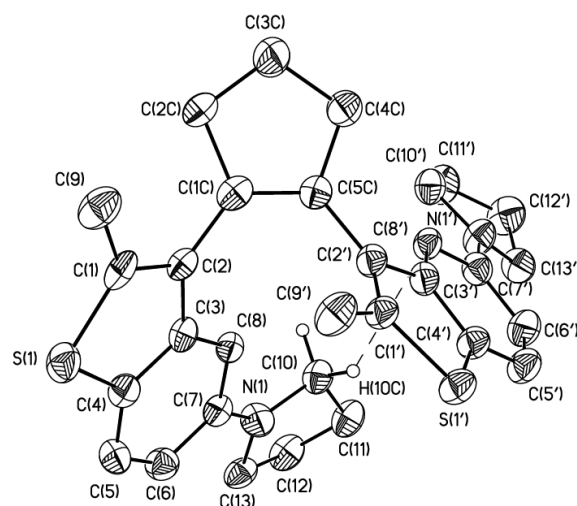


Fig. 12. General view of diamine **18** in representation of atoms by thermal ellipsoids ($p = 50\%$).

Despite additional intermolecular interactions found in the crystalline packing, such as O=C...C (π) stacking (C...C = 3.343(3) Å) for diketone **12**, hydrogen bonding N-H...O (N...O = 2.862(2) Å) for dibenzamide **15**, and various H... π and H...H contacts for diamine **18**, all the intramolecular contacts calculated for the isolated molecules were also located in the crystal. Not only these R...R and R...benzothiophene intramolecular

interactions persisted in the crystal, but moreover, their geometric parameters turned out to be rather close to those estimated for the isolated molecules. The comparison of these data describing the mutual disposition of benzothiophene rings had also revealed that the crystal packing effects could only insignificantly disturb the molecular parameters in the parallel orientation.

Thus, for at least three dibenzothiénylenes with diverse substituents ($R = \text{NHCOPh}$, COCH_3 , and NC_4H_8) the domination of the parallel conformation in the solid state can be considered as an inherent feature of these compounds, i.e. a result of specific intramolecular interactions of the introduced groups in the benzothiophene core. Therefore, it would be logical to propose that DFT calculations should be considered as a helpful practical way to exclude the potential substituent that would stabilize the parallel conformation of the molecule, which is strictly unfavorable while pursuing a search for the photochromic phenomenon in the solid state.

Although DFT modeling can be used to define particular substituents that will stabilize the parallel conformation, and as a consequence, identifying the antiparallel orientation of molecules in the crystal for others, it still cannot assure a photochromic behavior of the latter in the solid state due to indispensability of a certain proximity ($< 4.2 \text{ \AA}$) between the reaction centers $\text{C}(1)\dots\text{C}(1')$ for photocyclization reaction to proceed. Indeed, the mutual position of benzothiophene units in the antiparallel conformation, where no intramolecular interactions had been restraining these rings, could notably vary, as a result of crystal packing, affecting the crucial $\text{C}(1)\dots\text{C}(1')$ distance in this conformation. Besides the mentioned distance, orientation of two benzothiophene fragments could also be characterized by a pseudotorsion angle $\text{C}(2)\text{--}\text{C}(1)\text{--}\text{C}(1')\text{--}\text{C}(2')$ (ϕ). As was calculated for the isolated molecules in the antiparallel orientation, both these parameters turned out to be very similar varying in the ranges of $3.641 - 3.671 \text{ \AA}$ and $81.1 - 81.8^\circ$, thus satisfying the photochromism requirements.

However, this was not the case for most crystallized dibenzothiénylcyclopentenes with the antiparallel arrangement in the packing. In fact, only diphenoxy-substituted **16** had displayed a possession of this uncommon attribute with its crystals turning orange (Fig. 13) under UV-irradiation while other crystallized compounds (halide-, CHO -, and CN -substituted) remained uncolored under same conditions. It was established, that the distances between two reactive centers in the crystals for all these benzothiénylenes varied from $3.570(1) \text{ \AA}$ to $5.401(2) \text{ \AA}$, while ϕ diverged from 80.5° to 126.9° .

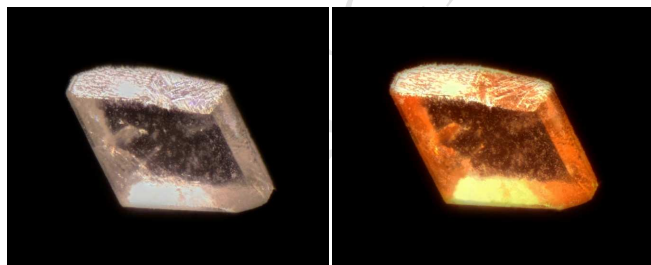


Fig. 13. Microscope photographs of a crystal of diphenoxy-substituted **16** before and after photoirradiation with UV light.

Thus, in the series of halide- and CN -substituted dibenzothiénylenes, all of these compounds, but the diiodide **9**, were found isostructural (when the molecule is on the C_2 axis) while the diiodide itself crystallized in another space group (with the molecule in a general position). Although the crystal packing pattern for dibenzothiénylenes **4** (Cl), **6** (Br), **9** (I), and **14** (CN) was ascertained to be, in principle, rather different (with

predominantly $\text{H}\dots\text{H}$ and $\text{H}\dots\pi$ interactions in **4**, **6**, and **14**; and $\text{I}\dots\text{I}$ (3.913 \AA) and $\text{I}\dots\text{S}$ $3.614(3) \text{ \AA}$ interactions in **9**), the $\text{C}(1)\dots\text{C}(1')$ distances and ϕ values appeared in a rather close range for these compounds amounting to $5.36 - 5.40 \text{ \AA}$ and 5.302 \AA (**9**), $121.6 - 124.3^\circ$ and 126.9° (**9**), respectively.

For dialdehyde **11** the molecular structure parameters were much closer to the threshold values from the standpoint of photochromic properties. In fact, for this molecule (which was also on a C_2 -axis) the key distance between two photoreactive centers $\text{C}(1)\dots\text{C}(1')$ equaled $4.162(3) \text{ \AA}$ which accurately coincided with the border value needed for photochromism in a crystal established by Irie. At the same time, the angle $\phi = 92.8^\circ$ in **11** became much closer to the calculated "ideal" values of $81 - 82^\circ$ than it was in the halide- and CN -substituted series. It is worth mentioning, that in both dialdehyde **11** and similarly structured diketone **12** the molecules in the crystal were assembled into stacks by interactions formed between the $\text{C}=\text{O}$ group and the aromatic cycle of the neighboring benzothiophene ring. We presume that this type of intermolecular interactions should be mainly governed by the nature of a substituent rather than by the conformation of the corresponding molecule in the crystal, which was antiparallel for **11** and parallel for **12**.

Hence, only in case of photochromic diphenoxy-substituted **16** (Fig. 7), the found $\text{C}(1)\dots\text{C}(1')$ distance equaled $3.571(2) \text{ \AA}$ – the distance that was not only shorter than the calculated threshold but even shorter than it was estimated in the gas phase, while the ϕ value was almost identical (80.5°) to that obtained from DFT-modeling ($81.1 - 81.8^\circ$).

Why had this compound with the phenoxy substituents appeared to be so different from the others? Surprisingly, but the phenoxy groups itself were not involved in any specific interactions in the crystal packing. Yet, another unique type of interactions has been determined for this compound: the sulfur atoms had interacted simultaneously with two benzothiophene moieties of the neighboring molecule by means of $\text{S}\dots\pi$ ($\text{S}\dots\text{C}$ $3.397 - 3.489 \text{ \AA}$) and weak $\text{S}\dots\text{H}_3\text{C}$ contacts (Fig. 14). It is worth noting, that similarly to the role of sulfur atoms in this crystal structure, multiple various intramolecular interactions had kept the benzothiophene fragments together in the parallel orientation, as was observed for **12** (COCH_3), **15** (NHCOPh), and **18** (NC_4H_8). Moreover, the cell dimensions for **16** remained unchanged in the crystal of this compound obtained from the polar system of solvents: on slow methanol diffusion into the acetone solution. This experiment proved the domination of certain intra- and intermolecular interactions in governing the crystal structure formation with little or no impact of the media.

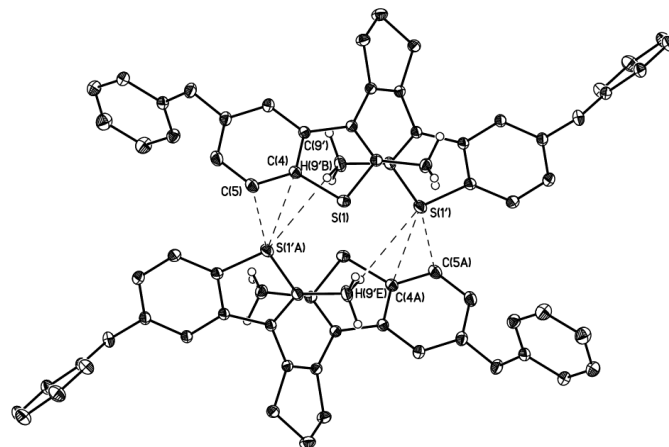


Fig. 14. Illustration of the formation of $\text{S}\dots\pi$ and $\text{S}\dots\text{H}_3\text{C}$ contacts in the centrosymmetric dimer of diphenoxy-substituted **16**.

Besides, the shortening of the C(1)...C(1') distance in the crystal of **16** as compared to the same parameter obtained for the isolated molecule attested to some influential attractive interactions developed in the crystalline state. In order to find out whether these interactions appeared to be the described S... π and S...H contacts or resulted from the transannular C(1)...C(1') interaction we have performed a high resolution X-ray diffraction experiment for **16** followed by topological analysis of the resulting experimental electron density.

According to these experimental data, the main features of the electron density distribution in this dibenzothiophenylene followed the rather typical pattern for the organic compounds. In particular, deformation electron density maps showed the maxima corresponding to covalent bonds and electron lone pairs of the sulphur atoms. The topological parameters of $\rho(\mathbf{r})$ in the crystal of **16** were rather close to those in the isolated molecule with the antiparallel arrangement; however, in the crystalline state the shortening of the interplane distance between the benzothiophene rings had led to two additional CH₃...C(2) and CH₃...C(2') contacts with an energy as small as ~2.1 kJ/mol (Fig. 15). The essential S... π and S...H contacts that had drawn the cycles together were both characterized by the presence of BCP, at the same time, no C(1)...C(1') interaction was detected. While the energy of an individual interaction was found to be rather low; yet, combining together it added up to 8.9 kJ/mol in total. In fact, this value is comparable with those of the corresponding intramolecular contacts in the parallel arrangement described earlier for dibenzothiophenylenes **12**, **15**, and **18**, the interactions that were proven to be responsible for stabilization of such conformation in the solid state for these compounds.

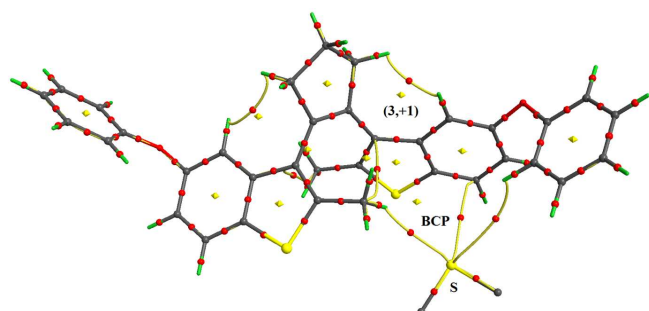


Fig. 15. Molecular graph for diphenoxy-substituted **16** according to the high resolution XRD. Red and yellow dots correspond to (3,-1) and (3,+1) critical points, respectively. Part of the neighboring molecule is omitted for clarity.

Hence, the combination of DFT and XRD investigations has enabled us to explain the forces responsible for a certain conformation of a dibenzothiophenylene molecule in the crystalline state. On one hand, its parallel orientation in the crystal is being governed by intramolecular interactions of specific substituents in the benzothiophene rings, and therefore, can be predicted by DFT calculations. On the other hand, the antiparallel arrangement is caused by various intermolecular interactions that can stabilize the particular mutual disposition of aromatic rings. Depending on the origin of such interactions and their spatial orientation the parameters of the crystal structure, including the crucial C(1)...C(1') distance, might vary greatly, thus making the target search for photochromic properties of dibenzothiophenylenes in the crystalline phase rather problematical. However, *a priori* exclusion of potentially "parallel" structures with a help of DFT analysis should considerably assist a researcher in this pursuit.

Synthetic approach to diverse 5,5'-substituted symmetric dibenzothiophenylcyclopentenes has been developed via straightforwardly accessible dibromide **6** that could be considered as a universal starting material for this purpose. Chemical substitution of bromides in **6** via either the dilithiation procedure, followed by the reaction with different electrophiles, or catalytically induced coupling with various nucleophiles provided a symmetric formation of new C-C, C-N, C-O, C-Si, and C-I bonds in the body of the molecule. The obtained compounds were profoundly studied in both solution and solid state in order to explore the dependence of photochromic properties of this class of dithienylethenes on the substituent in the benzothiophene ring. It was shown that all compounds displayed standard for dithienylethenes photochromic properties in solution, with the exception for diiodide **9**, which underwent decomposition under UV irradiation. Besides, an introduction of the substituents of an electron-donating nature led to the bathochromic shift of the absorption maxima and the raise of the light-sensitivity for the corresponding compounds in solution. At the same time, an improvement of the resistance to photodegradation for this class of photochromes was observed with an increase of electron-withdrawing ability of the groups introduced to 5- and 5'-positions of the benzothiophene rings. NMR studies revealed that two distinct rotamers with antiparallel and parallel orientation of benzothiophenyl fragments existed in solution, interconversion of which could be completely suppressed at -50 °C. The ratio of two conformers was established to be dependant on both nature of the chemical substituent in the molecular core and a value of the dielectric constant of the solvent. Moreover, symmetric dibenzothiophenylcyclopentenes also occupied either antiparallel or parallel conformation in the crystalline phase. It was found that the latter was controlled by intramolecular interactions of particular substituents in the benzothiophene rings, and hence could be predicted by DFT calculations for the isolated molecules. On the contrary, the antiparallel arrangement of the rings was being governed by different intermolecular interactions in the crystal packing, thus excluding the possibility of a predictive foresight towards photochromic properties in a single crystal. Only diphenoxy-substituted **16** had displayed photochromism in the crystalline state in the whole series of compounds. High resolution X-ray analysis showed that intermolecular S... π and S...H contacts were primarily responsible for this phenomenon by drawing the benzothiophene cycles together, and therefore, shortening the distance between two reactive centers C(1)...C(1'), thus allowing the photocyclization reaction to proceed.

Overall, we have presented a comprehensive research for this class of dithienylethenes both in solution and solid state. The obtained data and observed regularities in photochromic behavior should greatly assist a researcher in this field in designing of future photochromic dithienylethenes.

4. Experimental section

4.1. General

All reactions were carried out under argon atmosphere. Solvents were dried by the usual methods and then distilled prior to use. NMR spectra were obtained at 300 MHz for ¹H NMR and at 75 MHz for ¹³C NMR with chemical shift values in the spectra being referenced to the solvent. Temperature dependant ¹H NMR spectra were recorded using Bruker Avance 600 spectrometer (working frequency 600.13 MHz). Variable temperature unit was calibrated using ethylene glycol and methanol samples for high

and low temperature, respectively. The measurements were done using deuterated solvent's residual signal as an internal reference. 2D ^1H - ^1H EXSY spectra were obtained using 400 ms mixing time. Data acquisition and processing were performed with Topspin 2.1 and Mestrenova 9.0.0 software, respectively. Elemental analyses were carried out with a Perkin-Elmer CHN analyser (2400 series II). High resolution mass spectra (HR MS) were measured on the Bruker micrOTOF II instrument using electrospray ionization (ESI).⁴⁸ The measurements were done in a positive ion mode (interface capillary voltage – 4500 V) or in a negative ion mode (3200 V); mass range from m/z 50 to m/z 3000 Da; external or internal calibration was done with Electrospray Calibrant Solution (Fluka). A syringe injection was used for solutions in acetonitrile, methanol, or water (flow rate 3 $\mu\text{L}/\text{min}$). Nitrogen was applied as a dry gas; interface temperature was set at 180 °C. IR spectra were recorded on Nicolet Magna-IR 750 spectrometer. Spectral and kinetic studies were conducted with «Cary 50 bio» (Varian) spectrophotometer using a quartz cell with a path length of 0.2 cm. Irradiation was performed by Hamamatsu LC-8 spot light source equipped with either light filters UFS-1 (240-400 nm) for photocoloration (with irradiance $I = 11 \text{ mW}/\text{cm}^2$) or ZHS-16 (460-2800 nm) for photobleaching (with irradiance $I = 11 \text{ mW}/\text{cm}^2$) processes; no filter was used for photodegradation studies (with irradiance $I = 94 \text{ mW}/\text{cm}^2$). Concentration of the photochromic compounds in solution was $C = 2 \times 10^{-4} \text{ M}$. Toluene and acetonitrile from «Aldrich» were used as solvents. Polymer films and solid-phase films were prepared by casting method on quartz plates with an estimated thickness of the formed film being 100-150 μm . Preparation of a polymer included addition of 100 mg of polymethyl methacrylate (PMMA) to the solution of 0.5 mg of the corresponding dibenzothienylcyclopentene in chloroform (1 mL). Solid-phase films were prepared from solutions of dibenzothienylcyclopentenenes in toluene ($C = 2 \times 10^{-3} \text{ M}$). Photos of crystals of **16**: Olympus BH2, Olympus Splan Apo 4, NFK 2.5, reflected light.

4.2. Synthesis of dibromide **6**

4.2.1. 5-Bromo-2-methylbenzo[b]thiophene (7). On cooling *t*-BuOK (27.4 g, 245 mmol) was dissolved in absolute EtOH (200 mL) and to the clear solution 4-bromothiophenol (38.6 g, 204 mmol) was added in one portion. The formed homogeneous solution was stirred at rt for 1 h. 2-Bromopropionaldehyde diethyl acetal (51.6 g, 245 mmol) was then added and the suspension was kept at reflux for 24 h, after this time TLC analysis showed no 4-bromothiophenol left in the reaction mixture. EtOH was evaporated and the residue was dissolved in CH_2Cl_2 and water. The organic layer was combined with CH_2Cl_2 extracts of the aqueous phase, washed sequentially with water and brine, and dried over Na_2SO_4 . The liquid residue after evaporation of the solvents was distilled in vacuo to give 57.3 g of slightly yellow liquid (136-137 °C / 1 mm), which was used in the next step without additional purification.

To a well-stirred suspension of polyphosphoric acid (> 84 %, 120 g) in boiling chlorobenzene (350 mL) intermediate diethyl acetal was added in small portions within 3 h. The mixture was kept at reflux for a total of 8 h, after this time TLC analysis showed no starting material left in the reaction mixture. At this point water was added with formation of two clear layers. The organic layer was separated, combined with ethyl acetate extracts of the aqueous phase, then washed sequentially with water and brine, and dried over Na_2SO_4 . The residue after evaporation of the solvents was sublimed in vacuo (95-100 °C / 1 mm) to give 37.9 g (82% for two steps) of white solid: mp 93-95 °C; ^1H NMR (300 MHz, CDCl_3) δ 2.60 (s, 3H), 6.92 (s, 1H), 7.35 (dd, 1H, $J =$

8.4 Hz, $J = 1.8$ Hz), 7.61 (d, 1H, $J = 8.4$ Hz), 7.80 (d, 1H, $J = 1.8$ Hz); ^{13}C NMR (75 MHz, $\text{DMSO}-d_6$) δ 16.1, 118.0, 120.8, 123.2, 125.1, 126.2, 138.2, 142.0, 142.9; anal. calcd for $\text{C}_9\text{H}_7\text{BrS}$: C, 47.60; H, 3.11; S, 14.12; found: C, 47.45; H, 3.09; S, 14.18.

4.2.2. 1,5-Bis(5-bromo-2-methylbenzo[b]thiophen-3-yl)pentane-1,5-dione (8). To a solution of 5-bromo-2-methylbenzo[b]thiophene (4.2 g, 18.4 mmol) and glutaryl chloride (1.55 g, 9.2 mmol) in dry dichloromethane (60 mL) at -15 °C aluminum (III) chloride (2.7 g, 20.3 mmol) was added in portions within 30 min under argon atmosphere. The reaction mixture was stirred at 0 °C for 2 h and then at rt for 12 h. The solvent was evaporated, and water was added to the solid residue on cooling. The suspension was filtered, and the solid on filter was consequently washed with water, ethanol, and acetone to give 4.5 g (89%) of beige solid after drying: ^1H NMR (300 MHz, $\text{DMSO}-d_6$) δ 2.01-2.11 (m, 2H, $J = 6.5$ Hz), 2.81 (s, 6H), 3.09 (t, 4H, $J = 6.5$ Hz), 7.52 (d, 2H, $J = 8.4$ Hz), 7.92 (d, 2H, $J = 8.4$ Hz), 8.38 (s, 2H); ^{13}C NMR (75 MHz, $\text{DMSO}-d_6$) δ 16.6, 18.7, 42.1, 118.8, 123.8, 125.9, 127.2, 132.0, 135.7, 139.9, 149.9, 198.1; HRMS (m/z) [$M + H$]⁺ calcd for $\text{C}_{23}\text{H}_{18}\text{Br}_2\text{O}_2\text{S}_2$, 550.9168; found 550.9163.

4.2.3. 1,2-Bis(5-bromo-2-methylbenzo[b]thiophen-3-yl)cyclopent-1-ene (6). Titanium (IV) chloride (8.9 g, 46.8 mmol) was added in a dropwise manner to a well-stirred suspension of zinc dust (12 g, 185 mmol) in dry tetrahydrofuran (180 mL) at -15 °C under argon atmosphere. The suspension was stirred at rt for 1 h, then dry pyridine (3.7 g, 46.8 mmol) was added followed by addition of diketone **8** (8.6 g, 15.6 mmol) in one portion. The suspension was refluxed for 10 h, after this time TLC analysis showed no starting material left in the reaction mixture. Water (2.8 g, 155 mmol) was added with stirring, and the suspension was filtered through a silica plug. The filtrate was partially evaporated, and hexane was added under reflux. The product crystallizes on cooling as colorless crystals. The filtrate was evaporated and the solid residue was subjected to silica gel flash column chromatography (hexanes) to additionally give pure product as white powder. Combined weight amounted 6.9 g (85%). High quality single crystals suitable for X-ray diffraction were grown from ethyl acetate solution by slow evaporation: mp 216-218 °C; ^1H NMR (300 MHz, CDCl_3) δ 2.05 (s, 6H), 2.10-2.23 (m, 2H, $J = 7.2$ Hz), 2.70-3.10 (broad m, 4H), 7.12 (d, 2H, $J = 8.5$ Hz), 7.33 (d, 2H, $J = 8.5$ Hz), 7.61 (s, 2H); ^{13}C NMR (75 MHz, $\text{DMSO}-d_6$) δ 15.1, 23.9, 37.6, 118.0, 123.1, 124.4, 124.9, 125.5, 126.3, 136.7, 136.8, 140.7; IR (KBr, cm^{-1}) ν 2920, 2840, 1579, 1553, 1433, 1413, 1247, 1147, 1067, 958, 869, 798, 741; anal. calcd for $\text{C}_{23}\text{H}_{18}\text{Br}_2\text{S}_2$: C, 53.30; H, 3.50; Br, 30.83; S, 12.37; found: C, 53.35; H, 3.31; Br, 30.71; S, 12.32.

4.3. General experimental procedure for dilithiation

To a stirred clear solution of dibenzothienylethene **6** (206 mg, 0.4 mmol) in freshly distilled THF (15 mL) at -80 °C *n*-BuLi (1 mL, 1.6 M) was gradually injected. After 20 min at this temperature the corresponding electrophile (I_2 in THF – 3.2 mmol; TMSCl – 4.5 mmol; DMF – 4.1 mmol; CH_3CONH_2 – 3.5 mmol; CH_3CHO – 4.5 mmol) was added, and the temperature was allowed to rise to 0 °C. After addition of water (0.2 g, 11 mmol) the formed suspension was evaporated and subjected to silica gel flash column chromatography to give target material.

4.3.1. 1,2-Bis(5-iodo-2-methylbenzo[b]thiophen-3-yl)cyclopent-1-ene (9) via dilithiation. The general procedure was slightly modified at work up. To the reaction mixture saturated $\text{Na}_2\text{S}_2\text{O}_3$ solution and brine were added, and the organic layer was separated and combined with ethyl acetate extracts of the aqueous phase. Evaporation of the solvents provided an oily

residue which was dissolved in THF and filtered through a silica plug. After evaporation of the filtrate the residue was subjected to silica gel flash column chromatography (hexanes/ethyl acetate) to give 200 mg (82%) of white solid. High quality single crystals suitable for X-ray diffraction were grown by slow diffusion of hexanes into the chloroform solution: mp 170-171 °C; ¹H NMR (300 MHz, CDCl₃) δ 2.22 (s, 6H), 2.16-2.32 (m, 2H), 2.85-3.05 (m, 4H), 7.32 (d, 2H, *J* = 8.3 Hz), 7.39 (d, 2H, *J* = 8.3 Hz), 7.78 (s, 2H); ¹³C NMR (75 MHz, CDCl₃) δ 15.0, 23.9, 37.6, 89.0, 123.4, 129.4, 131.1, 131.8, 136.7, 137.4, 137.5, 141.0; IR (KBr, cm⁻¹) ν 2914, 2840, 1571, 1548, 1428, 1405, 1250, 1150, 1067, 964, 869, 804, 732; anal. calcd for C₂₃H₁₈I₂S₂: C, 45.12; H, 2.96; I, 41.45; S, 10.47; found: C, 44.64; H, 2.88; I, 40.49; S, 10.23; HRMS (*m/z*) [*M* + *H*]⁺ calcd for C₂₃H₁₈I₂S₂, 612.9012; found 612.8992.

4.3.2. *1,2-Bis(2-methyl-5-(trimethylsilyl)benzo[b]thiophen-3-yl)cyclopent-1-ene (10)*. 180 mg (90%) of colorless foam (hexanes) were obtained; ¹H NMR (300 MHz, CDCl₃) δ 0.08 (s, 9H), 0.33 (s, 9H), 1.92 (s, 3H), 2.19-2.32 (m, 5H), 2.67-2.82 (m, 1H), 2.82-2.98 (m, 1H), 3.10-3.29 (m, 2H), 7.22-7.40 (m, 2H), 7.56-7.73 (m, 3H), 7.78-7.89 (m, 1H); ¹³C NMR (75 MHz, CDCl₃) δ -0.9, 15.0, 24.6, 38.1, 121.4, 123.3, 127.4, 127.9, 130.2, 135.0, 135.8, 137.4, 139.2; IR (KBr, cm⁻¹) ν 2954, 2846, 1433, 1399, 1267, 1247, 1176, 1098, 1053, 838, 804, 755; HRMS (*m/z*) [*M* + *H*]⁺ calcd for C₂₉H₃₆S₂Si₂, 504.1791; found 504.1774.

4.3.3. *3,3'-(Cyclopentene-1,2-diyl)bis(2-methylbenzo[b]thiophene-5-carbaldehyde (11))*. 138 mg (83%) of white solid (hexanes/ethyl acetate) were obtained. High quality single crystals suitable for X-ray diffraction were grown by slow evaporation of the chloroform solution: mp 195 °C dec.; ¹H NMR (300 MHz, CDCl₃) δ 2.21 (s, 6H), 2.35 (quin, 2H, *J* = 7.4 Hz), 2.93-3.17 (m, 4H), 7.65 (d, 2H, *J* = 8.2 Hz), 7.71 (d, 2H, *J* = 8.2 Hz), 8.02 (s, 2H), 9.77-10.03 (broad s, 2H); ¹³C NMR (75 MHz, CDCl₃) δ 15.2, 23.9, 37.9, 122.5, 123.5, 124.7, 130.8, 132.8, 137.0, 138.2, 139.2, 144.4, 192.0; IR (KBr, cm⁻¹) ν 2914, 2720, 1685, 1588, 1553, 1433, 1376, 1304, 1193, 1141, 1067, 806, 715; HRMS (*m/z*) [*M* + *H*]⁺ calcd for C₂₅H₂₀O₂S₂, 417.0977; found 417.0966.

4.3.4. *1,1'-(3,3'-(Cyclopentene-1,2-diyl)bis(2-methylbenzo[b]thiophene-5,3-diyl))diethanone (12)*. 92 mg (52%) of white solid (hexanes/ethyl acetate) were obtained. High quality single crystals suitable for X-ray diffraction were grown by slow evaporation of the chloroform solution: mp 185-186 °C; ¹H NMR (300 MHz, CDCl₃) δ 2.08-2.20 (m, 3H), 2.23-2.41 (m, 8H), 2.60-2.71 (m, 3H), 2.83-3.01 (m, 2H), 3.09-3.24 (m, 2H), 7.66 (d, 2H, *J* = 8.2 Hz), 7.71-7.79 (m, 2H), 8.01-8.10 (m, 1H), 8.11-8.23 (m, 1H); ¹³C NMR (75 MHz, CDCl₃) δ 15.2, 23.9, 26.3, 38.0, 121.9, 122.6, 122.9, 130.8, 133.4, 136.8, 137.8, 138.9, 143.0, 197.8; IR (KBr, cm⁻¹) ν 2926, 2846, 1677, 1585, 1428, 1362, 1307, 1267, 1230, 1050, 907, 821, 809; HRMS (*m/z*) [*M* + *H*]⁺ calcd for C₂₇H₂₄O₂S₂, 445.1290; found 445.1296.

4.3.5. *1,1'-(3,3'-(Cyclopentene-1,2-diyl)bis(2-methylbenzo[b]thiophene-5,3-diyl))diethanol (13)*. 145 mg (81%) of white solid (hexanes/ethyl acetate) were obtained: mp 111-112 °C; ¹H NMR (300 MHz, CDCl₃) δ 0.96-1.04 (m, 1H), 1.08-1.19 (m, 1H), 1.39-1.51 (m, 4H), 2.10-2.43 (broad m, 10H), 2.82-3.18 (broad m, 4H), 4.73-4.90 (m, 2H), 6.96-7.13 (m, 2H), 7.48-7.59 (m, 2H), 7.66-7.78 (m, 2H); ¹³C NMR (75 MHz, CDCl₃) δ 15.0, 23.8, 25.4, 37.9, 70.6, 118.6, 121.0, 121.6, 130.6, 136.4, 136.9, 137.2, 139.4, 142.0; IR (KBr, cm⁻¹) ν 3411, 2971, 2926, 2846, 1545, 1442, 1370, 1293, 1199, 1150, 1075, 895, 802; HRMS (*m/z*) [*M* + *H*]⁺ calcd for C₂₇H₂₈O₂S₂, 448.1525; found 448.1503.

4.4. Copper (I) iodide catalyzed coupling of dibromide 6

4.4.1. *1,2-Bis(5-iodo-2-methylbenzo[b]thiophen-3-yl)cyclopent-1-ene (9) via halogen exchange*. Dibenzothienylethene **6** (150 mg, 0.29 mmol), copper (I) iodide (55 mg, 0.29 mmol), sodium iodide (348 mg, 2.32 mmol), and N,N'-dimethylethylenediamine (102 mg, 1.16 mmol) were sequentially placed into a Schott tube under argon atmosphere. Dioxane (4 mL) was then added washing all the solids from the walls of the tube. The reaction mixture was stirred at 115 °C for 24 h, after this time TLC analysis showed no starting material left in the reaction mixture. THF was added, and the formed suspension was filtered through a silica plug. After evaporation of the filtrate, the residue was subjected to silica gel flash column chromatography (hexanes/ethyl acetate) to give 165 mg (93%) of white solid.

4.4.2. *3,3'-(Cyclopentene-1,2-diyl)bis(2-methylbenzo[b]thiophene-5-carbonitrile) (14)*. Dibenzothienylethene **6** (150 mg, 0.29 mmol), copper (I) iodide (55 mg, 0.29 mmol), potassium iodide (48 mg, 0.29 mmol), sodium cyanide (57 mg, 1.16 mmol), and N,N'-dimethylethylenediamine (102 mg, 1.16 mmol) were sequentially placed into a Schott tube under argon atmosphere. Toluene (2 mL) was then added washing all the solids from the walls of the tube. The reaction mixture was stirred at 120 °C for 20 h, after this time TLC analysis showed some of monosubstituted intermediate left in the reaction mixture. All reagents were added at this point once again in the same quantities followed by 2 mL of toluene, and the well-stirred reaction was additionally kept at 120 °C for 20 h to complete the transformation. Hot reaction mixture was filtered through a silica plug followed by hot ethyl acetate. After evaporation of the combined filtrate the residue was subjected to silica gel flash column chromatography (hexanes/ethyl acetate) to give 105 mg (88%) of white solid. High quality single crystals suitable for X-ray diffraction were grown by slow diffusion of hexanes into the chloroform solution: mp 272 °C dec.; ¹H NMR (300 MHz, CDCl₃) δ 2.16 (s, 6H), 2.32 (quin, 2H, *J* = 7.4 Hz), 2.90-3.10 (m, 4H), 7.39 (d, 2H, *J* = 8.2 Hz), 7.69 (d, 2H, *J* = 8.2 Hz), 7.80 (s, 2H); ¹³C NMR (75 MHz, CDCl₃) δ 15.1, 24.0, 37.8, 107.6, 119.3, 122.9, 125.5, 126.4, 129.9, 137.0, 138.9, 139.2, 142.5; IR (KBr, cm⁻¹) ν 2914, 2840, 2223, 1594, 1445, 1385, 1227, 1141, 1064, 895, 809, 741; HRMS (*m/z*) [*M* + *H*]⁺ calcd for C₂₅H₁₈N₂S₂, 411.0984; found 411.0975.

4.4.3. *N,N'-(3,3'-(cyclopentene-1,2-diyl)bis(2-methylbenzo[b]thiophene-5,3-diyl))dibenzamide (15)*. Dibenzothienylethene **6** (150 mg, 0.29 mmol), benzamide (140 mg, 1.16 mmol), copper (I) iodide (55 mg, 0.29 mmol), potassium carbonate (320 mg, 2.32 mmol), and N,N'-dimethylethylenediamine (102 mg, 1.16 mmol) were sequentially placed into a Schott tube under argon atmosphere. Dioxane (4 mL) was then added washing all the solids from the walls of the tube. The reaction mixture was stirred at 115 °C for 24 h, after this time TLC analysis showed no starting material left in the reaction mixture. THF was added, and the formed suspension was filtered through a silica plug. After evaporation of the filtrate the residue was subjected to silica gel flash column chromatography (hexanes/ethyl acetate) to give 104 mg (60%) of white solid. High quality single crystals suitable for X-ray diffraction were grown by slow diffusion of MeOH into the DMSO solution: mp 279 °C dec.; ¹H NMR (300 MHz, CDCl₃) δ 2.22-2.39 (m, 8H), 2.83-3.01 (m, 4H), 7.21-7.29 (m, 4H), 7.32-7.37 (m, 2H), 7.38 (d, 2H, *J* = 8.4 Hz), 7.53 (d, 2H, *J* = 8.4 Hz), 7.53-7.61 (m, 4H), 7.79 (s, 2H), 8.10 (s, 2H); ¹³C NMR (75 MHz, DMSO-*d*₆) δ 14.7, 23.7, 37.1, 113.5, 117.3, 121.9, 127.5, 128.3, 129.8, 131.4, 132.4, 135.0, 136.1, 136.3, 136.5, 139.3, 165.5; IR (KBr, cm⁻¹) ν 3349, 3297, 2920, 2846, 1651, 1599, 1574, 1511,

1445, 1327, 1273, 1153, 1027, 864, 798, 718; HRMS (m/z) [$M + H$]⁺ calcd for C₃₇H₃₀N₂O₂S₂, 599.1821; found 599.1815.

4.4.4. *1,2-Bis(2-methyl-5-phenoxybenzo[b]thiophen-3-yl)cyclopent-1-ene (16)*. Phenol (110 mg, 1.17 mmol) and *t*-BuOK (97 mg, 0.87 mmol) were stirred in warm dioxane (2.5 mL) in a Schott tube under argon atmosphere until a formation of a clear homogeneous solution. Then dibenzothienylethene **6** (150 mg, 0.29 mmol) and copper (I) iodide (55 mg, 0.29 mmol) were added followed by dioxane (1.5 mL) to wash all the solids from the walls of the tube. The reaction mixture was stirred at 135 °C for several days, with addition of the reagents and CuI as solids each time. TLC analysis showed no further progress of the reaction. When neither starting material nor monosubstituted intermediate could be detected by TLC analysis, the solvent was evaporated, and the residue was stirred in CHCl₃ / aqueous Na₂CO₃ system. After filtration of the two-layered mixture, the organic layer was evaporated and subjected to silica gel flash column chromatography (hexanes/ethyl acetate) to give 175 mg (82%) of white solid. High quality single crystals suitable for X-ray diffraction were grown by slow diffusion of either hexanes into the chloroform solution or MeOH into the acetone solution: mp 137-138 °C; ¹H NMR (300 MHz, CDCl₃) δ 1.95 (s, 3H), 2.18 (quin, 2H, *J* = 7.3 Hz), 2.19-2.37 (m, 3H), 2.63-2.82 (m, 2H), 2.90-3.09 (m, 2H), 6.63-6.80 (m, 2H), 6.82-6.94 (m, 4H), 6.97-7.10 (m, 2H), 7.17-7.36 (m, 6H), 7.45-7.63 (m, 2H); ¹³C NMR (75 MHz, CDCl₃) δ 15.1, 24.0, 37.5, 113.5, 116.7, 117.5, 122.4, 122.9, 129.6, 130.2, 133.6, 136.9, 138.0, 140.6, 153.5, 158.6; IR (KBr, cm⁻¹) ν 2960, 2840, 1588, 1562, 1488, 1445, 1259, 1227, 1136, 872, 749, 689; HRMS (m/z) [$M + H$]⁺ calcd for C₃₅H₂₈O₂S₂, 544.1525; found 544.1520.

4.5. Palladium (0) catalyzed amination of dibromide **6**

4.5.1. *3,3'-(Cyclopentene-1,2-diyl)bis(2-methyl-N-pentylbenzo[b]thiophen-5-amine) (17)*. Dibenzothienylethene **6** (150 mg, 0.29 mmol), tris(dibenzylideneacetone)dipalladium (0) (3 mg, 2 mol %), BINAP (10 mg, 6 mol %), sodium *t*-BuONa (167 mg, 1.74 mmol), and *n*-amylamine (101 mg, 1.16 mmol) were sequentially placed into a Schott tube under argon atmosphere. Toluene (2 mL) was then added washing all the solids from the walls of the tube. The reaction mixture was stirred at 85 °C for 7 h, after this time TLC analysis showed no starting material left in the reaction mixture. Ethyl acetate was added, and the formed suspension was filtered through a silica plug. After evaporation of the filtrate the residue was subjected to silica gel flash column chromatography (hexanes/ethyl acetate) to give 143 mg (93%) of white solid: mp 116-117 °C; ¹H NMR (300 MHz, CDCl₃) δ 0.92 (t, 6H, *J* = 6.7 Hz), 1.30-1.42 (m, 8H), 1.54-1.67 (m, 4H), 1.90-2.25 (broad s, 6H), 2.21 (quin, 2H, *J* = 7.1 Hz), 2.70-3.21 (m, 10H), 6.51-6.59 (m, 2H), 6.70-6.83 (m, 2H), 7.39 (d, 2H, *J* = 8.3 Hz); ¹³C NMR (75 MHz, CDCl₃) δ 14.0, 15.1, 22.6, 24.3, 29.3, 29.3, 37.5, 44.5, 104.8, 112.2, 122.0, 127.4, 129.9, 136.6, 136.7, 140.7, 145.7; IR (CCl₄, cm⁻¹) ν 2959, 2928, 2854, 1604, 1564, 1454, 1261, 1118, 1094, 1020, 932, 844; HRMS (m/z) [$M + H$]⁺ calcd for C₃₃H₄₂N₂S₂, 531.2862; found 531.2862.

4.5.2. *1,2-Bis(2-methyl-5-(pyrrolidin-1-yl)benzo[b]thiophen-3-yl)cyclopent-1-ene (18)*. Dibenzothienylethene **6** (150 mg, 0.29 mmol), tris(dibenzylideneacetone)dipalladium (0) (3 mg, 2 mol %), BINAP (10 mg, 6 mol %), *t*-BuONa (167 mg, 1.74 mmol), and pyrrolidine (92 mg, 1.3 mmol) were sequentially placed into a Schott tube under argon atmosphere. Toluene (2 mL) was then added washing all the solids from the walls of the tube. The reaction mixture was stirred at 85 °C for 7 h, after this time TLC analysis showed no starting material left in the reaction mixture. Ether and ethyl acetate were added, and the formed suspension

was filtered through an Al₂O₃ plug. After evaporation of the filtrate the residue was subjected to Al₂O₃ column chromatography (hexanes/ethyl acetate) to give 111 mg (77%) of air sensitive white solid. High quality single crystals suitable for X-ray diffraction were grown by slow diffusion of hexanes into the chloroform solution: mp 239-240 °C; ¹H NMR (300 MHz, CDCl₃) δ 1.84 (s, 6H), 2.00-2.10 (m, 5H), 2.19-2.34 (m, 5H), 2.61-2.73 (m, 1H), 2.84-2.95 (m, 3H), 3.02-3.19 (m, 4H), 3.29-3.46 (m, 4H), 6.50-6.82 (broad m, 4H), 7.37-7.51 (m, 2H); ¹³C NMR (75 MHz, CDCl₃) δ 15.2, 24.4, 25.3, 37.7, 48.1, 104.6, 110.5, 121.9, 126.0, 130.3, 136.2, 136.5, 140.7, 145.6; IR (KBr, cm⁻¹) ν 2960, 2886, 2823, 1602, 1453, 1367, 1307, 1153, 832, 792; HRMS (m/z) [$M + H$]⁺ calcd for C₃₁H₃₄N₂S₂, 499.2236; found 499.2224.

4.6. X-ray crystallography

X-ray diffraction data were collected on a APEX II DUO CCD diffractometer using molybdenum radiation [λ (MoK α) = 0.71072 Å, ω -scans] for **3**, **4**, **6**, **9**, **11**, **12**, **14**, **15**, **16** and using copper radiation [λ (CuK α) = 1.54178 Å, ω -scans] for **18** at 100K. The substantial redundancy in data allowed empirical absorption correction to be applied with SADABS by multiple measurements of equivalent reflections. The structures were solved by direct methods and refined by the full-matrix least-squares technique against F^2 in the anisotropic-isotropic approximation. In **4**, **6**, **11** and **14**, the local C₂ symmetry led to a significant anisotropy of displacement parameters of the atom C(3C), which in case of **11** resulted in its disorder by two positions with equal occupancies. In **11**, the analysis of the Fourier maps has also revealed a disorder of the oxygen atom of the C=O group by two positions with the occupancies 0.630(2) and 0.370(2); the positional and anisotropic displacement parameters of these two components were refined with the constraints on the C=O bond length (DFIX) and anisotropic displacement parameters (EADP). Hydrogen atoms in all structures were placed in calculated positions and refined within the riding model. All calculations were performed with the SHELXTL software package.⁴⁹ Crystal data and structure refinement parameters are listed in Table S1 (Supplementary data). Crystallographic data (excluding structure factors) for the structures reported in this paper have been deposited to the Cambridge Crystallographic Data Centre as supplementary no.: CCDC-997775 (for **3**), CCDC-997776 (for **4**), CCDC-997777 (for **6**), CCDC-997778 (for **9**), CCDC-997779 (for **11**), CCDC-997780 (for **12**), CCDC-997781 (for **14**), CCDC-997782 (for **15**), CCDC-997783 (for **16**), CCDC-997784 (for **18**). These data can be obtained free of charge from The Cambridge Crystallographic Data via www.ccdc.cam.ac.uk/data_request/cif.

Multipole refinement for **16** was performed within the Hansen-Coppens formalism,⁵⁰ with a total pseudostatic charge density distribution $\rho(\mathbf{r})$ calculated as a sum of pseudoatomic charge densities. The refinement in this study was done with XD2006 software.⁵¹ The multipole expansion was truncated at the hexadecapole level ($l = 4$) for heavy atoms and at the octupole level ($l = 3$) for C and O atoms. For hydrogen atoms, only the populations of monopoles and D₁₀ harmonics were refined. In each case, we used low-angle reflections with $\sin \theta/\lambda \leq 0.904 \text{ \AA}^{-1}$ to refine multipole parameters and high angle reflections with $\sin \theta/\lambda \geq 0.504 \text{ \AA}^{-1}$ to refine positions and anisotropic displacement parameters of heavy atoms. Multipole and monopole populations and corresponding κ coefficients in **16** were refined separately in the first steps of the refinement and together in the last steps. The overall quality of the experiment and the refinement was supported by analysis of differences of mean-squares displacement amplitudes (DMSDA) along

interatomic vectors in molecule; those values did not exceed $9 \times 10^{-4} \text{ \AA}^{-2}$. Electron density residuals were randomly distributed in the unit cell of **16** and didn't exceed 0.36 e \AA^{-3} . The refinement for **16** was carried out against F and converged to $R = 0.0305$, $R_w = 0.0248$ and $GOF = 1.52$ (for 22613 merged reflections with $I > 3\sigma(I)$). The estimation of the kinetic energy $g(\mathbf{r})$ was based on the Kirzhnits's approximation⁵² relating it to the values of the $\rho(\mathbf{r})$ and its derivatives: $g(\mathbf{r}) = (3/10)(3\pi^2)^{2/3} [\rho(\mathbf{r})]^{5/3} + (1/72)|\nabla\rho(\mathbf{r})|^2/\rho(\mathbf{r}) + 1/6\nabla^2\rho(\mathbf{r})$. The use of this relation in conjunction with the virial theorem ($2g(\mathbf{r}) + v(\mathbf{r}) = 1/4\nabla^2\rho(\mathbf{r})$) provided the value of the potential energy density $v(\mathbf{r})$ in a critical points from experimental diffraction data. For the critical point search in intermolecular areas, we have used the following procedure: 1) each atom has been surrounded by the cluster with the radii 6 Å and each contact with distance up to 4 Å has been analysed; 2) for all the critical points found, we have calculated bond paths to verify for what particular pair of atoms the interaction occurred. By means of this procedures, we have checked all interatomic interactions, and thus obtained the molecular graph for supramolecular organization. The topological analysis of the experimental $\rho(\mathbf{r})$ distribution and data visualization were performed with WinXPRO program suite.⁵³

Topological analysis of the theoretical $\rho(\mathbf{r})$ distribution, as well as integration of $\rho(\mathbf{r})$ and its derivatives over atomic basis, was performed with AIMAll⁵⁴ and AIM2002⁵⁵ software packages.

Acknowledgements

We thank Dr. Roman A. Kunetskiy for making microscope photos of crystals of **16**. Prof. K. A. Lyssenko also thanks Russian Science foundation (grant 14-13-00884) for financial support of structural studies.

Supplementary data

Supplementary data for this article can be found at ...

References and notes

- Irie, M. *Chem. Rev.* **2000**, *100*, 1685-1716.
- (a) Irie, M. In *Organic Photochromic and Thermochromic Compounds, Vol.1: Main Photochromic Families*; Crano, J. C., Gugliemetti, R. J., Eds.; N.Y.: Plenum Press, 1999; pp 207-221. (b) Bertarelli, C.; Bianco, A.; Castagna, R.; Pariani, G. *J. Photochem. Photobiol. C: Photochem. Rev.* **2011**, *12*, 106-125.
- (a) Natali, M.; Giordani, S. *Chem. Soc. Rev.* **2012**, *41*, 4010-4029. (b) Feringa, B. L. *Molecular Switches*; Wiley-VCH: Verlag, GmbH, 2001. (c) Kudernac, T.; Katsonis, N.; Browne, W. R.; Feringa, B. L. *J. Mater. Chem.* **2009**, *19*, 7168-7177. (d) Tian, H.; Feng, Y. *J. Mater. Chem.* **2008**, *18*, 1617-1622. (e) Zhang, J.; Wang, J.; Tian, H. *Mater. Horiz.* **2014**, *1*, 169-184. (f) Tian, H.; Yang, S. *Chem. Soc. Rev.* **2004**, *33*, 85-97.
- Irie, M. *Proc. Jpn. Acad., Ser. B* **2010**, *86*, 472-483.
- (a) Krayushkin, M. M.; Kalik, M. A. *Adv. Heterocycl. Chem.* **2011**, *103*, 1-59. (b) Tsujioka, T.; Irie, M. *J. Photochem. Photobiol. C: Photochem. Rev.* **2010**, *11*, 1-14.
- (a) Yun, C.; You, J.; Kim, J.; Huh, J.; Kim, E. *J. Photochem. Photobiol. C: Photochem. Rev.* **2009**, *10*, 111-129. (b) Wigglesworth, T. J.; Myles, A. J.; Branda N. R. *Eur. J. Org. Chem.* **2005**, 1233-1238. (c) Hu, H.; Zhu, M.; Meng, X.; Zhang, Z.; Wei, K.; Guo, Q. *J. Photochem. Photobiol. A: Chemistry* **2007**, *189*, 307-313.
- (a) Yamaguchi, T.; Fujita, Y.; Nakazumi, H.; Kobatake, S.; Irie, M. *Tetrahedron* **2004**, *60*, 9863-9869. (b) Pu, S.; Yang, T.; Xu, J.; Shen, L.; Li, G.; Xiao, Q.; Chen, B. *Tetrahedron* **2005**, *61*, 6623-6629. (c) Pu, S.; Liu, H.; Liu, G.; Chen, B.; Tong, Z. *Tetrahedron* **2014**, *70*, 852-858. (d) Ding, H.; Liu, G.; Pu, S.; Zheng, C. *Dyes and Pigments* **2014**, *103*, 82-88. (e) Kudernac, T.; Kobayashi, T.; Uyama, A.; Uchida, K.; Nakamura, S.; Feringa, B. L. *J. Phys. Chem. A* **2013**, *117*, 8222-8229. (f) Pu, S.; Zheng, C. Sun, Q.; Liu, G.; Fan, C. *Chem. Commun.* **2013**, *49*, 8036-8038. (g) Liu, G.; Pu, S.; Wang, R. *Org. Lett.* **2013**, *15*, 980-983. (h) Pu, S.; Tong, Z.; Liu, G.; Wang, R. *J. Mater. Chem. C* **2013**, *1*, 4726-4739. (i) Pu, S.; Ding, H.; Liu, G.; Zheng, C.; Xu, H. *J. Phys. Chem. C* **2014**, *118*, 7010-7017. (j) Liu, H.; Pu, S.; Liu, G.; Chen, B. *Dyes and Pigments* **2014**, *102*, 159-168.
- (a) Hermes, S.; Dassa, G.; Toso, G.; Bianco, A.; Bertarelli, C.; Zerbi G. *Tetrahedron Lett.* **2009**, *50*, 1614-1617. (b) Kobatake, S.; Irie, M. *Tetrahedron* **2003**, *59*, 8359-8364.
- Krayushkin, M. M.; Kalik, M. A.; Migulin, V. A. *Russ. Chem. Rev.* **2009**, *78*, 329-336.
- (a) De Jong, J. J. D.; Lucas, L.N.; Hania, R.; Pugzlys, A.; Kellogg, R. M.; Feringa, B. L.; Duppen, K.; van Esch, J. H. *Eur. J. Org. Chem.* **2003**, 1887-1893. (b) Hania, P.R.; Pugzlys, A.; Lucas, L.N.; De Jong, J. J. D.; Feringa, B. L.; van Esch, J. H.; Jonkman, H. T.; Duppen, K. *J. Phys. Chem. A* **2005**, *109*, 9437-9442. (c) Yamaguchi, T.; Hosaka, M.; Shinohara, K.; Ozeki, T.; Fukuda, M.; Takami, S.; Ishibashi, Y.; Asahi, T.; Morimoto, M. *J. Photochem. Photobiol. A: Chemistry* **2014**, *285*, 44-51.
- Lucas, L.N.; van Esch, J.; Kellogg, R. M.; Feringa, B. L. *Chem. Commun.* **1998**, 2313-2314.
- (a) Piao, X.; Zou, Y.; Wu, J.; Li, C.; Yi, T. *Org. Lett.* **2009**, *11*, 3818-3821. (b) Tian, H.; Qin, B.; Yao, R.; Zhao, X.; Yang, S. *Adv. Mater.* **2003**, *15*, 2104-2107. (c) Hou, L.; Zhang, X.; Pijper, T. C.; Browne, W. R.; Feringa, B. L. *J. Am. Chem. Soc.* **2014**, *136*, 910-913.
- (a) Zhang, J.; Jin, J.; Zou, L.; Tian, H. *Chem. Commun.* **2013**, 9926-9928. (b) Akazawa, M.; Uchida, K.; De Jong, J. J. D.; Areephong, J.; Stuart, M.; Caroli, G.; Browne, W. R.; Feringa, B. L. *Org. Biomol. Chem.* **2008**, *6*, 1544-1547. (c) Wang, S.; Shen, W.; Feng, Y.; Tian, H. *Chem. Commun.* **2006**, 1497-1499.
- (a) Kudernac, T.; van der Molen, S. J.; van Wees, B. J.; Feringa, B. L. *Chem. Commun.* **2006**, 3597-3599. (b) van der Molen, S. J.; Liao, J.; Kudernac, T.; Agustsson, J. S.; Bernard, L.; Calame, M.; van Wees, B. J.; Feringa, B. L.; Schonenberger, C. *Nano Lett.* **2009**, *9*, 76-80.
- Areephong, J.; Browne, W. R.; Feringa, B. L. *Org. Biomol. Chem.* **2007**, *5*, 1170-1174.
- Zou, Y.; Yi, T.; Xiao, S.; Li, C.; Gao, X.; Wu, J.; Yu, M.; Huang, C. *JACS* **2008**, *130*, 15750-15751.
- Babii, O.; Afonin, S.; Berditsch, M.; Reißer, S.; Mykhailiuk, P. K.; Kubyshkin, V. S.; Steinbrecher, T.; Ulrich, A. S.; Komarov, I. V. *Angew. Chem. Int. Ed.* **2014**, *53*, 3392-3395.

18. (a) Kawata, S.; Kawata, Y. *Chem. Rev.* **2000**, *100*, 1777-1788. (b) Jeong, Y.-C.; Yang, S. I.; Ahn, K.-H.; Kim, E. *Chem. Commun.* **2005**, 2503-2505. (c) Jeong, Y.-C.; Yang, S. I.; Kim, E.; Ahn, K.-H. *Tetrahedron* **2006**, *62*, 5855-5861. (d) Yokoyama, Y.; Hasegawa, T.; Ubukata, T. *Dyes and Pigments* **2011**, *89*, 223-229. (e) Frigoli, M.; Mehl, G. H. *Chem. Eur. J.* **2004**, *10*, 5243-5250.
19. Huang, Z.-N.; Xu, B.-A.; Jin, S.; Fan, M.-G. *Synthesis* **1998**, 1092-1094.
20. Krayushkin, M. M.; Migulin, V. A.; Yarovenko, V. N.; Barachevskii, V. A.; Vorontsova, L. G.; Starikova, Z. A.; Zavarzin, I. V.; Bulgakova, V. N. *Mendeleev Commun.* **2007**, *17*, 125-127.
21. (a) Dunaev, A. A.; Alfimov, M. V.; Barachevsky, V. A.; Vasnev, V. A.; Zavarzin, I. V.; Ivanov, S. N.; Keshtov, M. L.; Kovalev, A. I.; Krayushkin, M. M.; Pyankov, Yu. A.; Rusanov, A. L.; Strokach, Yu. P.; Yarovenko, V. N. Patent, WO 2006080647 (A1), August 3, 2006. (b) Krayushkin, M. M.; Yarovenko, V. N.; Khristoforova, L. V.; Shashkov, A. S.; Grebennikov, E. P.; Devyatkov, A. G.; Adamov, G. E.; Levchenko, K. S.; Shmelin, P. S.; Barachevskii, V. A.; Valova, T. M.; Kobeleva, O. I. *Russ. Chem. Bull., Int. Ed.* **2011**, *60*, 2536-2543.
22. Krayushkin, M. M.; Vorontsova, L. G.; Yarovenko, V. N.; Zavarzin, I. V.; Bulgakova, V. N.; Starikova, Z. A.; Barachevskii, V. A. *Russ. Chem. Bull., Int. Ed.* **2008**, *57*, 2402-2404.
23. Migulin, V. A.; Krayushkin, M. M.; Barachevskii, V. A.; Kobeleva, O. I.; Valova, T. M.; Lyssenko, K. A. *J. Org. Chem.* **2012**, *77*, 332-340.
24. (a) Krayushkin, M. M.; Migulin, V. A. Patent, RU 2421453 (C1), June 20, 2011. (b) Singer, M.; Jaschke, A. *J. Am. Chem. Soc.* **2010**, *132*, 8372-8377. (c) Zuckerman, N. B.; Kang, X.; Chen, S.; Konopelski, J. P. *Tetrahedron Lett.* **2013**, *54*, 1482-1485.
25. Szaloki, G.; Pozzo, J.-L. *Chem. Eur. J.* **2013**, *19*, 11124-11132.
26. Luyksaar, S. I.; Migulin, V. A.; Nabatov, B. V.; Krayushkin, M. M. *Russ. Chem. Bull., Int. Ed.*, **2010**, *59*, 446-451.
27. (a) Barrois, S.; Wagenknecht, H.-A. *Beilstein J. Org. Chem.* **2012**, *8*, 905-914. (b) Barrois, S.; Beyer, C.; Wagenknecht, H.-A. *Synlett* **2012**, 23, 711-716.
28. Klapars, A.; Buchwald, S. L. *J. Am. Chem. Soc.* **2002**, *124*, 14844-14845.
29. Zanon, J.; Klapars, A.; Buchwald, S. L. *J. Am. Chem. Soc.* **2003**, *125*, 2890-2891.
30. Klapars, A.; Huang, X.; Buchwald, S. L. *J. Am. Chem. Soc.* **2002**, *124*, 7421-7428.
31. Shafir, A.; Buchwald, S. L. *J. Am. Chem. Soc.* **2006**, *128*, 8742-8743.
32. Wolfe, J. P.; Buchwald, S. L. *J. Org. Chem.* **2000**, *65*, 1144-1157.
33. Fan, C.; Pu, S.; Liu, G.; Yang, T. *J. Photochem. Photobiol. A: Chemistry* **2008**, *197*, 415-425.
34. (a) Walko, M.; Feringa, B. L. *Chem. Commun.* **2007**, 1745-1747. (b) Yamaguchi, T.; Irie, M. *J. Photochem. Photobiol. A: Chemistry* **2006**, *178*, 162-169.
35. Perrin, C. L.; Dwyer, T. J. *Chem. Rev.* **1990**, *90*, 935-967.
36. Lazzeretti, P. *Prog. NMR Spectrosc.* **2000**, *36*, 1-88.
37. Reichardt, C.; Welton, T. *Solvents and Solvent Effects in Organic Chemistry, Fourth Edition*; Wiley-VCH Verlag GmbH & Co.; KGaA, Weinheim, Germany, 2010.
38. Lide, D. R., ed. *CRC Handbook of Chemistry and Physics*; 90th Edition (CD-ROM Version 2010), CRC Press/Taylor and Francis, Boca Raton, FL.
39. Nakamura, S.; Irie, M. *J. Org. Chem.* **1988**, *53*, 6136-6138.
40. Kobatake, S.; Uchida, K.; Tsuchida, E.; Irie, M. *Chem. Commun.* **2002**, 2804-2805.
41. Kobatake, S.; Yamada, M.; Yamada, T.; Irie, M. *J. Am. Chem. Soc.* **1999**, *121*, 8450-8456.
42. Bader, R. F. W. *Atoms in Molecules. A Quantum Theory*; Clarendon Press, Oxford, 1990.
43. (a) Dittrich, B.; Koritsanszky, T.; Volkov, A.; Mebs, S.; Luger, P. *Angew. Chem. Int. Ed.* **2007**, *46*, 2935-2938. (b) Nelyubina, Y. V.; Glukhov, I. V.; Antipin, M. Y.; Lyssenko, K. A. *Chem. Commun.* **2010**, *46*, 3469-3471.
44. Lyssenko, K. A. *Mendeleev Commun.* **2012**, *22*, 1-7.
45. Monteiro, N. K. V.; Firme, C. L. *J. Phys. Chem. A* **2014**, *118*, 1730-1740.
46. Marder, S. R.; Cheng, L.-T.; Tiemann, B. G.; Friedli, A. C.; Blanchard-Desce, M.; Perry, J. W.; Skindhoj, J. *Science* **1994**, *263*, 511-514.
47. (a) Espinosa, E.; Molins, E.; Lecomte, C.; *Chem. Phys. Lett.* **1998**, *285*, 170-173. (b) Espinosa, E.; Alkorta, I.; Rozas, I.; Elguero, J.; Molins, E.; *Chem. Phys. Lett.* **2001**, *336*, 457-461.
48. Belyakov, P. A.; Kadentsev, V. I.; Chizhov, A. O.; Kolotyrkina, N. G.; Shashkov, A. S.; Ananikov, V. P. *Mendeleev Commun.*, **2010**, *20*, 125-131.
49. Sheldrick, G. M. *Acta. Cryst.* **2008**, *A64*, 112-122.
50. Hansen, N. K.; Coppens, P. *Acta Cryst.* **1978**, *A34*, 909-921.
51. Volkov, A.; Macchi, P.; Farrugia, L. J.; Gatti, C.; Mallinson, P.; Richter, T.; Koritsanszky, T. XD2006 – A Computer Program Package for Multipole Refinement, Topological Analysis of Charge Densities and Evaluation of Intermolecular Energies from Experimental and Theoretical Structure Factors, 2006.
52. Kirzhnits, D. A. *Sov. Phys. JETP* **1957**, *5*, 64-71.
53. Stash, A.; Tsirelson, V. *J. Appl. Cryst.* **2002**, *35*, 371-373.
54. Keith, T. A. *AIMAll, Version 13.05.06*, 2013.
55. Biegler-Konig, F.; Schonbohm, J.; Bayles, D. *J. Comput. Chem.* **2001**, *22*, 545-559.

Synthesis and studies of symmetric dibenzothienylcyclopentenes

Vasily A. Migulin ^{a,*}, Michael M. Krayushkin ^a, Valery A. Barachevsky ^b, Olga I. Kobeleva ^b,
Valentin V. Novikov ^c, Konstantin A. Lyssenko ^c

^a *N. D. Zelinsky Institute of Organic Chemistry, Russian Academy of Sciences, Leninsky prospect, 47, 119991
Moscow, Russian Federation*

^b *Photochemistry Center, Russian Academy of Sciences, Novatorov Str., 7a, 119421 Moscow, Russian Federation*

^c *A. N. Nesmeyanov Institute of Organoelement Compounds, Russian Academy of Sciences, Vavilov Str., 28, 119991
Moscow, Russian Federation*

vmiguli@mail.ru

Table of Contents

1. Materials and methods.....	S2
2. Absorption spectra.....	S3
3. Photocoloration and photobleaching kinetic curves.....	S13
4. Photodegradation kinetic curves.....	S25
5. ¹ H and ¹³ C NMR spectra.....	S35
6. X-ray crystallography and computational data.....	S54
7. References.....	S64

* Corresponding author. Tel.: +7-916-319-9665; fax: +7-499-135-5328; e-mail: vmiguli@mail.ru

1. Materials and methods.

NMR spectra were obtained at 300 MHz for ^1H NMR and at 75 MHz for ^{13}C NMR with chemical shift values in the spectra being referenced to the solvent. Temperature dependant ^1H NMR spectra were recorded using Bruker Avance 600 spectrometer (working frequency 600.13 MHz). Variable temperature unit was calibrated using ethylene glycol and methanol samples for high and low temperature, respectively. The measurements were done using deuterated solvent's residual signal as an internal reference. Spectral and kinetic studies were conducted with «Cary 50 bio» (Varian) spectrophotometer using a quartz cell with a path length of 0.2 cm. Irradiation was performed by Hamamatsu LC-4 spot light source equipped with either light filters UFS-1 (240-400 nm) for photocoloration (with irradiance $I = 14 \text{ mW/cm}^2$) or ZHS-16 (460-2800 nm) for photobleaching (with irradiance $I = 190 \text{ mW/cm}^2$) processes; no filter was used for photodegradation studies. Concentration of the photochromic compounds in solution was $C = 2 \times 10^{-4} \text{ M}$. Toluene and acetonitrile from «Aldrich» were used as solvents. Polymer films and solid-phase films were prepared by casting method on quartz plates with an estimated thickness of the formed film being 100-150 μm . Preparation of a polymer included addition of 100 mg of polymethyl methacrylate (PMMA) to the solution of 0.5 mg of the corresponding dibenzothienylcyclopentene in chloroform (1 mL). Solid-phase films were prepared from solutions of dibenzothienylcyclopentenones in toluene ($C = 2 \times 10^{-3} \text{ M}$).

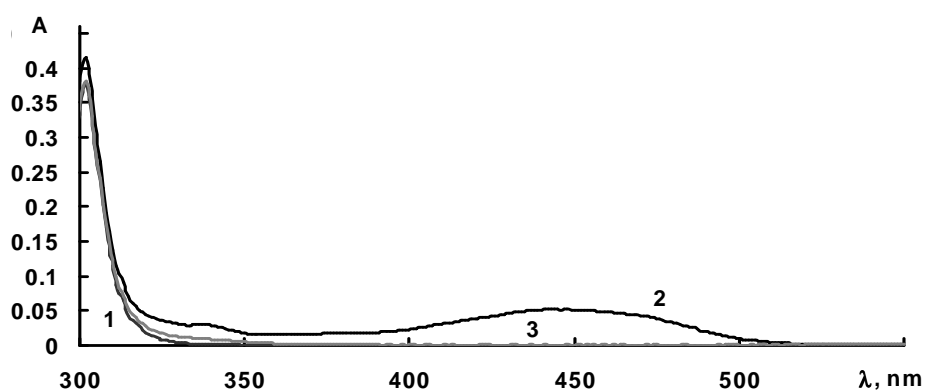
2. Absorption spectra.

FIGURE S1. Absorption spectra of dibenzothienylethene **3** in toluene before (1) and after (2) UV irradiation, and after visible light irradiation (3).

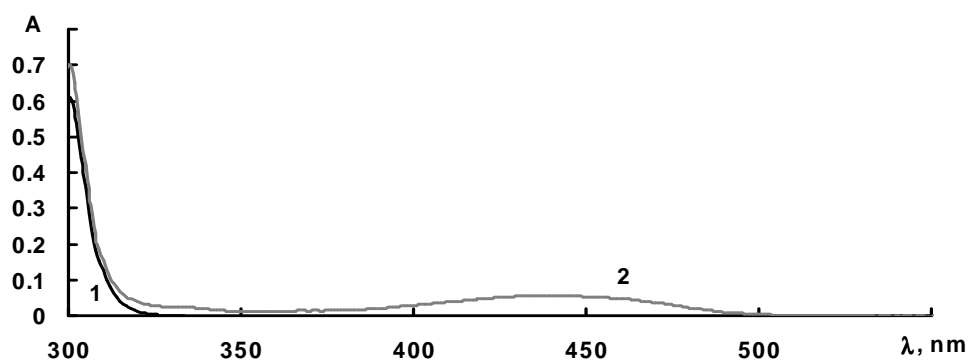


FIGURE S2. Absorption spectra of dibenzothienylethene **3** in acetonitrile before (1) and after (2) UV irradiation.

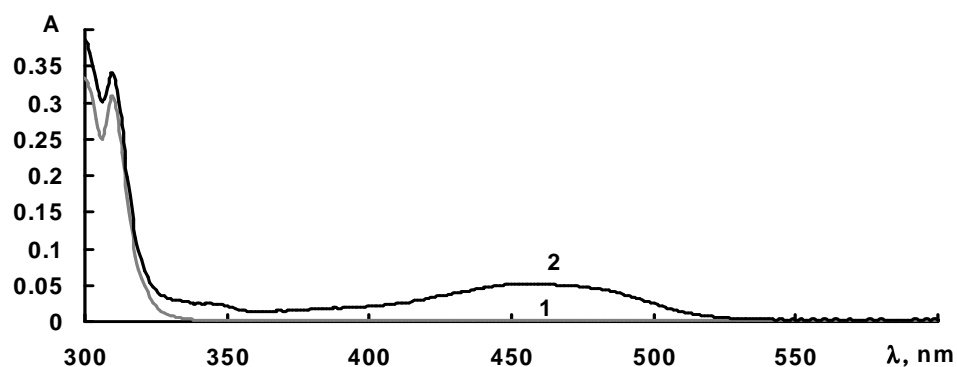


FIGURE S3. Absorption spectra of dibenzothienylethene **4** in toluene before (1) and after (2) UV irradiation.

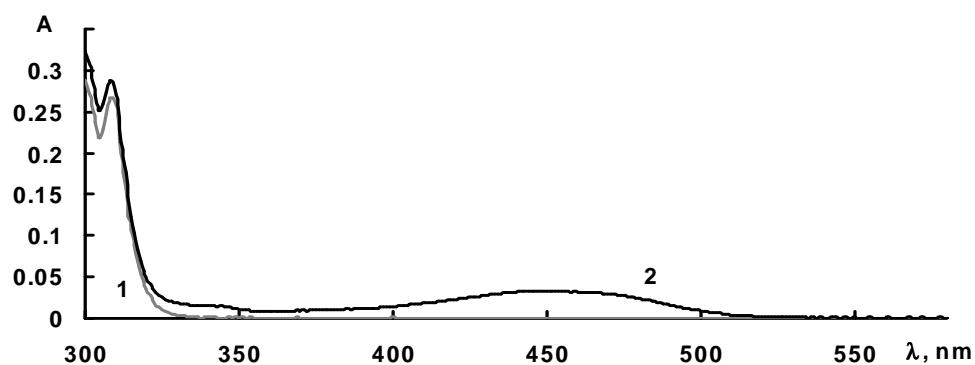


FIGURE S4. Absorption spectra of dibenzothienylethene **4** in acetonitrile before (1) and after (2) UV irradiation.

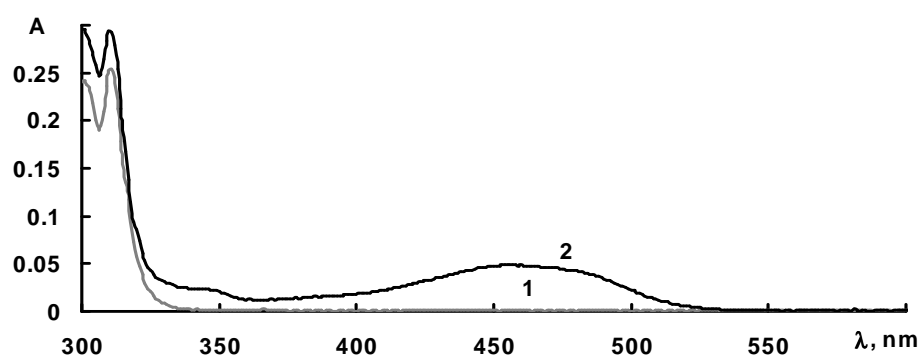


FIGURE S5 Absorption spectra of dibenzothienylethene **6** in toluene before (1) and after (2) UV irradiation.

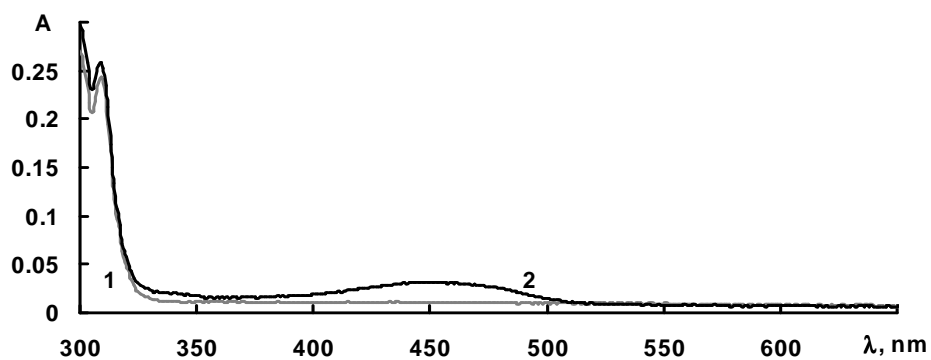


FIGURE S6. Absorption spectra of dibenzothienylethene **6** in acetonitrile before (1) and after (2) UV irradiation.

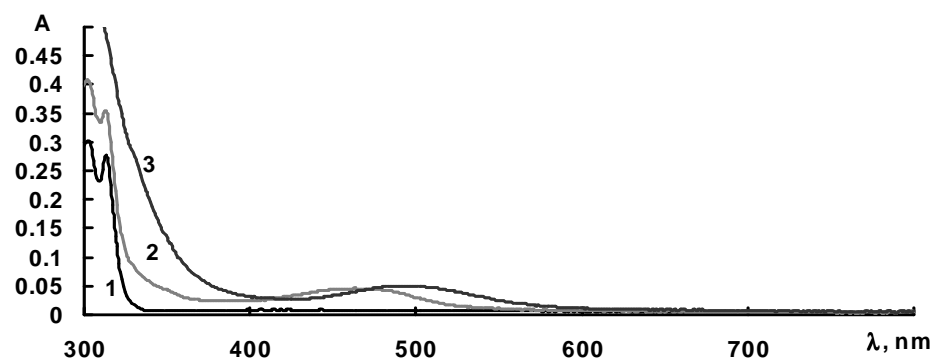


FIGURE S7. Absorption spectra of dibenzothienylethene **9** in toluene before (1) and after short (2) and long (3) exposition to UV irradiation.

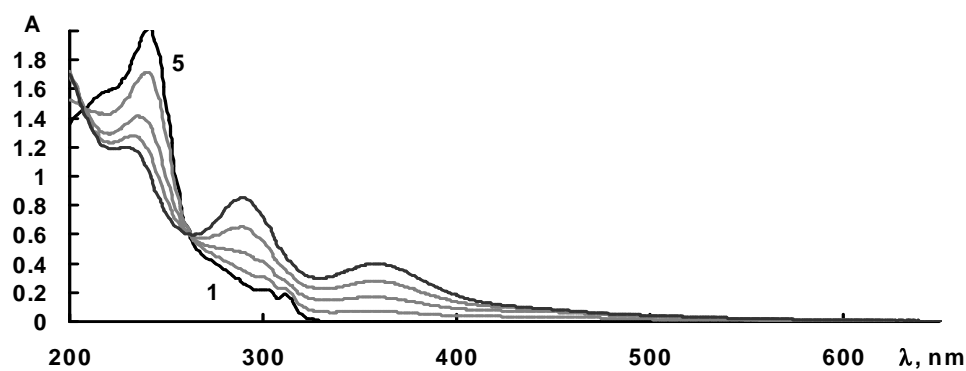


FIGURE S8. Absorption spectra of dibenzothienylethene **9** in acetonitrile before (1) and after (2-5) UV irradiation.

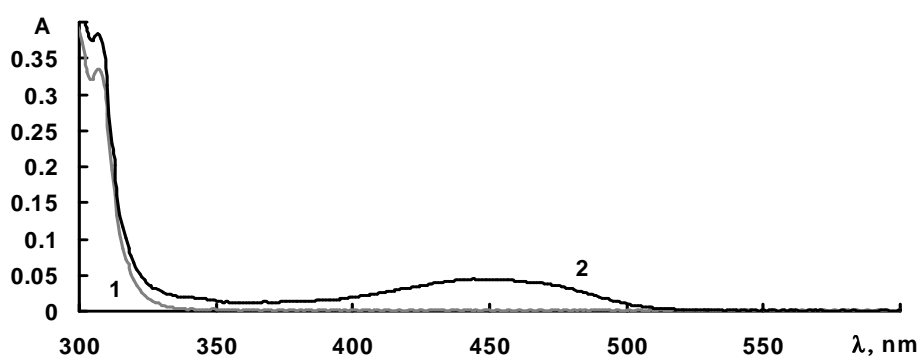


FIGURE S9. Absorption spectra of dibenzothienylethene **10** in toluene before (1) and after (2) UV irradiation.

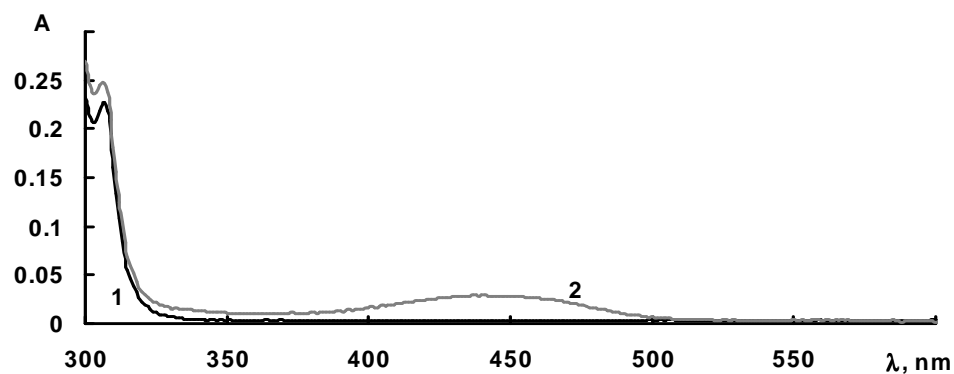


FIGURE S10. Absorption spectra of dibenzothienylethene **10** in acetonitrile before (1) and after (2) UV irradiation.

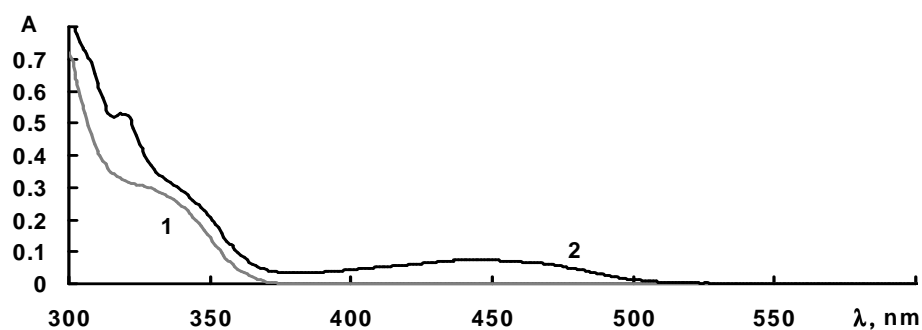


FIGURE S11. Absorption spectra of dibenzothienylethene **11** in toluene before (1) and after (2) UV irradiation.

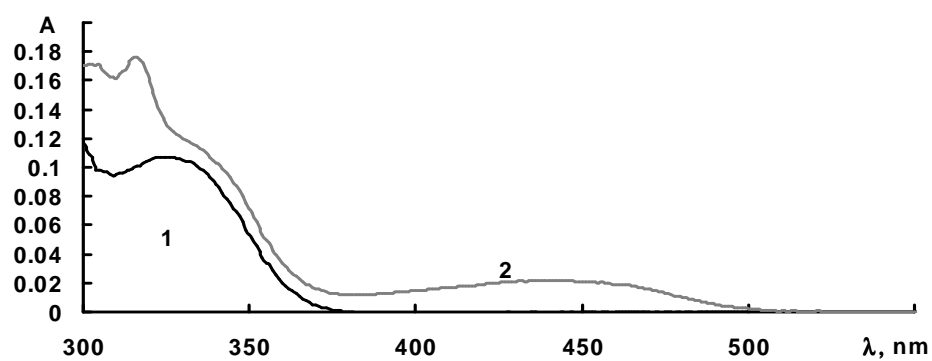


FIGURE S12. Absorption spectra of dibenzothienylethene **11** in acetonitrile before (1) and after (2) UV irradiation.

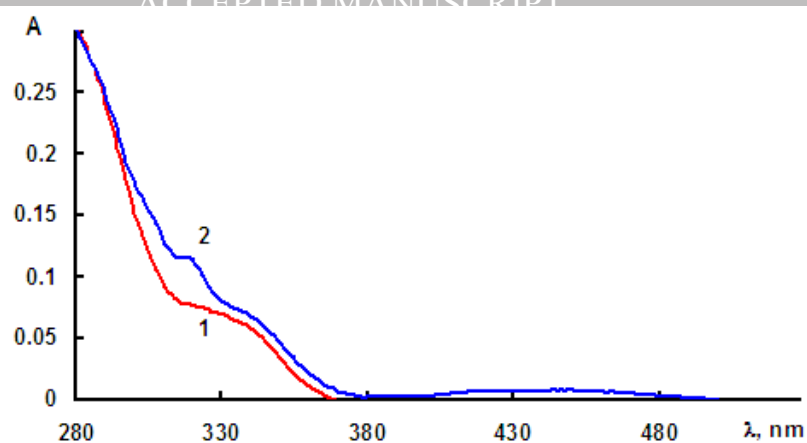


FIGURE S13. Absorption spectra of dibenzothienylethene **11** in PMMA film before (1) and after (2) UV irradiation.

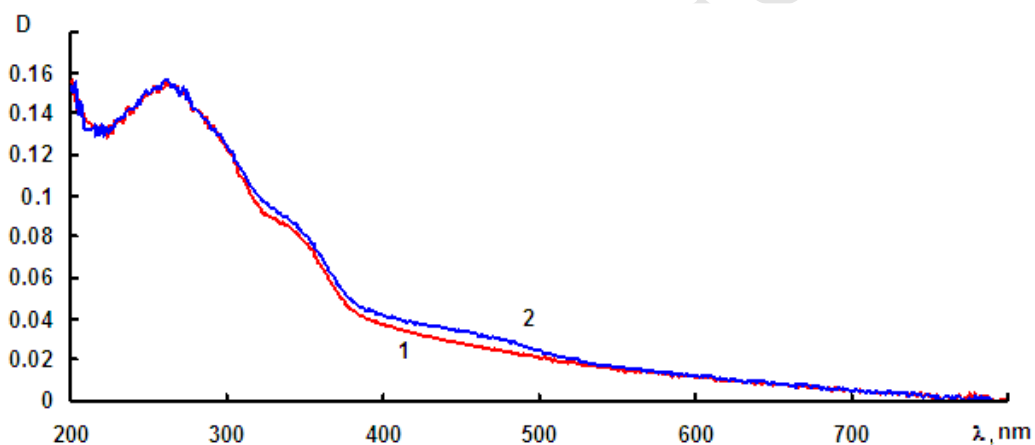


FIGURE S14. Absorption spectra of dibenzothienylethene **11** in solid-phase film before (1) and after (2) UV irradiation.

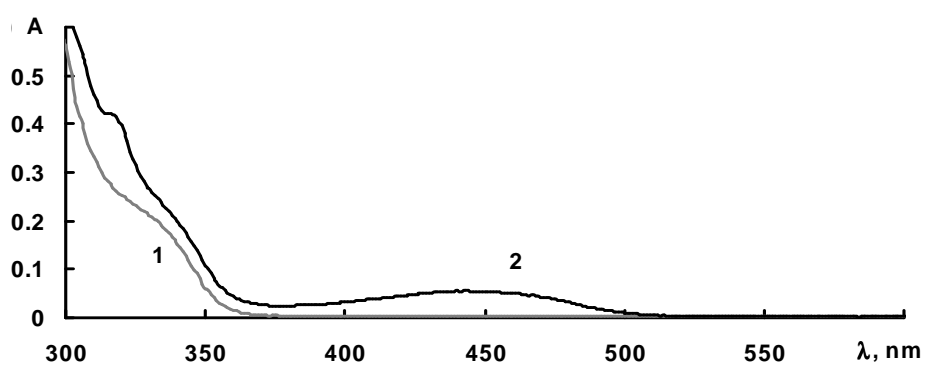


FIGURE S15. Absorption spectra of dibenzothienylethene **12** in toluene before (1) and after (2) UV irradiation.

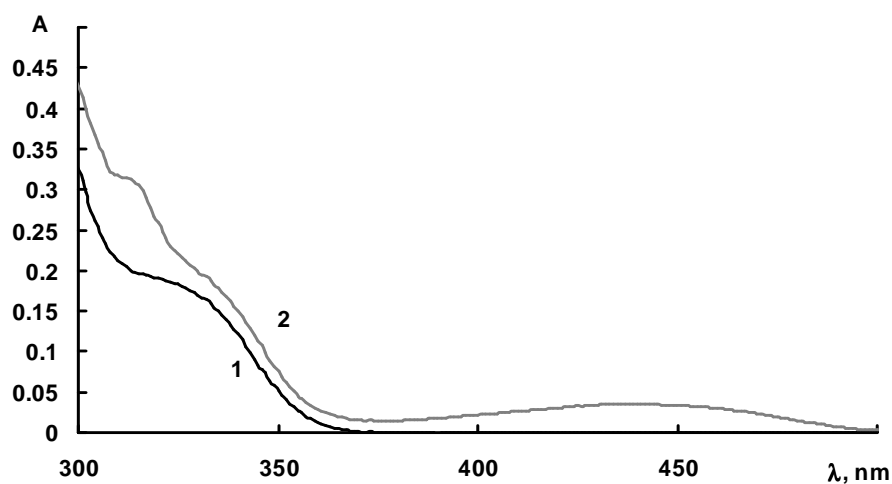


FIGURE S16. Absorption spectra of dibenzothienylethene **12** in acetonitrile before (1) and after (2) UV irradiation.

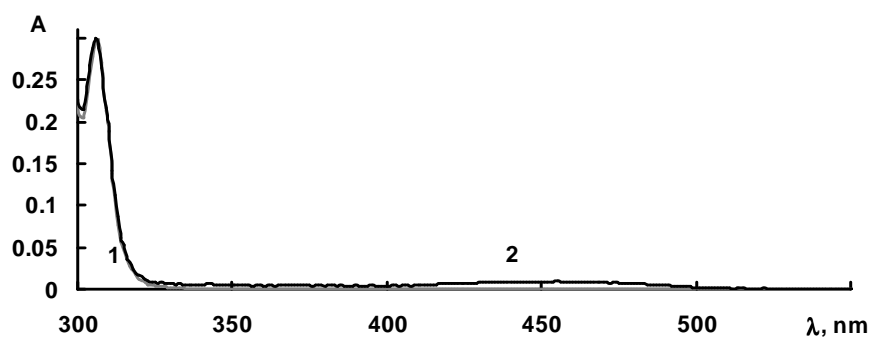


FIGURE S17. Absorption spectra of dibenzothienylethene **13** in toluene before (1) and after (2) UV irradiation.

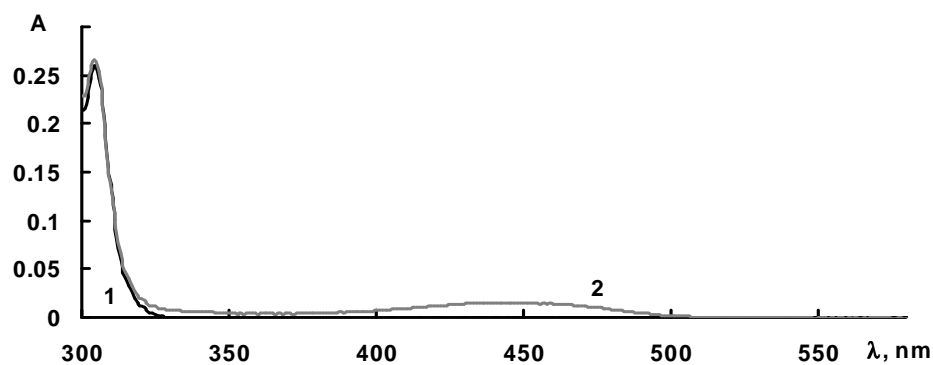


FIGURE S18. Absorption spectra of dibenzothienylethene **13** in acetonitrile before (1) and after (2) UV irradiation.

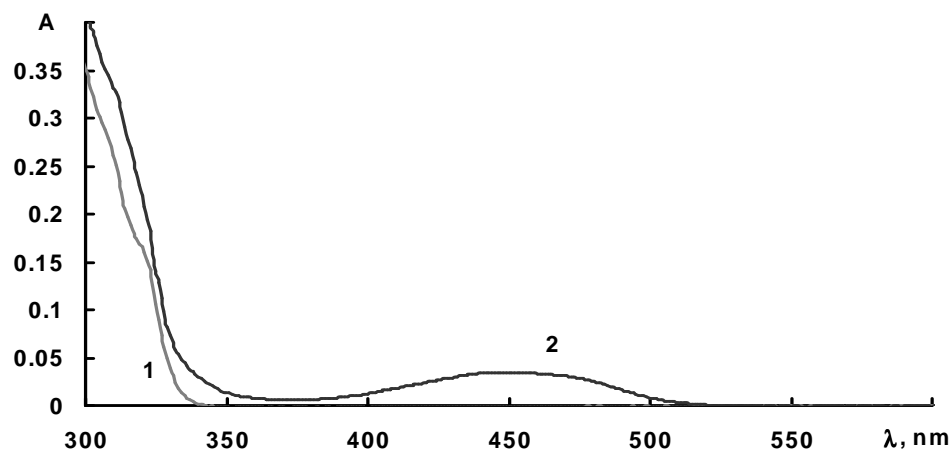


FIGURE S19. Absorption spectra of dibenzothienylethene **14** in toluene before (1) and after (2) UV irradiation.

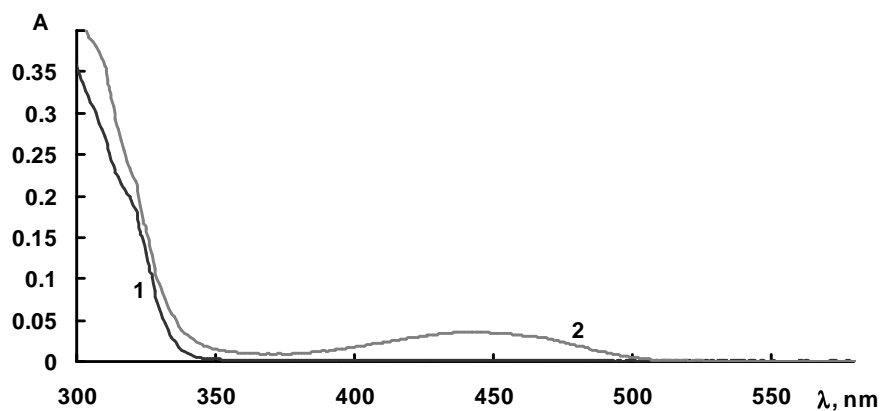


FIGURE S20. Absorption spectra of dibenzothienylethene **14** in acetonitrile before (1) and after (2) UV irradiation.

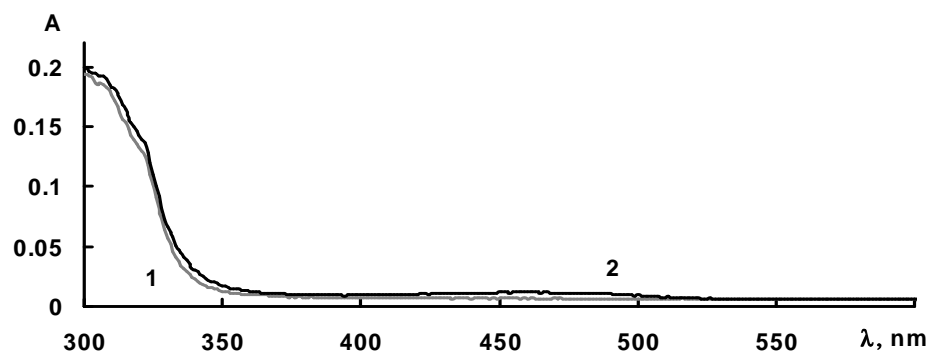


FIGURE S21. Absorption spectra of dibenzothienylethene **15** in toluene before (1) and after (2) UV irradiation.

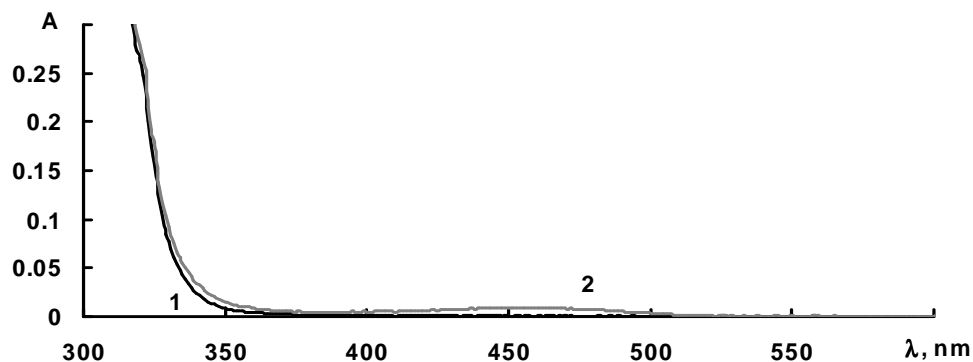


FIGURE S22. Absorption spectra of dibenzothienylethene **15** in acetonitrile before (1) and after (2) UV irradiation.

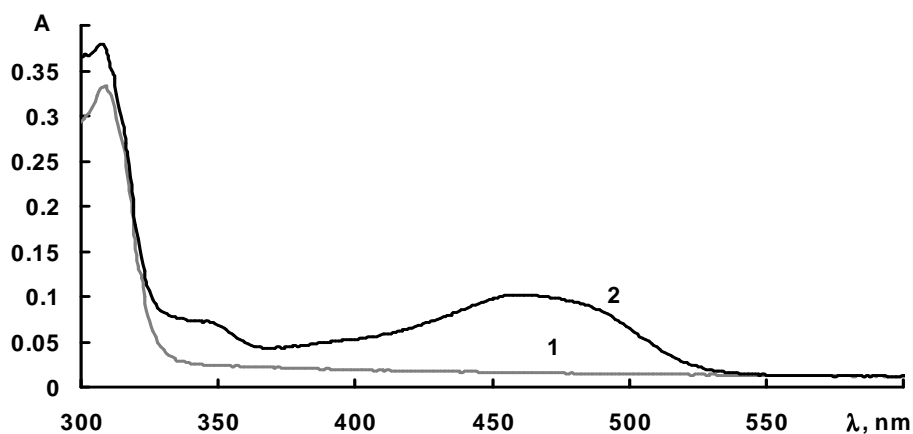


FIGURE S23. Absorption spectra of dibenzothienylethene **16** in toluene before (1) and after (2) UV irradiation.

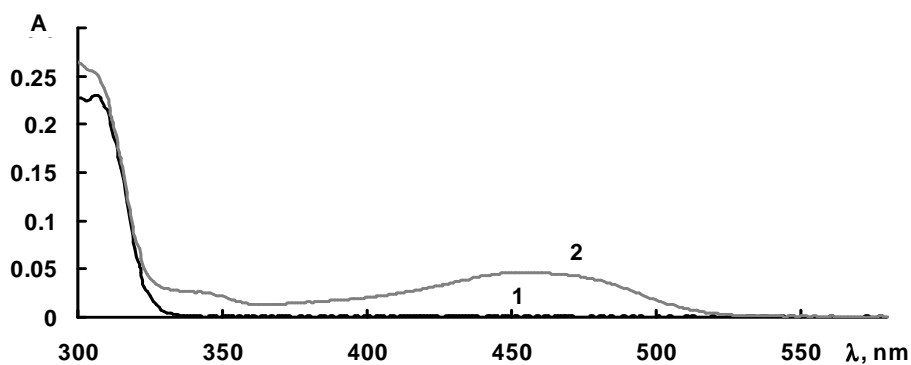


FIGURE S24. Absorption spectra of dibenzothienylethene **16** in acetonitrile before (1) and after (2) UV irradiation.

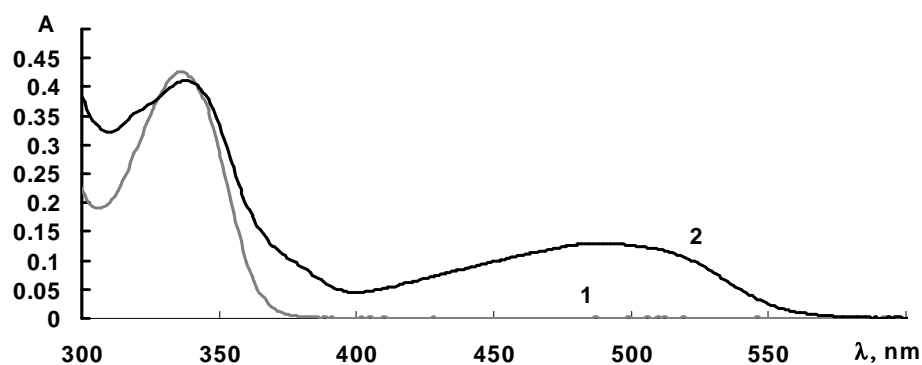


FIGURE S25. Absorption spectra of dibenzothienylethene **17** in toluene before (1) and after (2) UV irradiation.

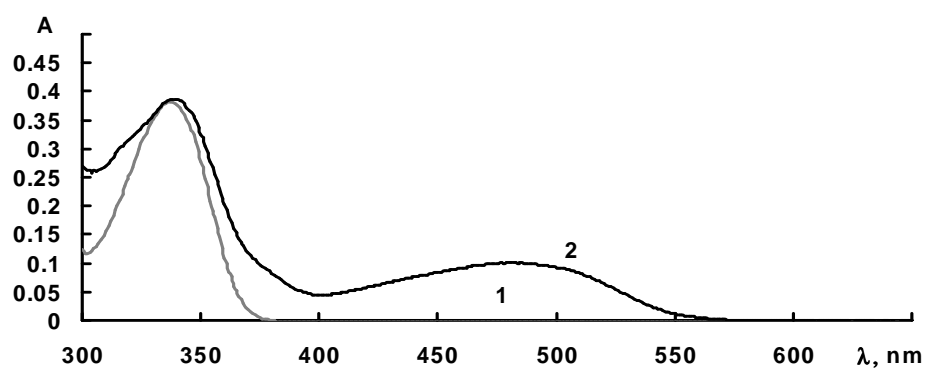


FIGURE S26. Absorption spectra of dibenzothienylethene **17** in acetonitrile before (1) and after (2) UV irradiation.

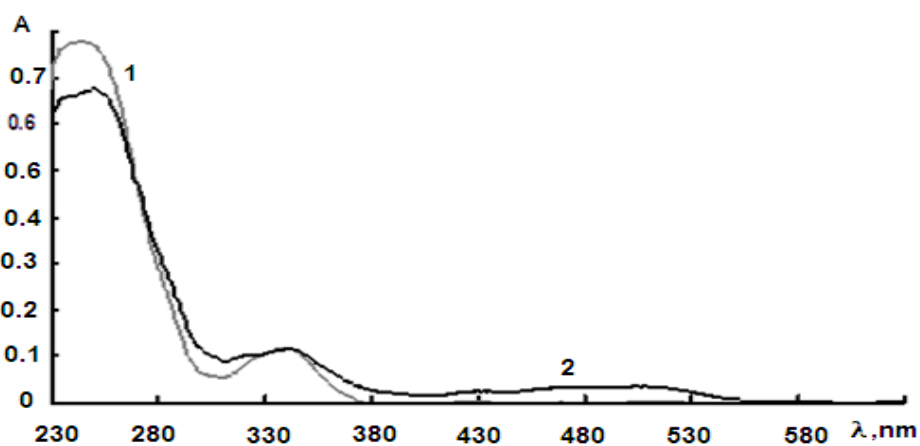


FIGURE S27. Absorption spectra of dibenzothienylethene **17** in PMMA film before (1) and after (2) UV irradiation.

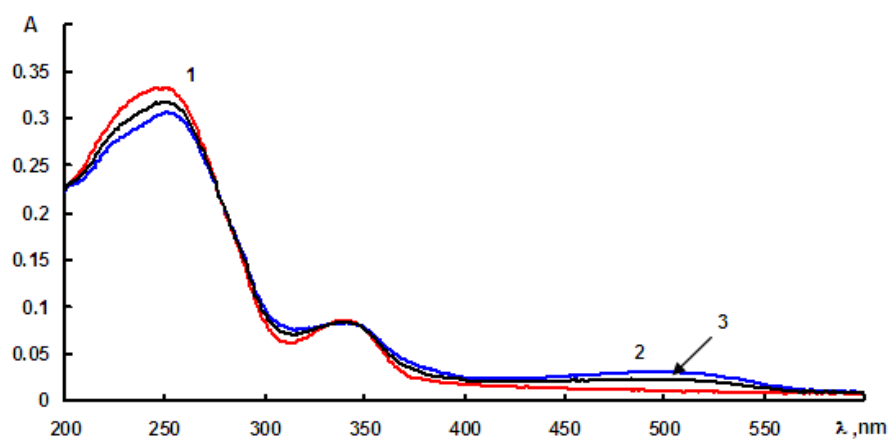


FIGURE S28. Absorption spectra of dibenzothienylethene **17** in solid-phase film before (1) and after (2) UV irradiation.

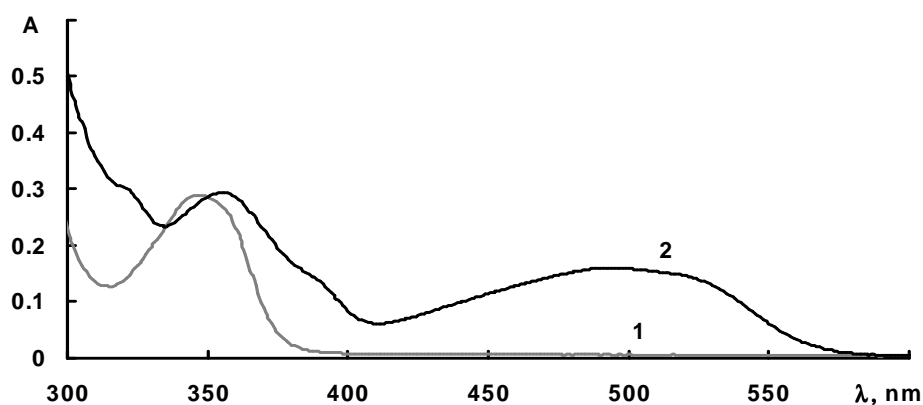


FIGURE S29. Absorption spectra of dibenzothienylethene **18** in toluene before (1) and after (2) UV irradiation.

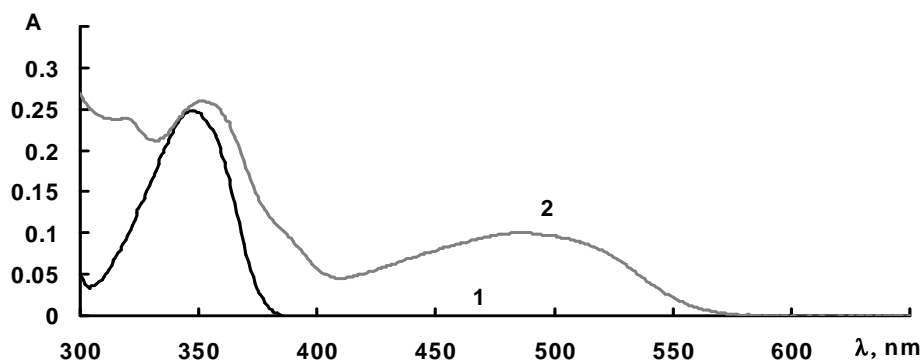


FIGURE S30. Absorption spectra of dibenzothienylethene **18** in acetonitrile before (1) and after (2) UV irradiation.

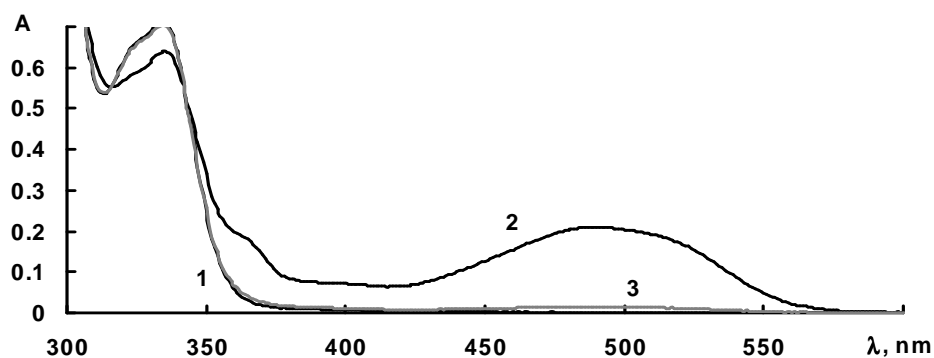


FIGURE S31. Absorption spectra of dibenzothienylethene **5** ($R = \text{COMe}$) in toluene before (1) and after (2) UV irradiation, and after visible light irradiation (3).

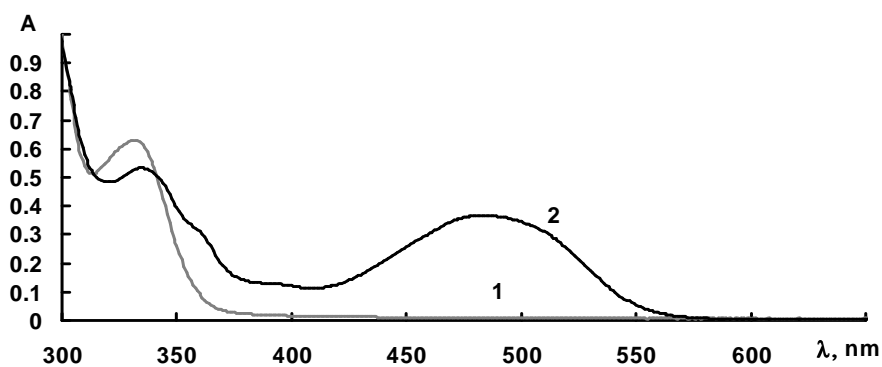


FIGURE S32. Absorption spectra of dibenzothienylethene **5** ($R = \text{COMe}$) in acetonitrile before (1) and after (2) UV irradiation.

3. Photocoloration and photobleaching kinetic curves.

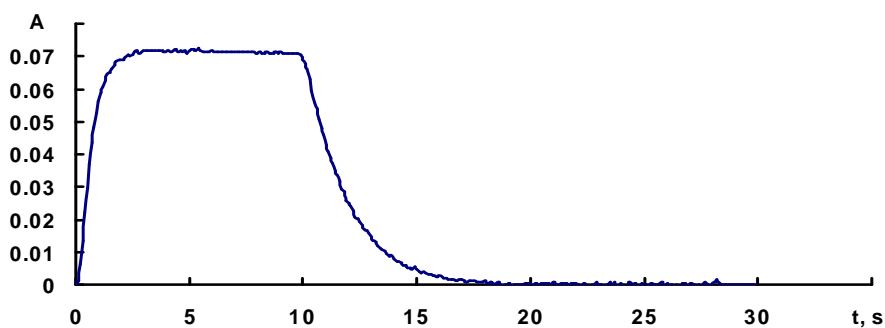


FIGURE S33. Kinetic curve for dibenzothienylethene **3** in toluene for processes of photocoloration under UV irradiation and photobleaching under visible light registered at 445 nm.

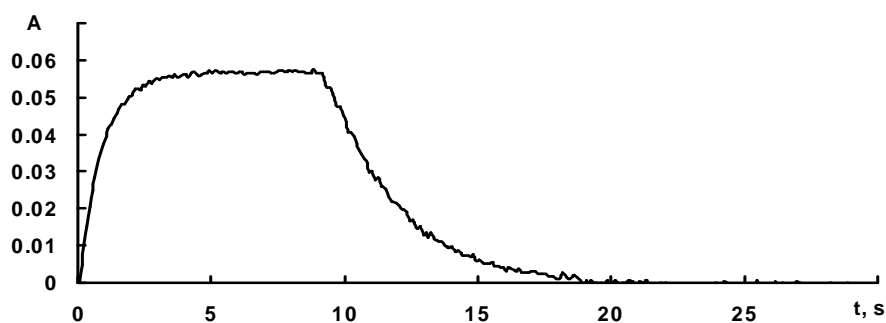


FIGURE S34. Kinetic curve for dibenzothienylethene **3** in acetonitrile for processes of photocoloration under UV irradiation and photobleaching under visible light registered at 440 nm.

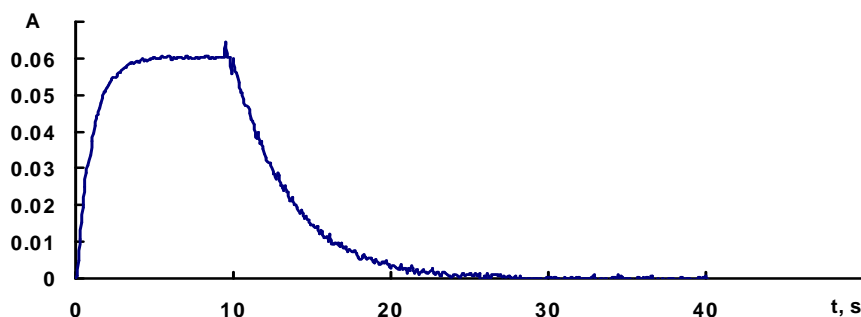


FIGURE S35. Kinetic curve for dibenzothienylethene **4** in toluene for processes of photocoloration under UV irradiation and photobleaching under visible light registered at 455 nm.

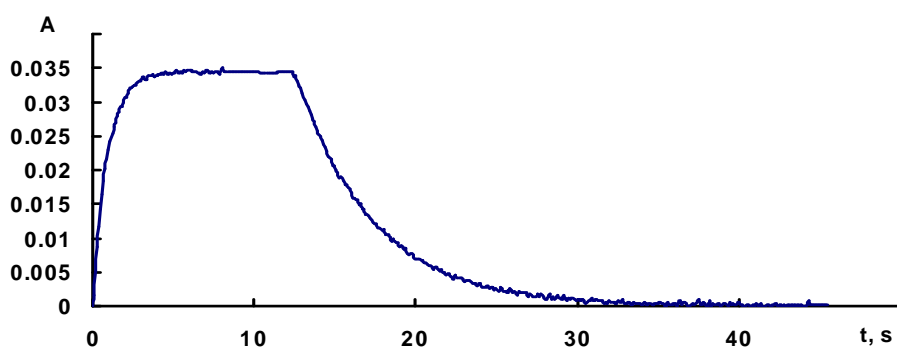


FIGURE S36. Kinetic curve for dibenzothienylethene **4** in acetonitrile for processes of photocoloration under UV irradiation and photobleaching under visible light registered at 450 nm.

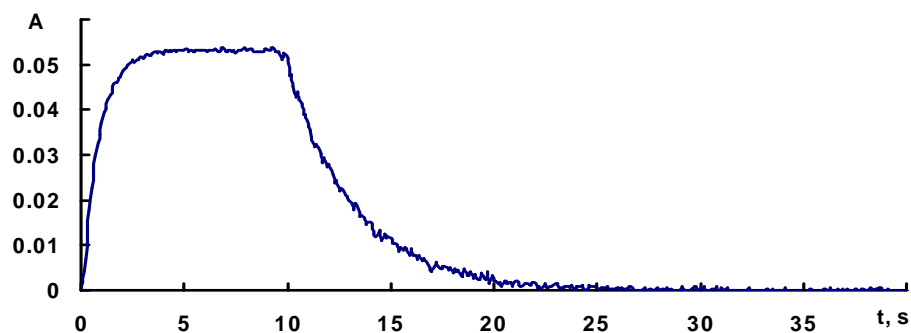


FIGURE S37. Kinetic curve for dibenzothienylethene **6** in toluene for processes of photocoloration under UV irradiation and photobleaching under visible light registered at 460 nm.

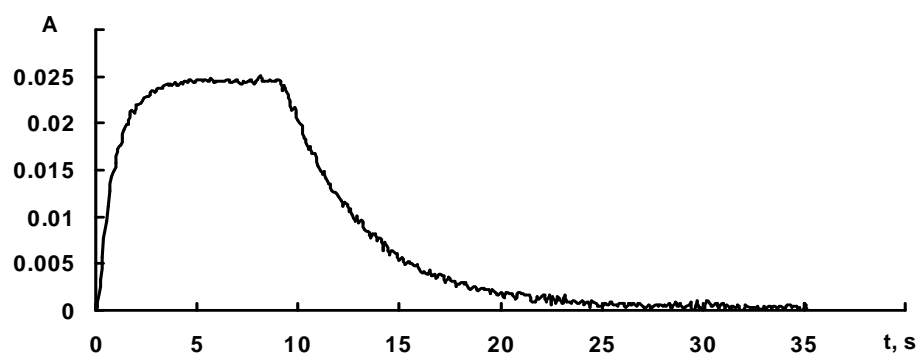


FIGURE S38. Kinetic curve for dibenzothienylethene **6** in acetonitrile for processes of photocoloration under UV irradiation and photobleaching under visible light registered at 450 nm.

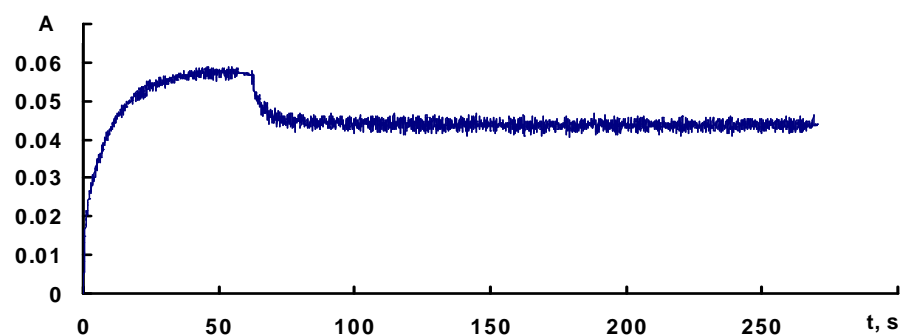


FIGURE S39. Kinetic curve for dibenzothienylethene **9** in toluene for processes of photocoloration under UV irradiation and photobleaching under visible light registered at 460 nm.

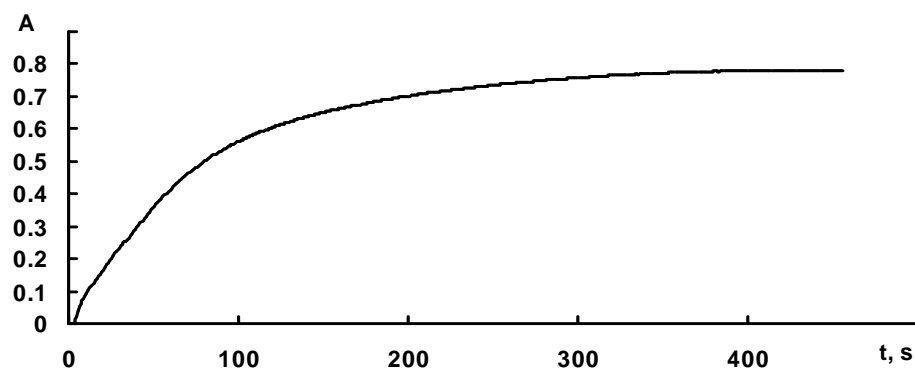


FIGURE S40. Kinetic curve for dibenzothienylethene **9** in acetonitrile for the process of photocoloration under UV irradiation registered at 360 nm.

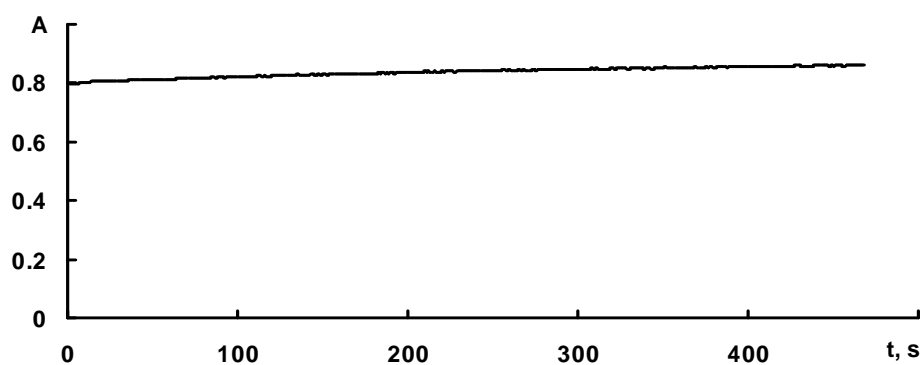


FIGURE S41. Kinetic curve for dibenzothienylethene **9** in acetonitrile for the process of photobleaching under visible light registered at 360 nm.



FIGURE S42. Kinetic curve for dibenzothienylethene **10** in toluene for processes of photocoloration under UV irradiation and photobleaching under visible light registered at 445 nm.

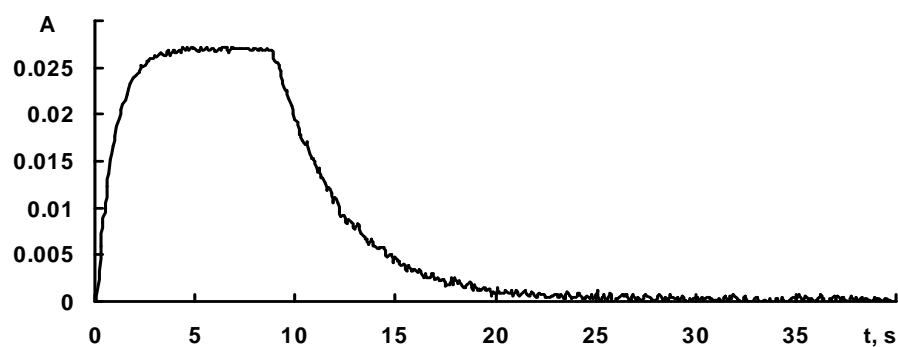


FIGURE S43. Kinetic curve for dibenzothienylethene **10** in acetonitrile for processes of photocoloration under UV irradiation and photobleaching under visible light registered at 440 nm.

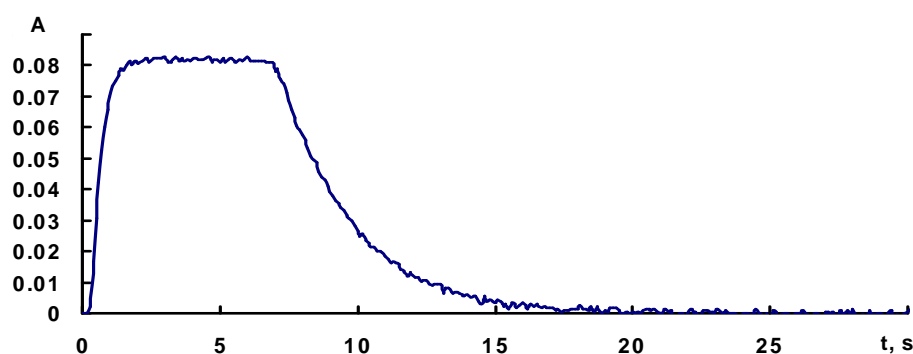


FIGURE S44. Kinetic curve for dibenzothienylethene **11** in toluene for processes of photocoloration under UV irradiation and photobleaching under visible light registered at 445 nm.

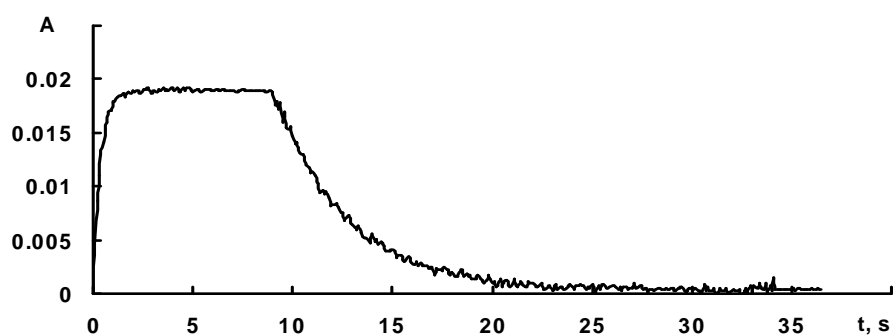


FIGURE S45. Kinetic curve for dibenzothienylethene **11** in acetonitrile for processes of photocoloration under UV irradiation and photobleaching under visible light registered at 440 nm.

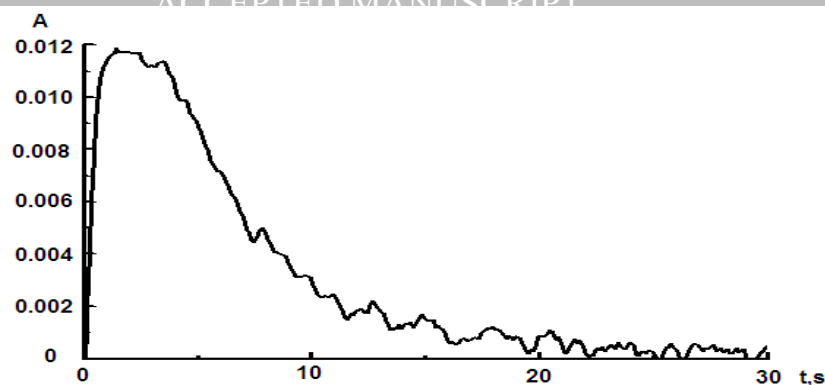


FIGURE S46. Kinetic curve for dibenzothienylethene **11** in PMMA film for processes of photocoloration under UV irradiation and photobleaching under visible light registered at 440 nm.



FIGURE S47. Kinetic curve for dibenzothienylethene **12** in toluene for processes of photocoloration under UV irradiation and photobleaching under visible light registered at 445 nm.

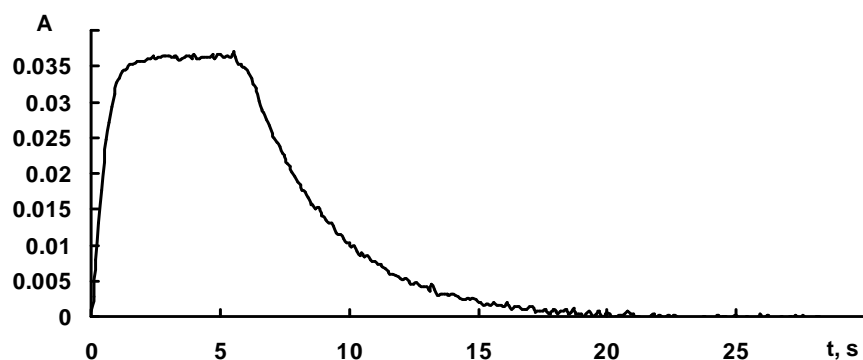


FIGURE S48. Kinetic curve for dibenzothienylethene **12** in acetonitrile for processes of photocoloration under UV irradiation and photobleaching under visible light registered at 440 nm.

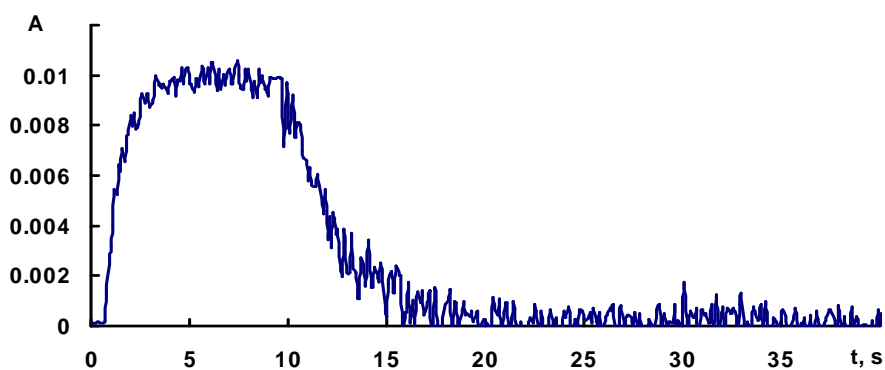


FIGURE S49. Kinetic curve for dibenzothienylethene **13** in toluene for processes of photocoloration under UV irradiation and photobleaching under visible light registered at 450 nm.



FIGURE S50. Kinetic curve for dibenzothienylethene **13** in acetonitrile for processes of photocoloration under UV irradiation and photobleaching under visible light registered at 445 nm.

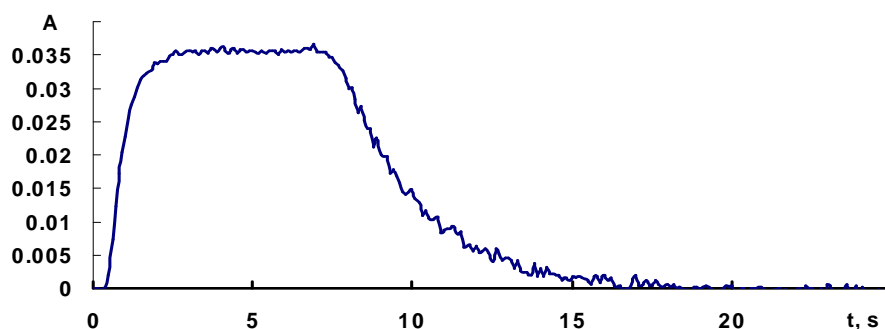


FIGURE S51. Kinetic curve for dibenzothienylethene **14** in toluene for processes of photocoloration under UV irradiation and photobleaching under visible light registered at 450 nm.

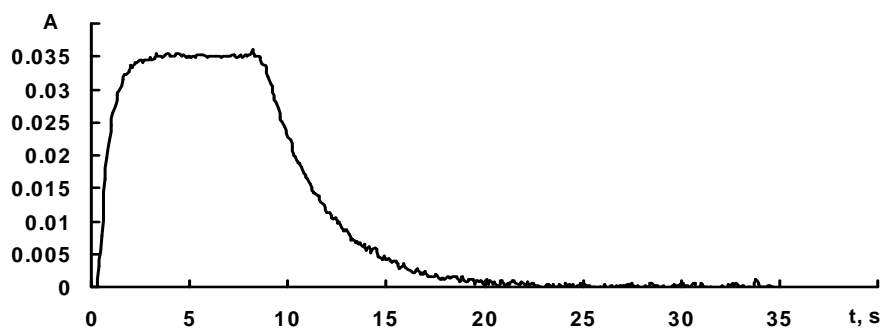


FIGURE S52. Kinetic curve for dibenzothienylethene **14** in acetonitrile for processes of photocoloration under UV irradiation and photobleaching under visible light registered at 445 nm.

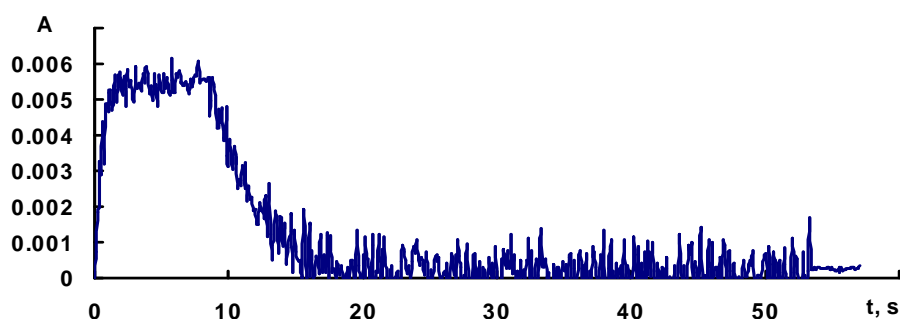


FIGURE S53. Kinetic curve for dibenzothienylethene **15** in toluene for processes of photocoloration under UV irradiation and photobleaching under visible light registered at 460 nm.

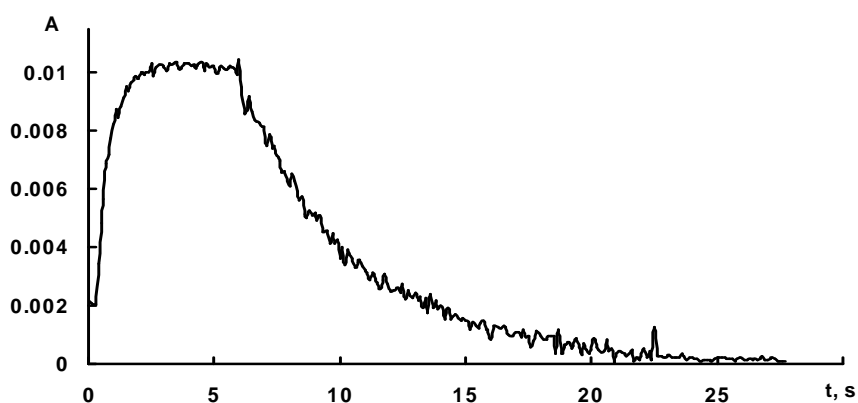


FIGURE S54. Kinetic curve for dibenzothienylethene **15** in acetonitrile for processes of photocoloration under UV irradiation and photobleaching under visible light registered at 460 nm.

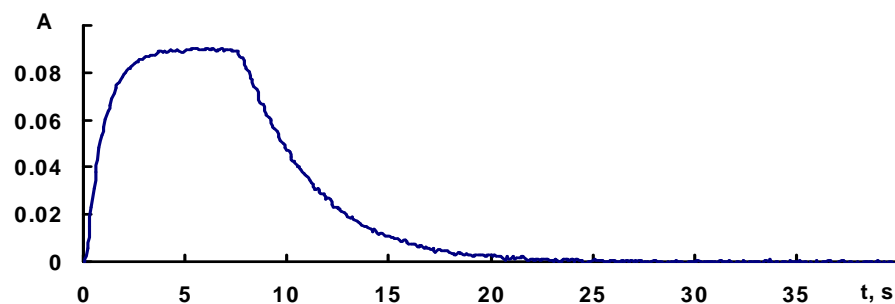


FIGURE S55. Kinetic curve for dibenzothienylethene **16** in toluene for processes of photocoloration under UV irradiation and photobleaching under visible light registered at 460 nm.

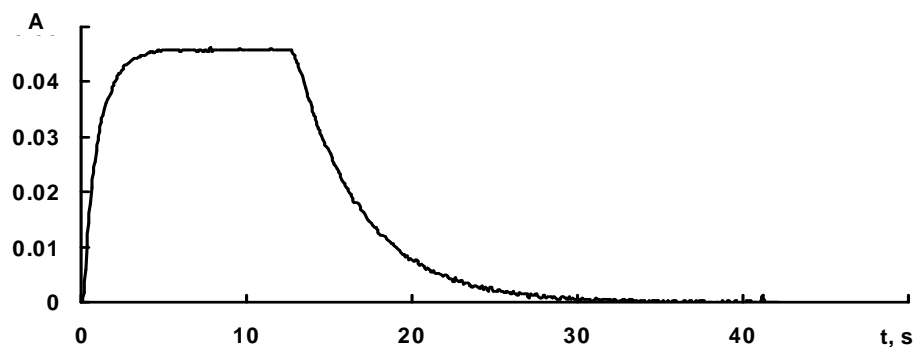


FIGURE S56. Kinetic curve for dibenzothienylethene **16** in acetonitrile for processes of photocoloration under UV irradiation and photobleaching under visible light registered at 460 nm.

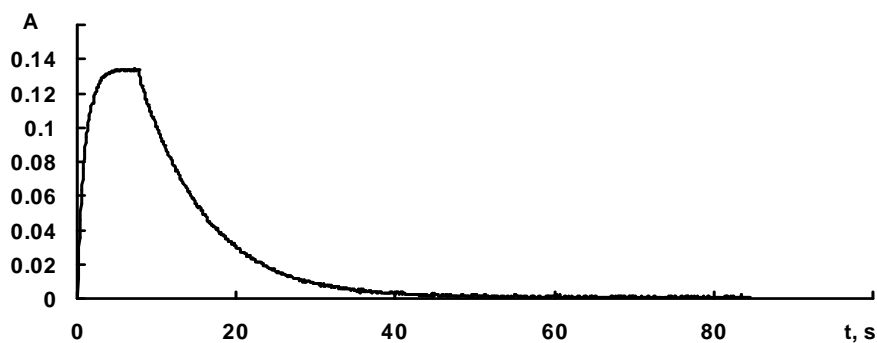


FIGURE S57. Kinetic curve for dibenzothienylethene **17** in toluene for processes of photocoloration under UV irradiation and photobleaching under visible light registered at 490 nm.

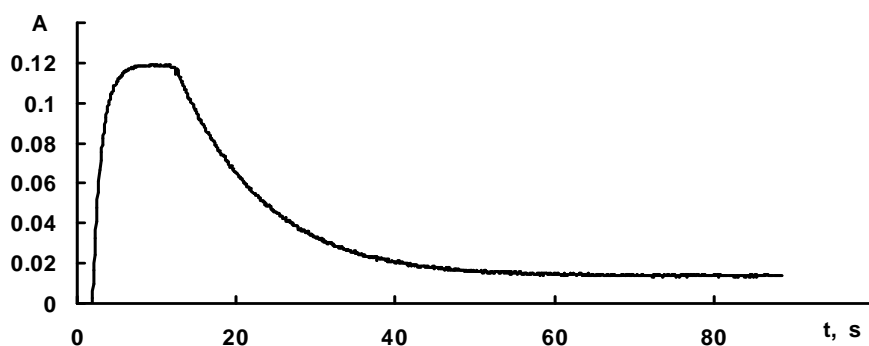


FIGURE S58. Kinetic curve for dibenzothienylethene **17** in acetonitrile for processes of photocoloration under UV irradiation and photobleaching under visible light registered at 480 nm.

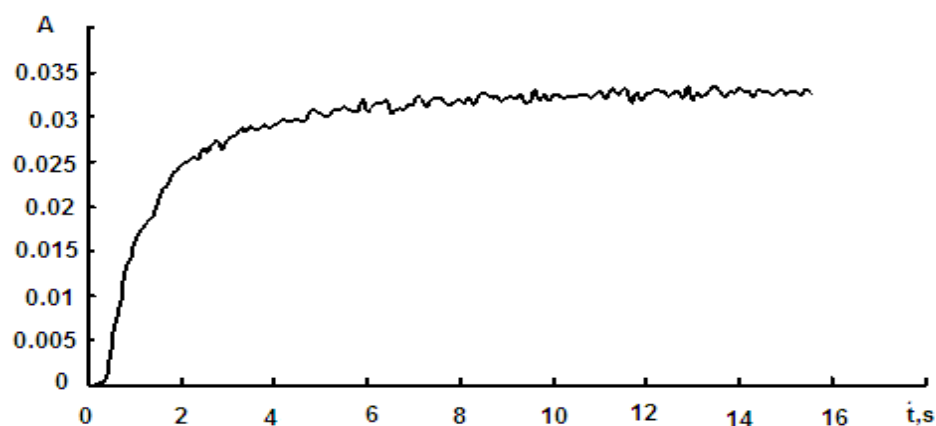


FIGURE S59. Kinetic curve for dibenzothienylethene **17** in PMMA film for the process of photocoloration under UV irradiation registered at 500 nm.

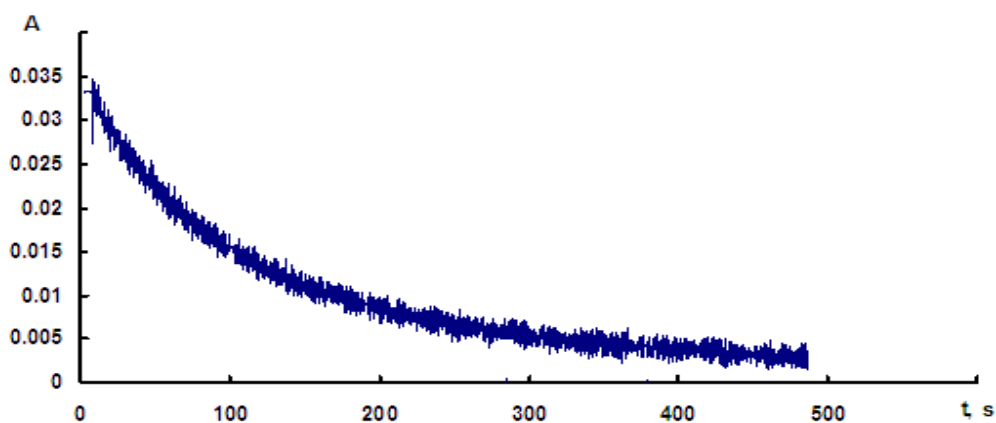


FIGURE S60. Kinetic curve for dibenzothienylethene **17** in PMMA film for the process of photobleaching under visible light registered at 500 nm.

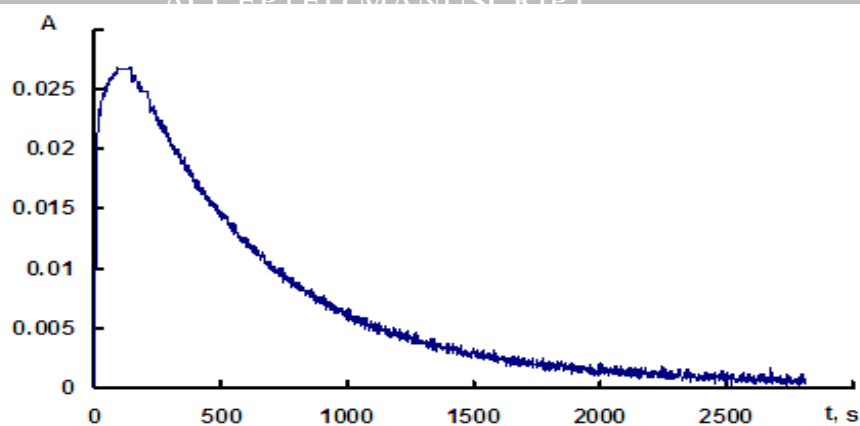


FIGURE S61. Kinetic curve for dibenzothienylethene **17** in solid-phase film for processes of photocoloration under UV irradiation and photobleaching under visible light registered at 495 nm.

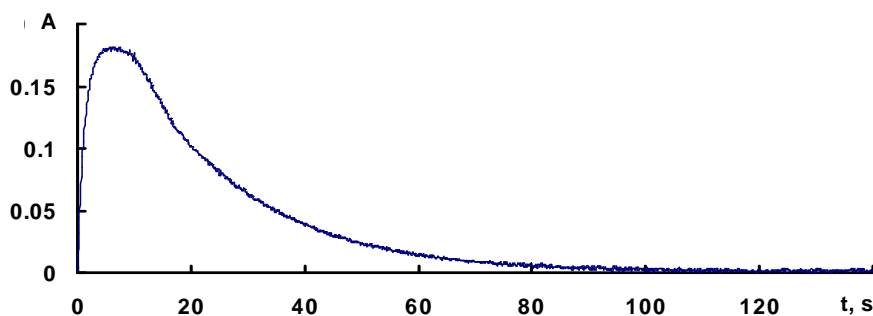


FIGURE S62. Kinetic curve for dibenzothienylethene **18** in toluene for processes of photocoloration under UV irradiation and photobleaching under visible light registered at 495 nm.

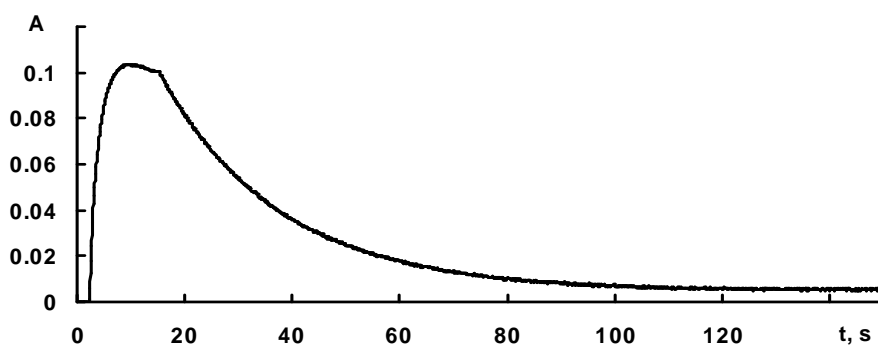


FIGURE S63. Kinetic curve for dibenzothienylethene **18** in acetonitrile for processes of photocoloration under UV irradiation and photobleaching under visible light registered at 490 nm.

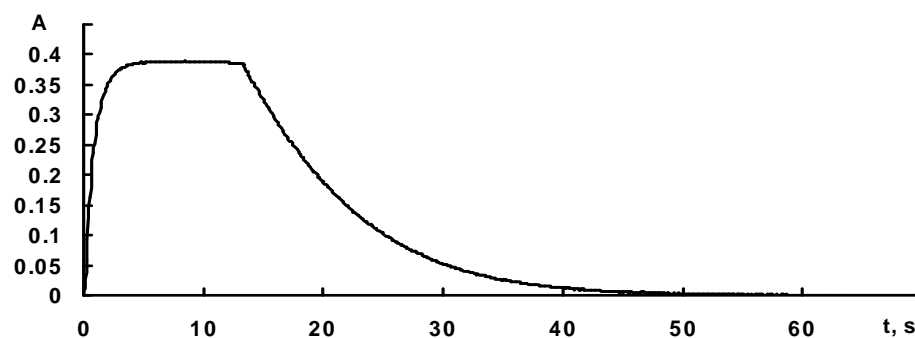


FIGURE S64. Kinetic curve for dibenzothienylethene **5** (R = COMe) in toluene for processes of photocoloration under UV irradiation and photobleaching under visible light registered at 490 nm.

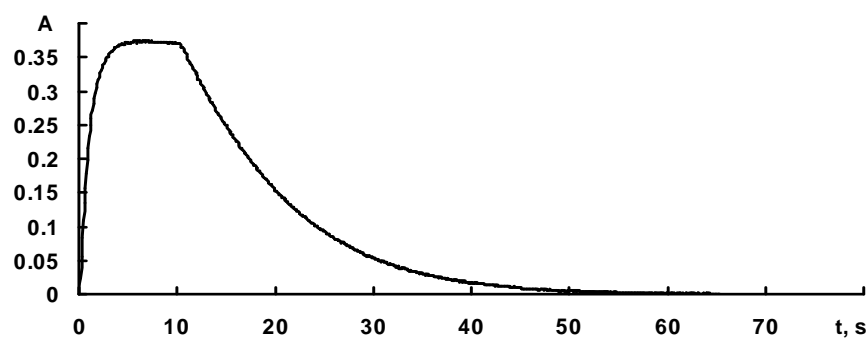


FIGURE S65. Kinetic curve for dibenzothienylethene **5** (R = COMe) in acetonitrile for processes of photocoloration under UV irradiation and photobleaching under visible light registered at 480 nm.

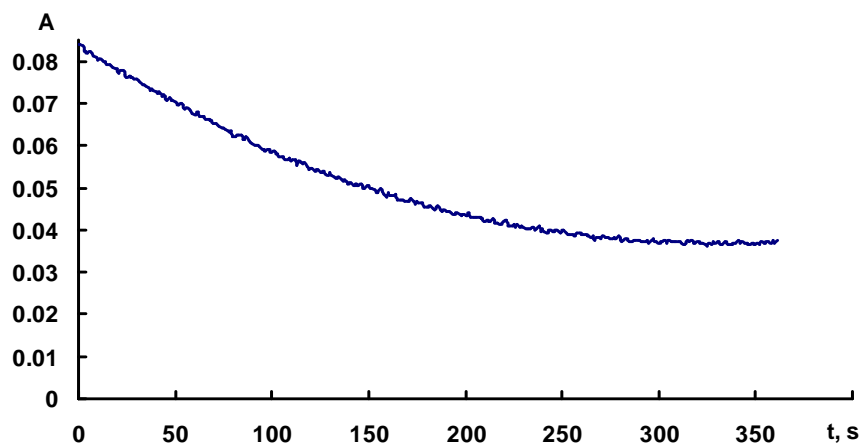
4. Photodegradation kinetic curves.

FIGURE S66. Photodegradation kinetic curve for dibenzothienylethene **3** in toluene registered at 445 nm.

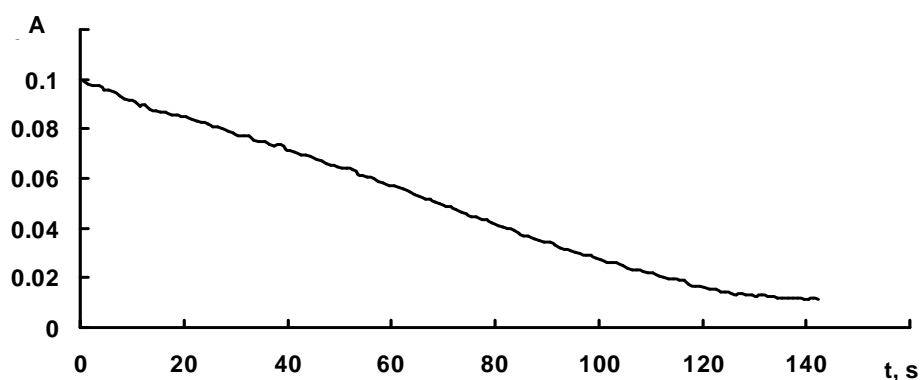


FIGURE S67. Photodegradation kinetic curve for dibenzothienylethene **3** in acetonitrile registered at 440 nm.

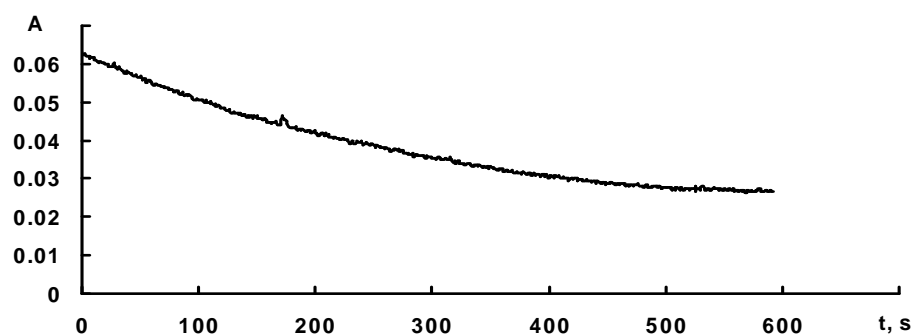


FIGURE S68. Photodegradation kinetic curve for dibenzothienylethene **4** in toluene registered at 455 nm.

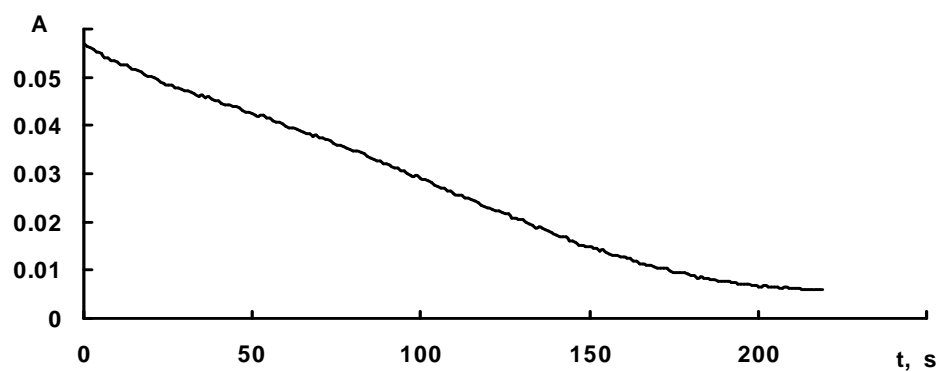


FIGURE S69. Photodegradation kinetic curve for dibenzothienylethene **4** in acetonitrile registered at 450 nm.

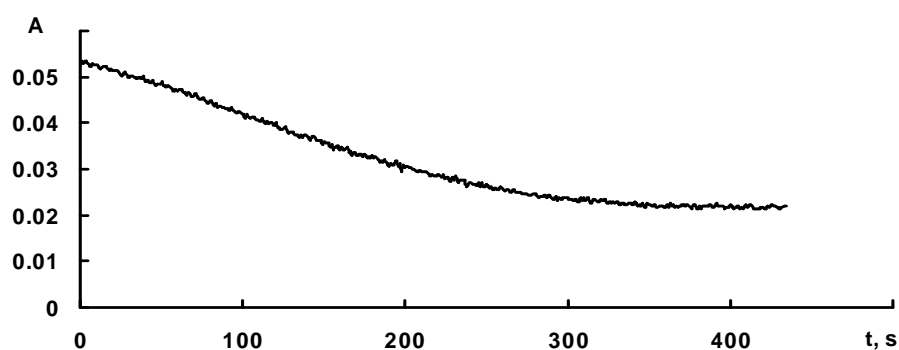


FIGURE S70. Photodegradation kinetic curve for dibenzothienylethene **6** in toluene registered at 455 nm.

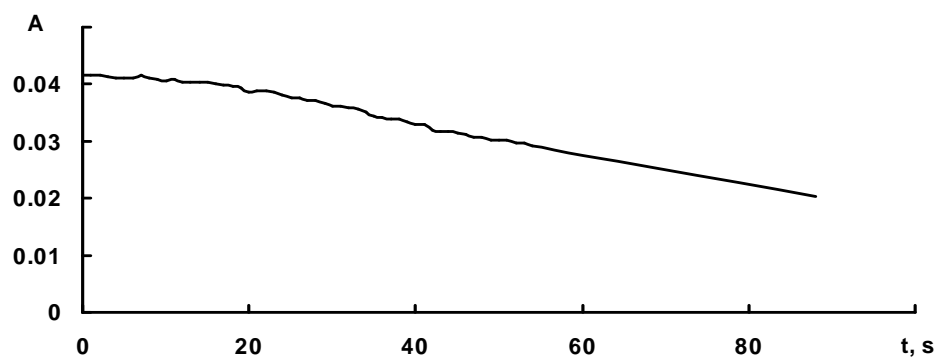


FIGURE S71. Photodegradation kinetic curve for dibenzothienylethene **6** in acetonitrile registered at 450 nm.

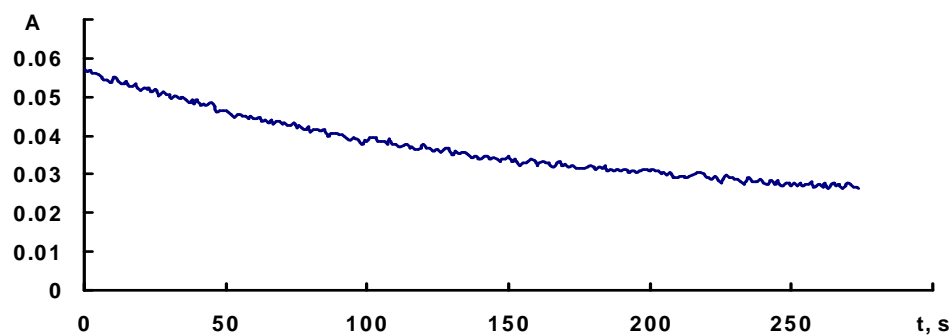


FIGURE S72. Photodegradation kinetic curve for dibenzothienylethene **9** in toluene registered at 460 nm.

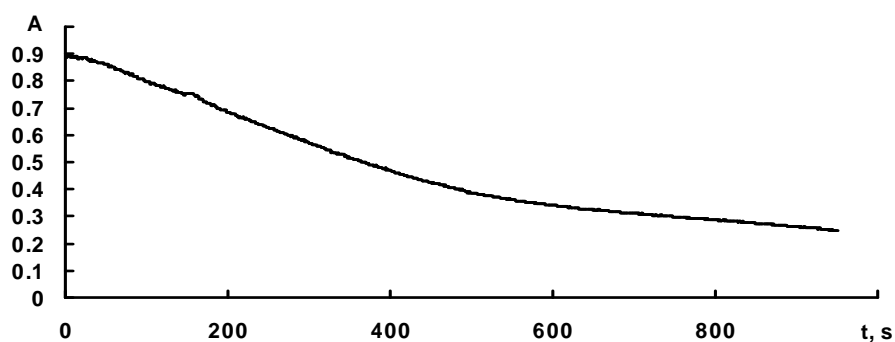


FIGURE S73. Photodegradation kinetic curve for dibenzothienylethene **9** in acetonitrile registered at 360 nm.

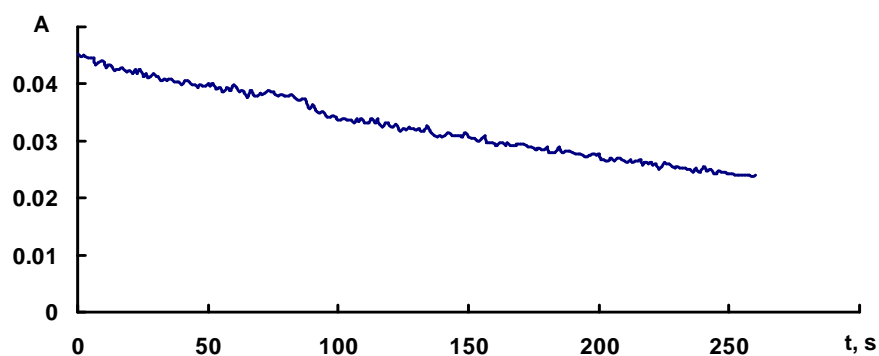


FIGURE S74. Photodegradation kinetic curve for dibenzothienylethene **10** in toluene registered at 445 nm.

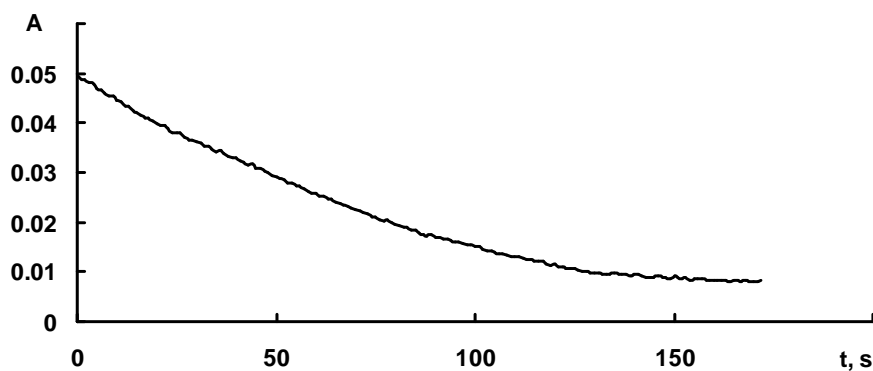


FIGURE S75. Photodegradation kinetic curve for dibenzothienylethene **10** in acetonitrile registered at 440 nm.

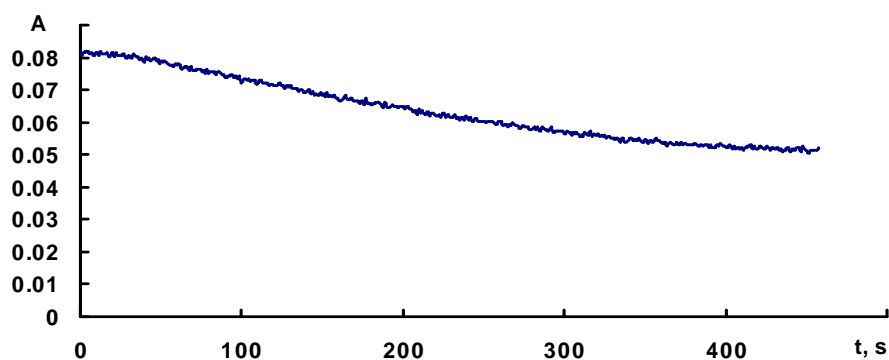


FIGURE S76. Photodegradation kinetic curve for dibenzothienylethene **11** in toluene registered at 445 nm.

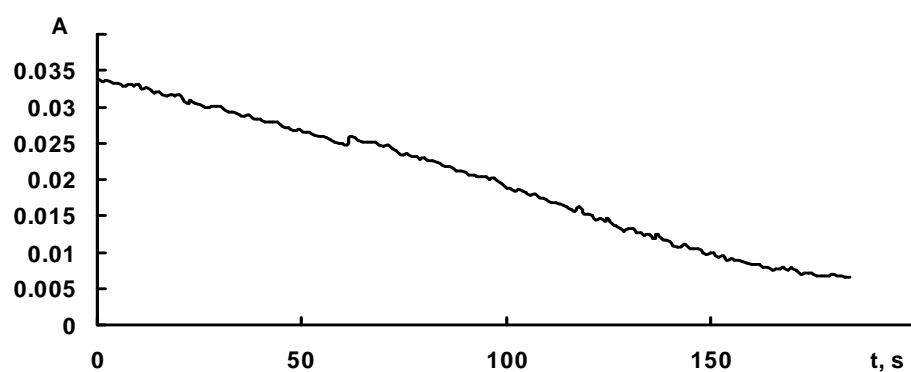


FIGURE S77. Photodegradation kinetic curve for dibenzothienylethene **11** in acetonitrile registered at 440 nm.

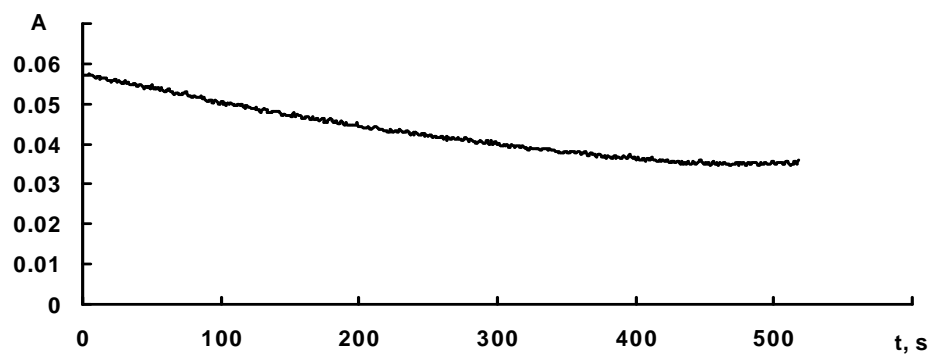


FIGURE S78. Photodegradation kinetic curve for dibenzothienylethene **12** in toluene registered at 445 nm.

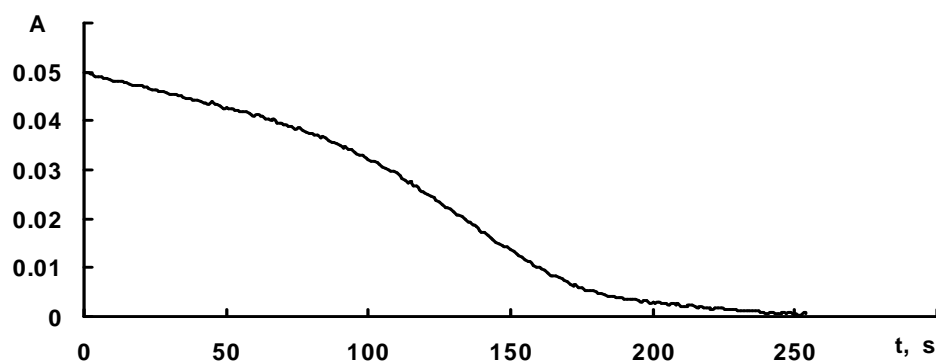


FIGURE S79. Photodegradation kinetic curve for dibenzothienylethene **12** in acetonitrile registered at 440 nm.

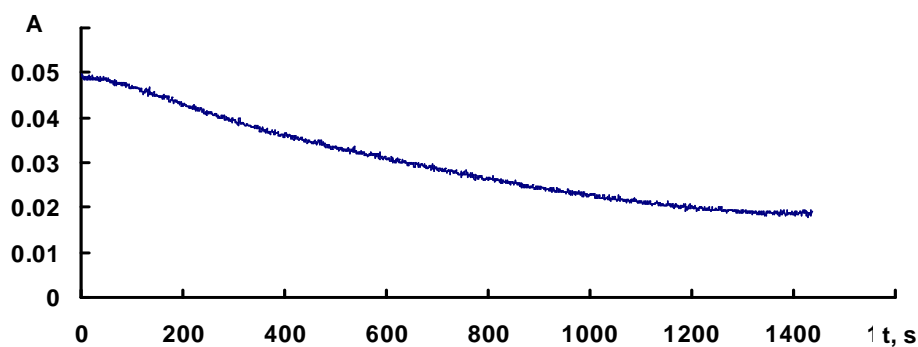


FIGURE S80. Photodegradation kinetic curve for dibenzothienylethene **13** in toluene registered at 450 nm.

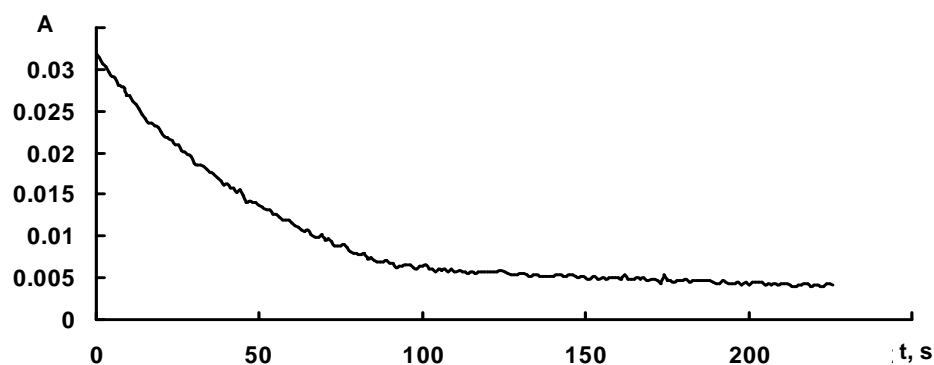


FIGURE S81. Photodegradation kinetic curve for dibenzothienylethene **13** in acetonitrile registered at 445 nm.

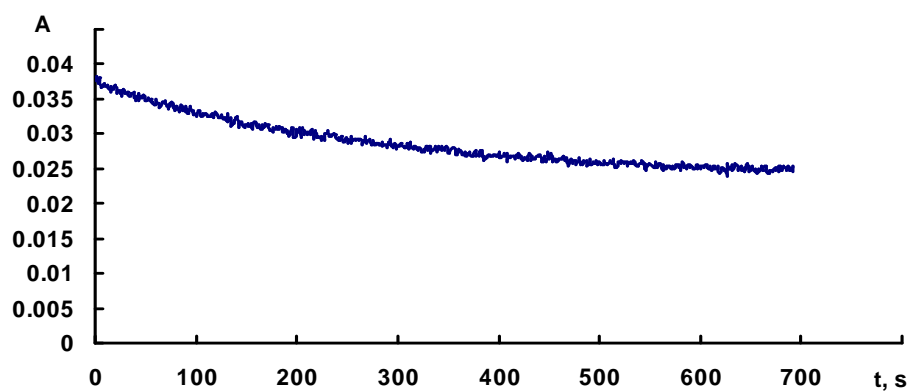


FIGURE S82. Photodegradation kinetic curve for dibenzothienylethene **14** in toluene registered at 450 nm.

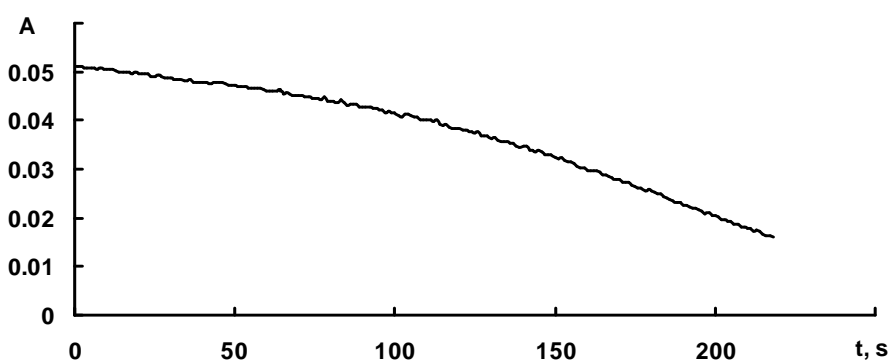


FIGURE S83. Photodegradation kinetic curve for dibenzothienylethene **14** in acetonitrile registered at 445 nm.

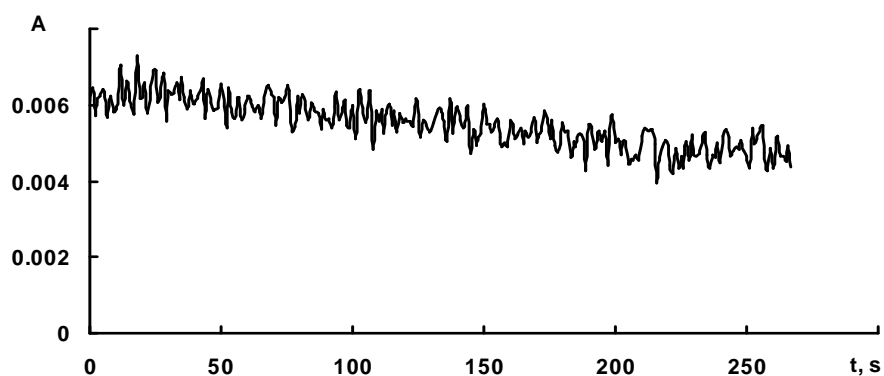


FIGURE S84. Photodegradation kinetic curve for dibenzothienylethene **15** in toluene registered at 460 nm.

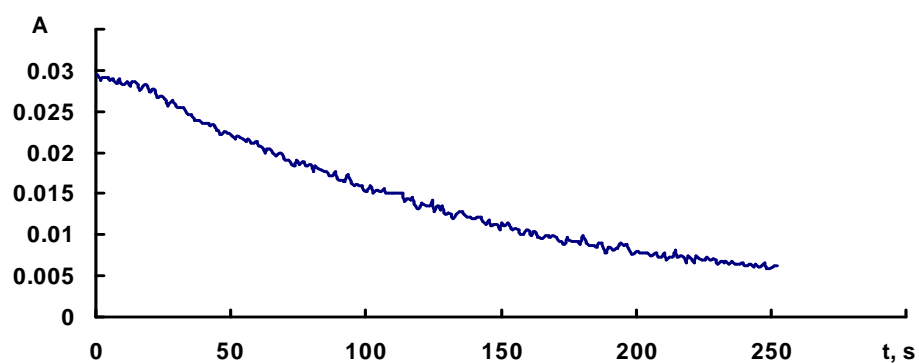


FIGURE S85. Photodegradation kinetic curve for dibenzothienylethene **15** in acetonitrile registered at 460 nm.

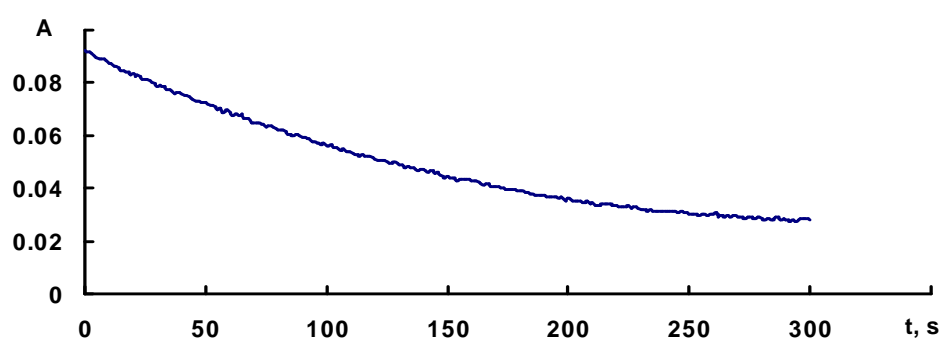


FIGURE S86. Photodegradation kinetic curve for dibenzothienylethene **16** in toluene registered at 460 nm.

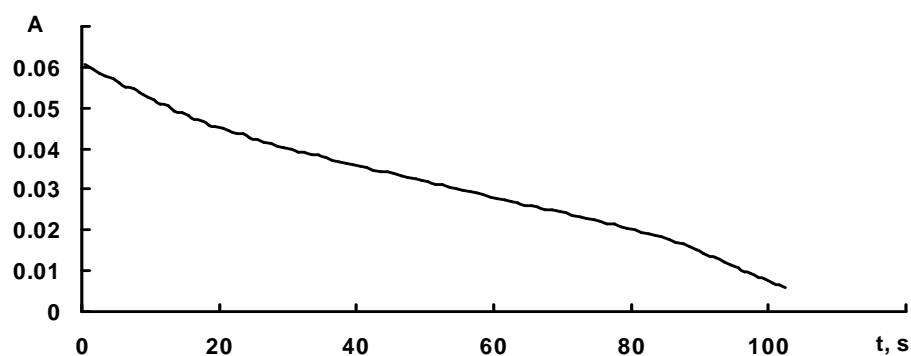


FIGURE S87. Photodegradation kinetic curve for dibenzothienylethene **16** in acetonitrile registered at 460 nm.

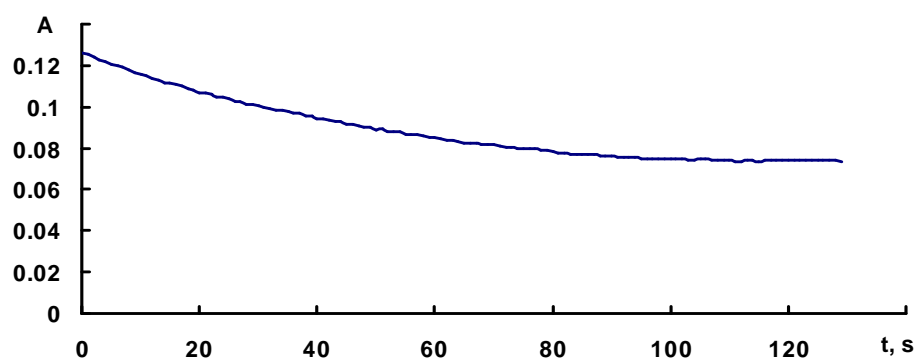


FIGURE S88. Photodegradation kinetic curve for dibenzothienylethene **17** in toluene registered at 490 nm.

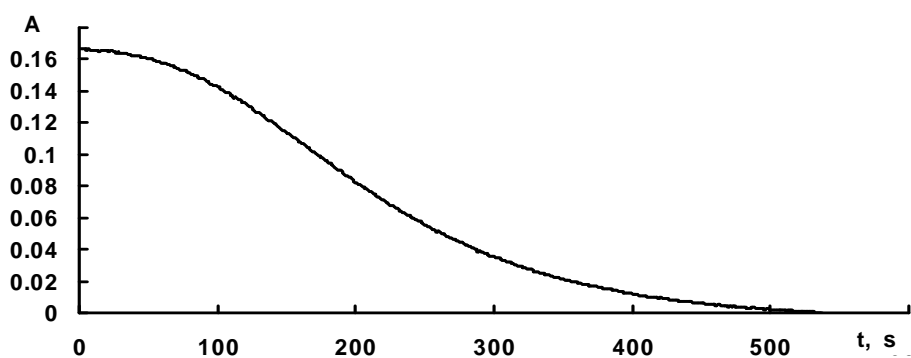


FIGURE S89. Photodegradation kinetic curve for dibenzothienylethene **17** in acetonitrile registered at 480 nm.

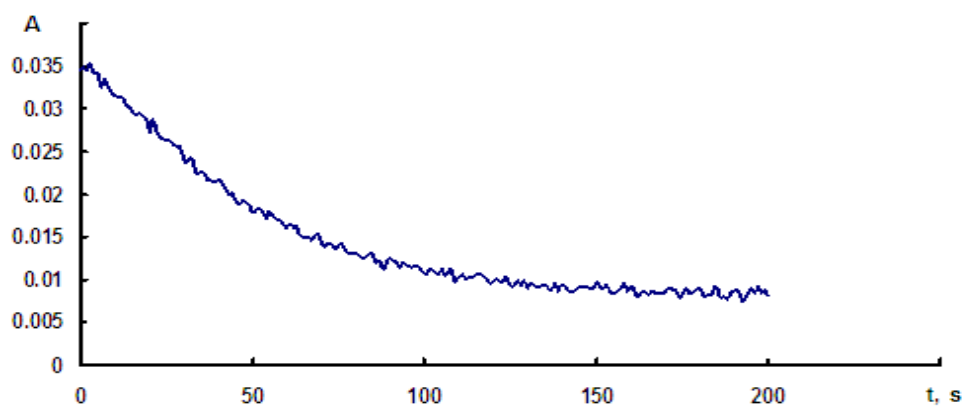


FIGURE S90. Photodegradation kinetic curve for dibenzothienylethene **17** in PMMA film registered at 500 nm.

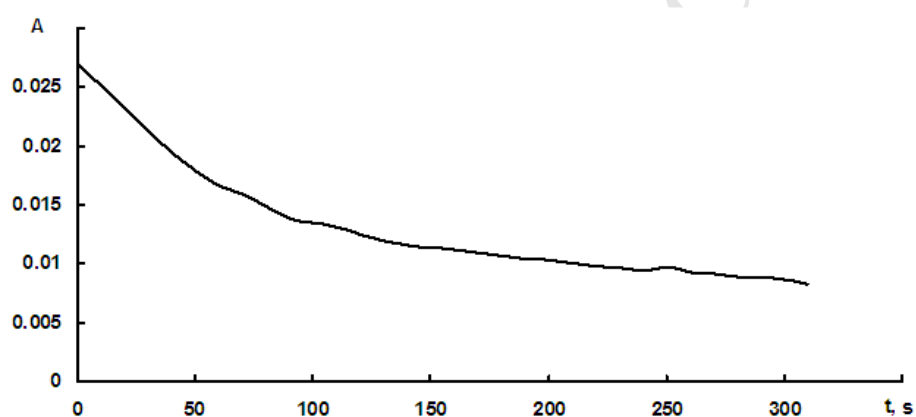


FIGURE S91. Photodegradation kinetic curve for dibenzothienylethene **17** in solid-phase film registered at 495 nm.

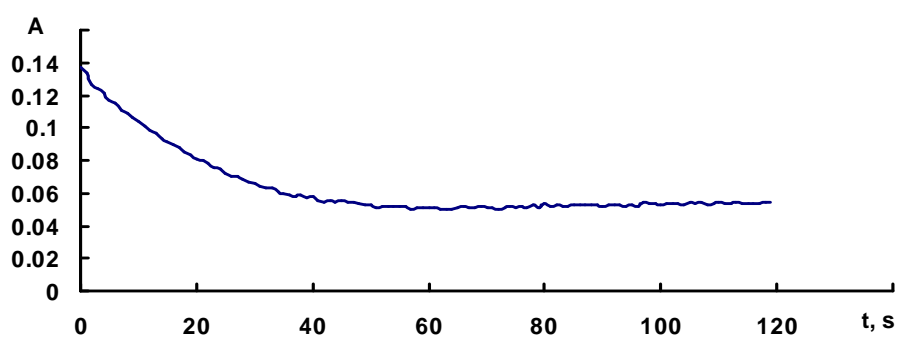


FIGURE S92. Photodegradation kinetic curve for dibenzothienylethene **18** in toluene registered at 495 nm.

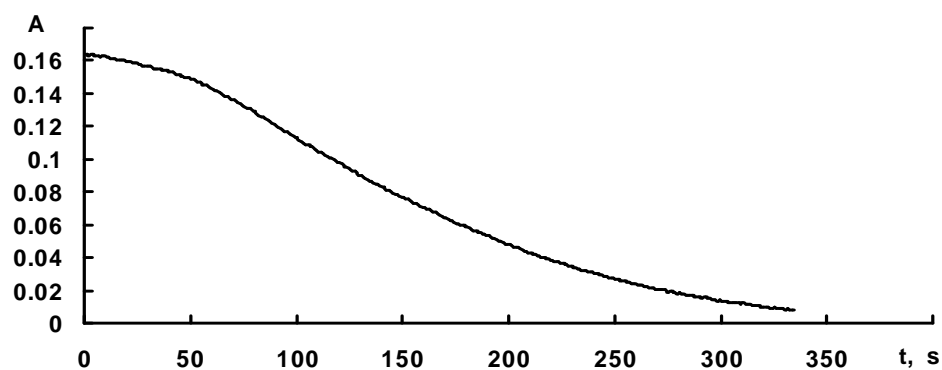


FIGURE S93. Photodegradation kinetic curve for dibenzothienylethene **18** in acetonitrile registered at 490 nm.

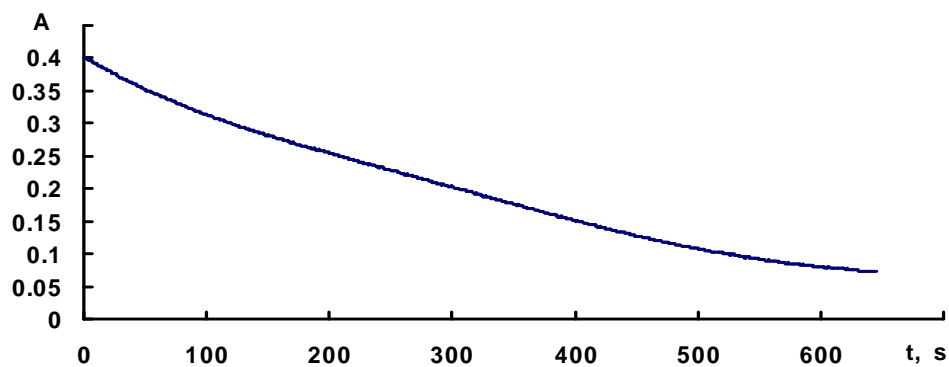


FIGURE S94. Photodegradation kinetic curve for dibenzothienylethene **5** (R = COMe) in toluene registered at 490 nm.

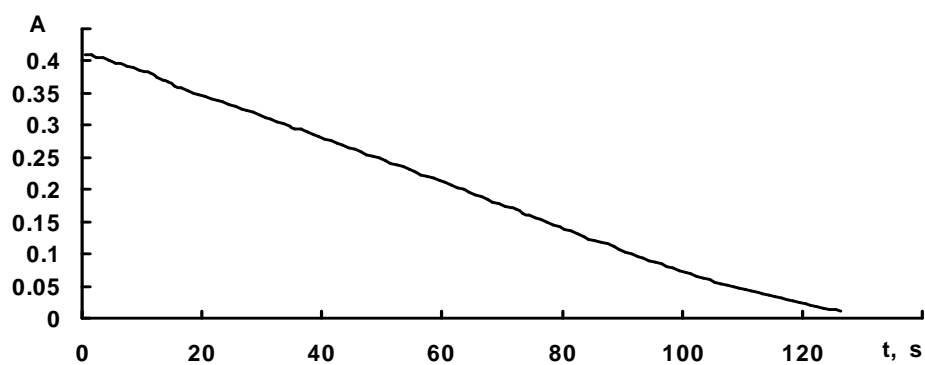


FIGURE S95. Photodegradation kinetic curve for dibenzothienylethene **5** (R = COMe) in acetonitrile registered at 480 nm.

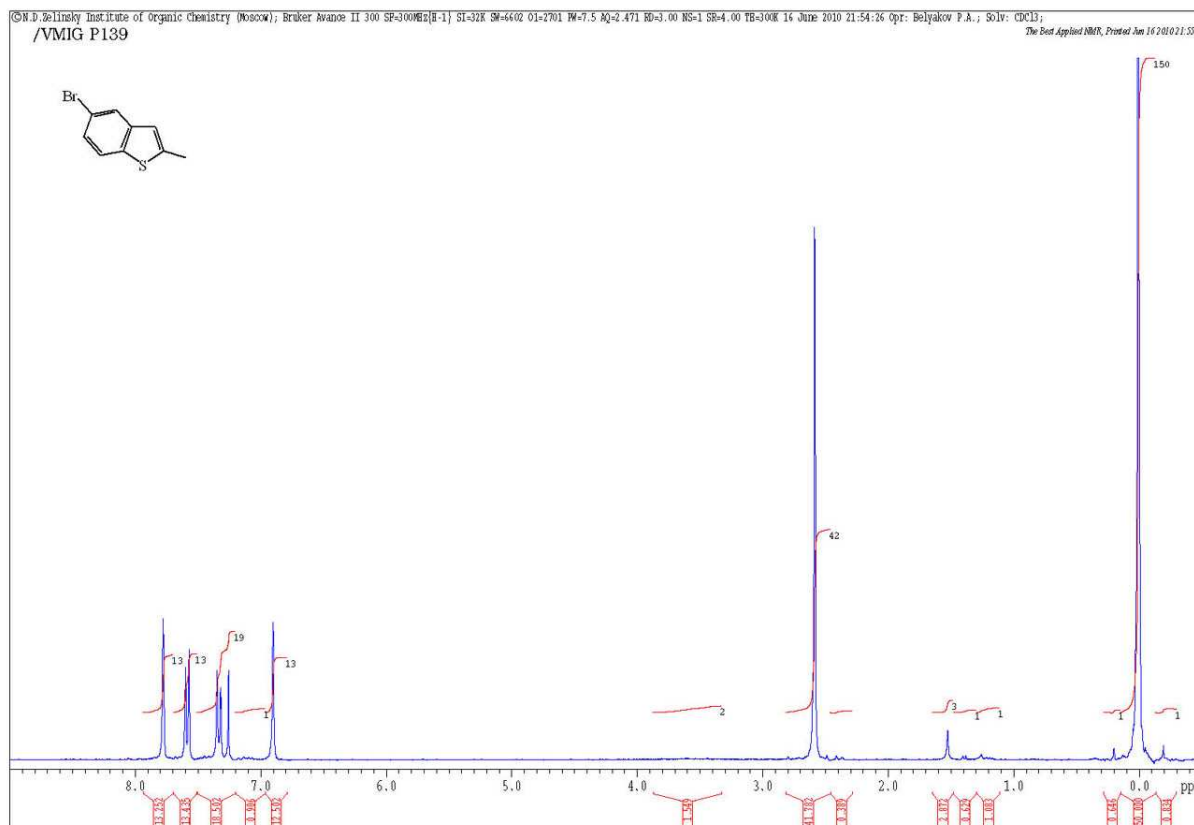


FIGURE S96. ^1H NMR spectrum of 5-bromo-2-methylbenzo[b]thiophene (7) in CDCl_3 .

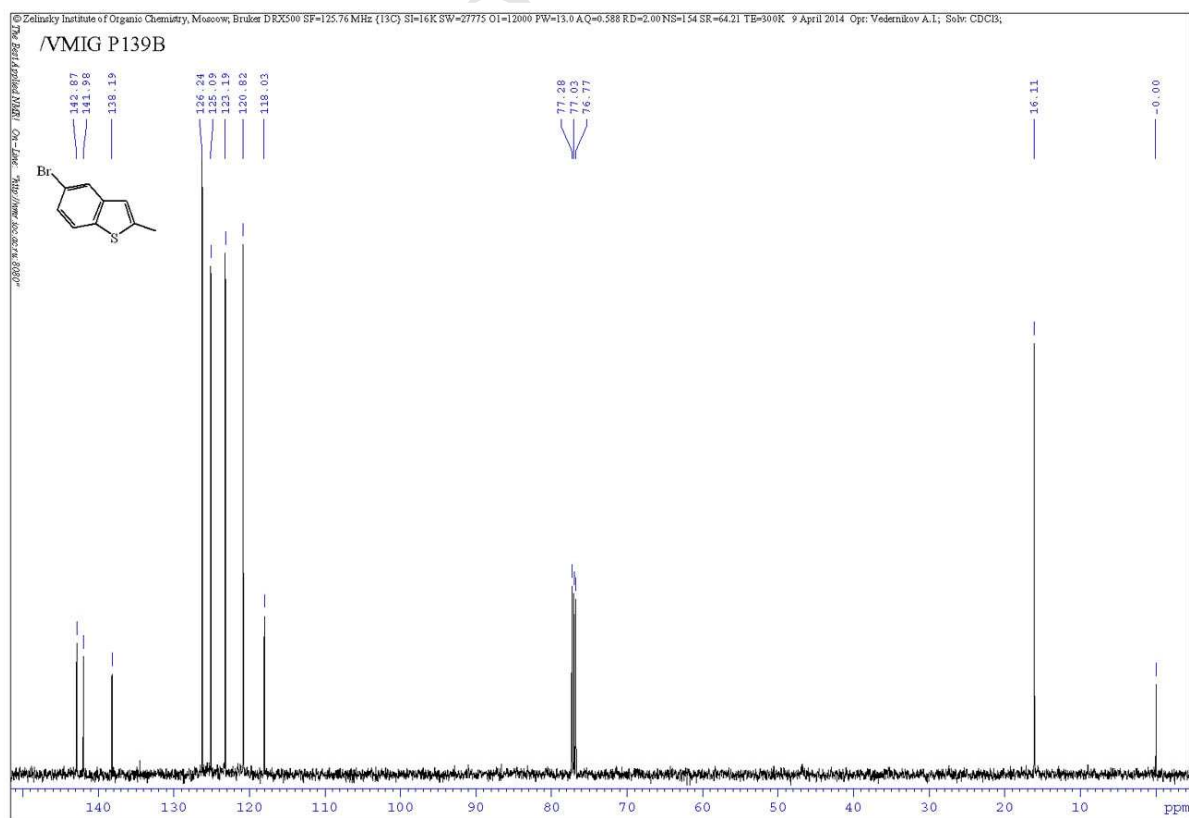
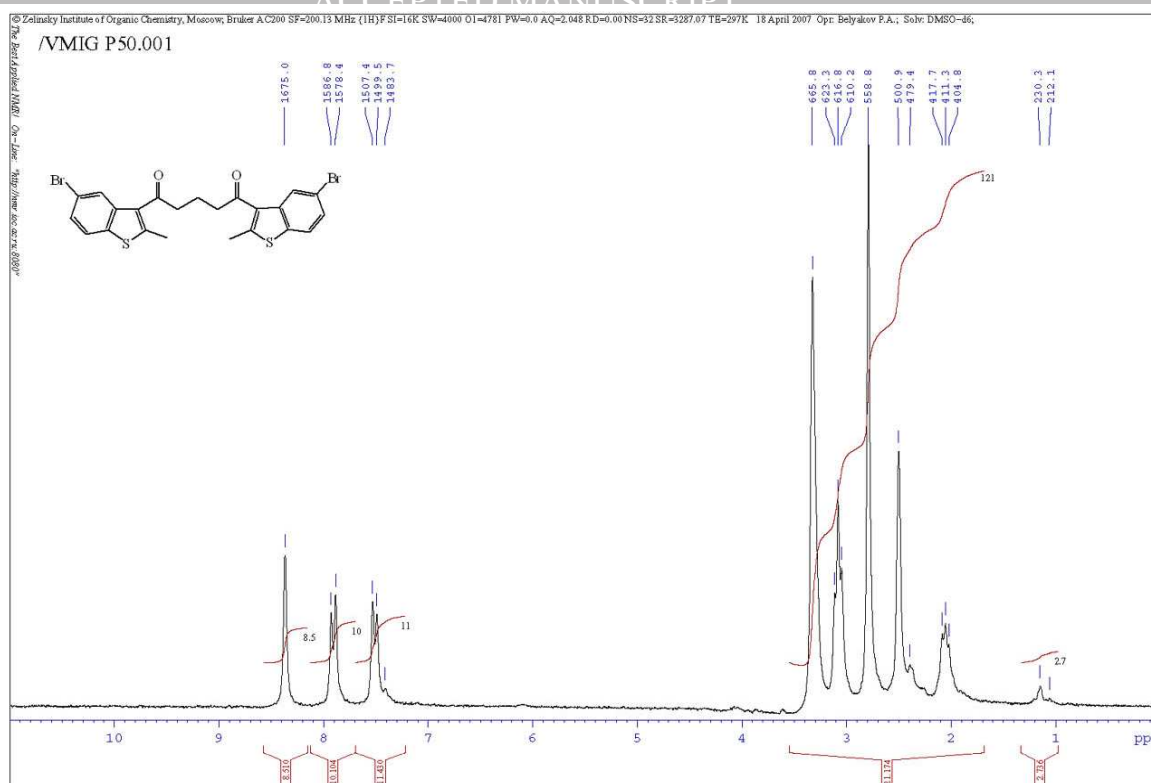


FIGURE S97. ^{13}C NMR spectrum of 5-bromo-2-methylbenzo[b]thiophene (7) in CDCl_3 .



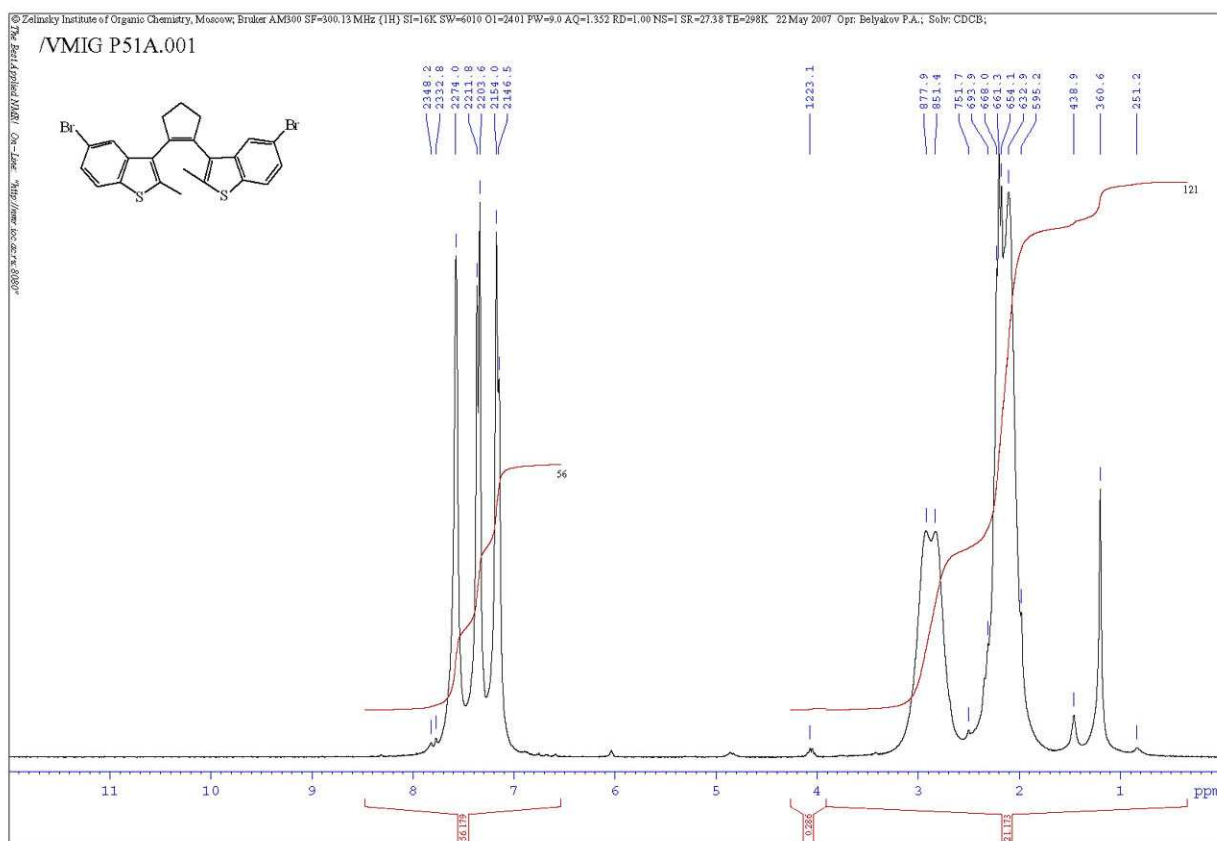


FIGURE S100. ^1H NMR spectrum of dibenzothienylethene **6** in CDCl_3 .

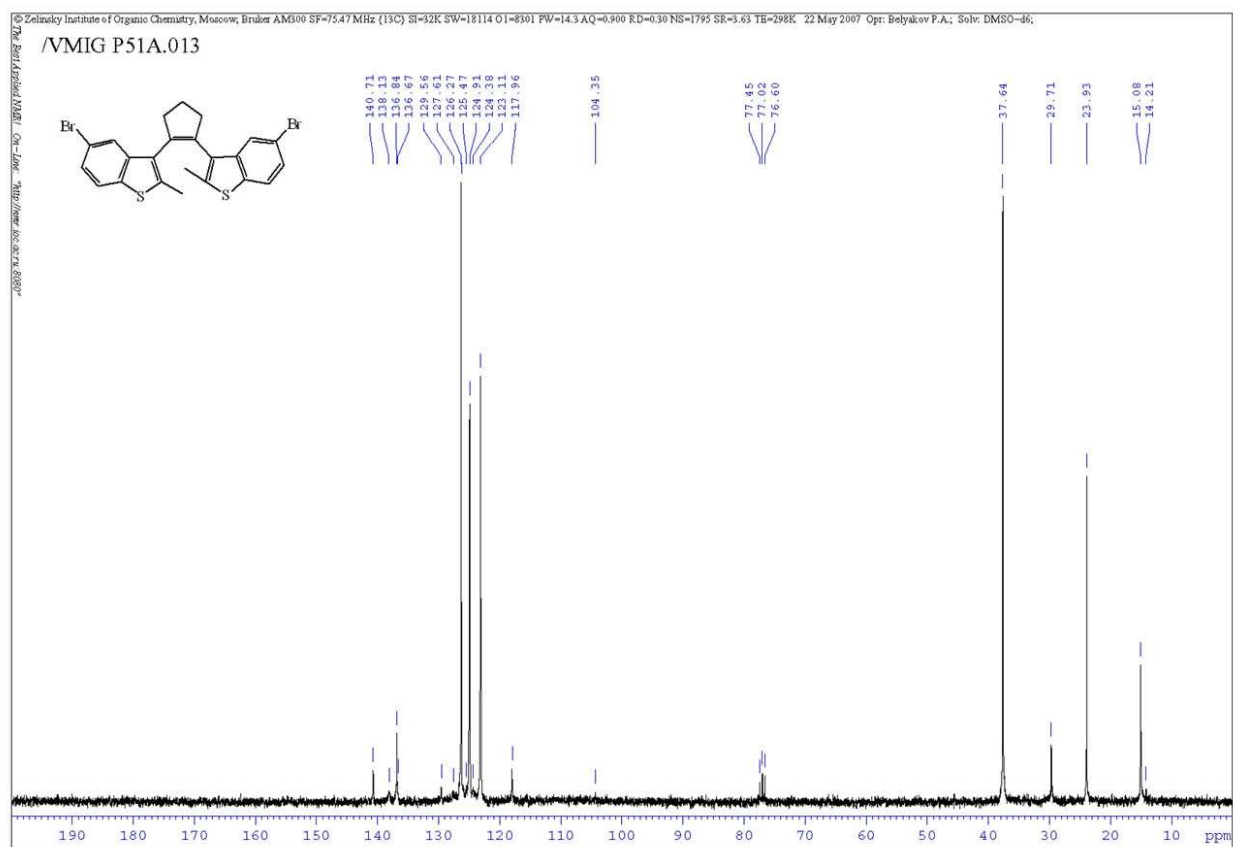


FIGURE S101. ^{13}C NMR spectrum of dibenzothienylethene **6** in $\text{DMSO}-d_6$.

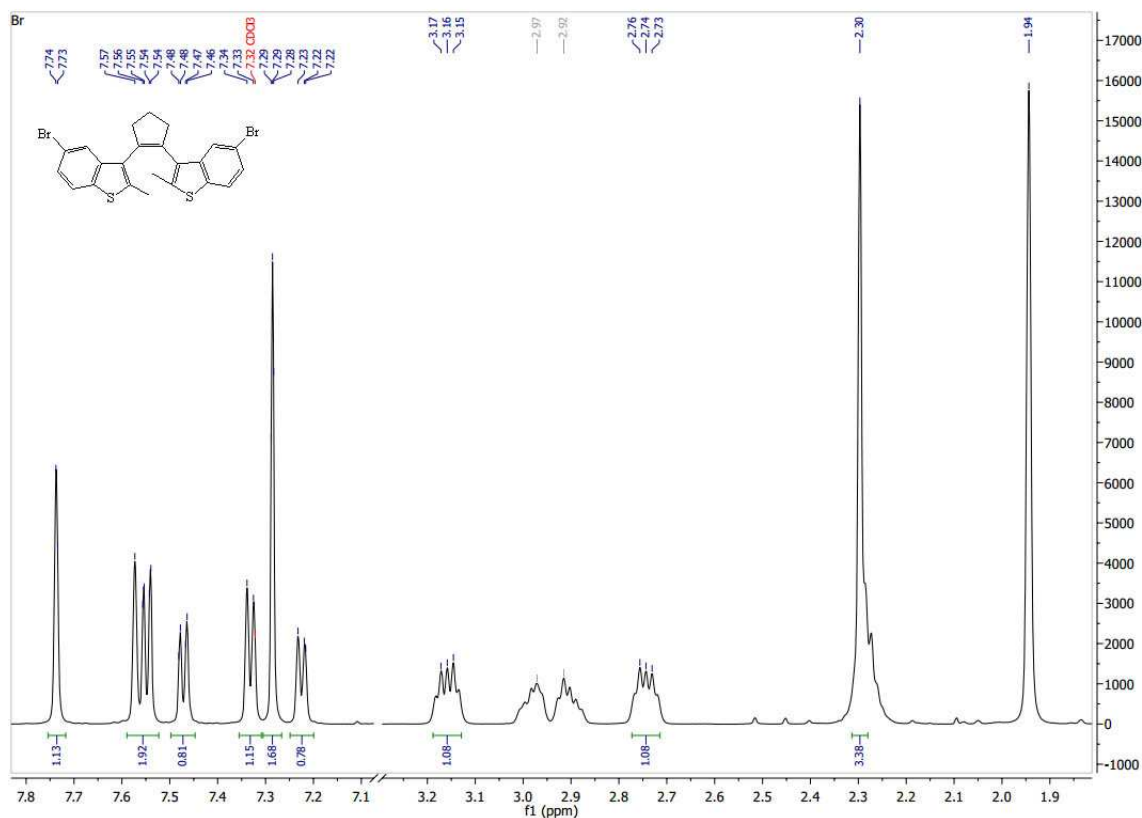


FIGURE S102. ¹H NMR spectrum of dibenzothienylethene **6** at 600 MHz in CDCl₃ at 235 K.

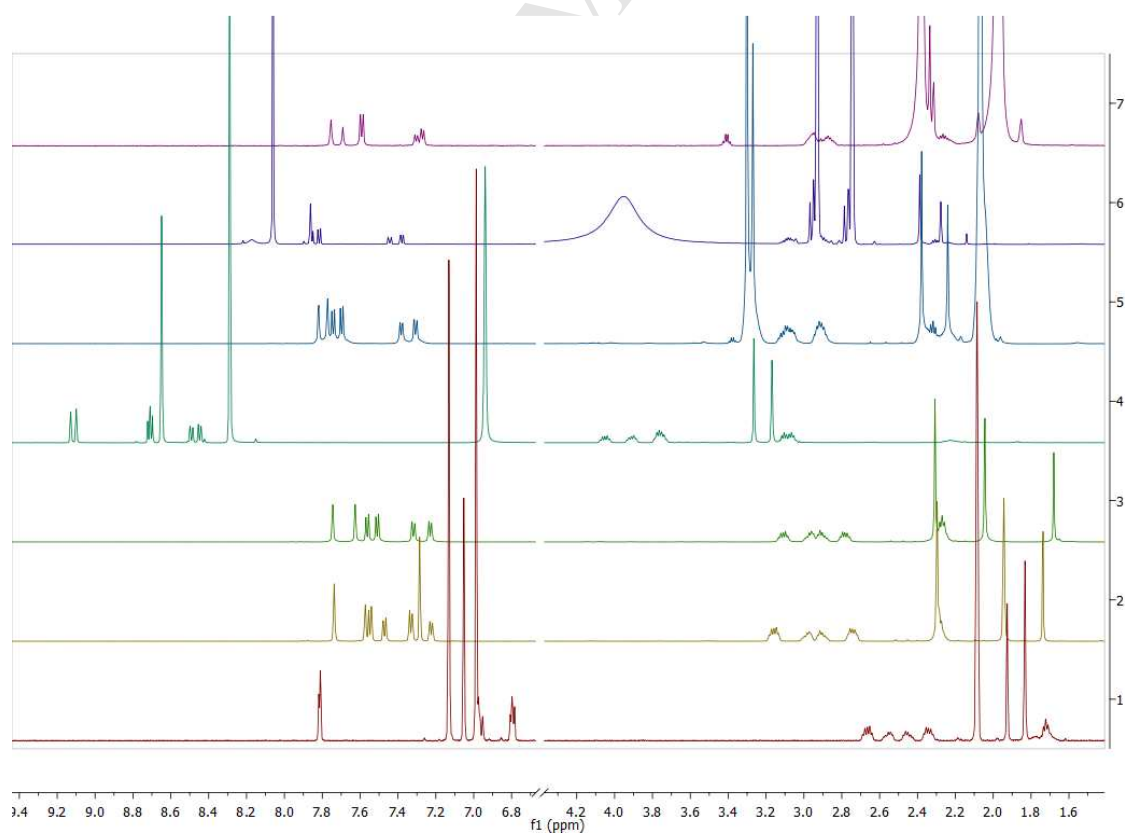
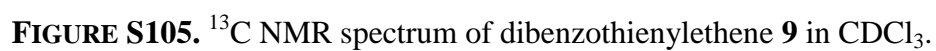
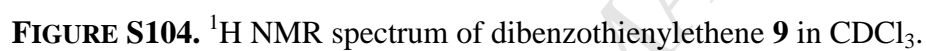


FIGURE S103. ¹H NMR spectrum of dibenzothienylethene **6** at 600 MHz in toluene-*d*₈ (1), CDCl₃ (2), CD₂Cl₂ (3), pyridine-*d*₅ (4), acetone-*d*₆ (5), DMF-*d*₇ (6), and CD₃CN (7) at 235 K.



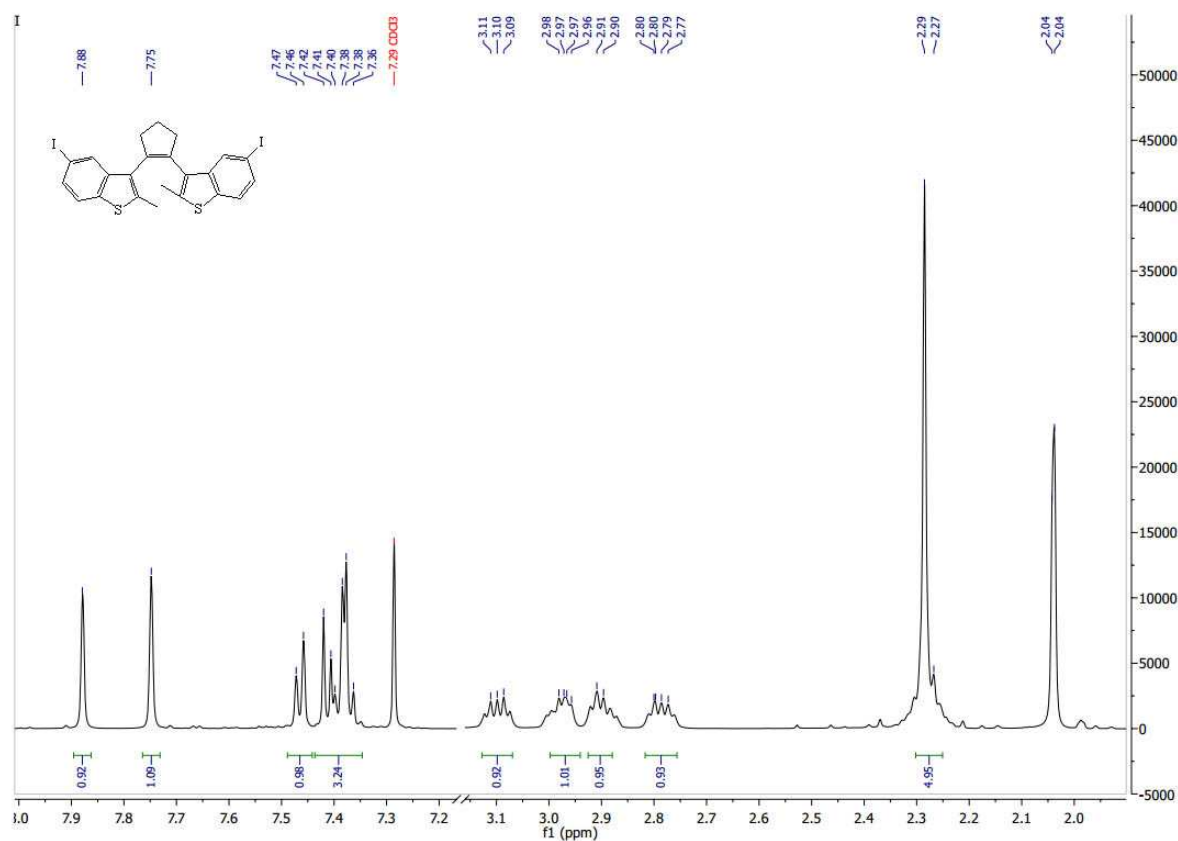


FIGURE S106. ^1H NMR spectrum of dibenzothiophene **9** at 600 MHz in CDCl_3 at 235 K.

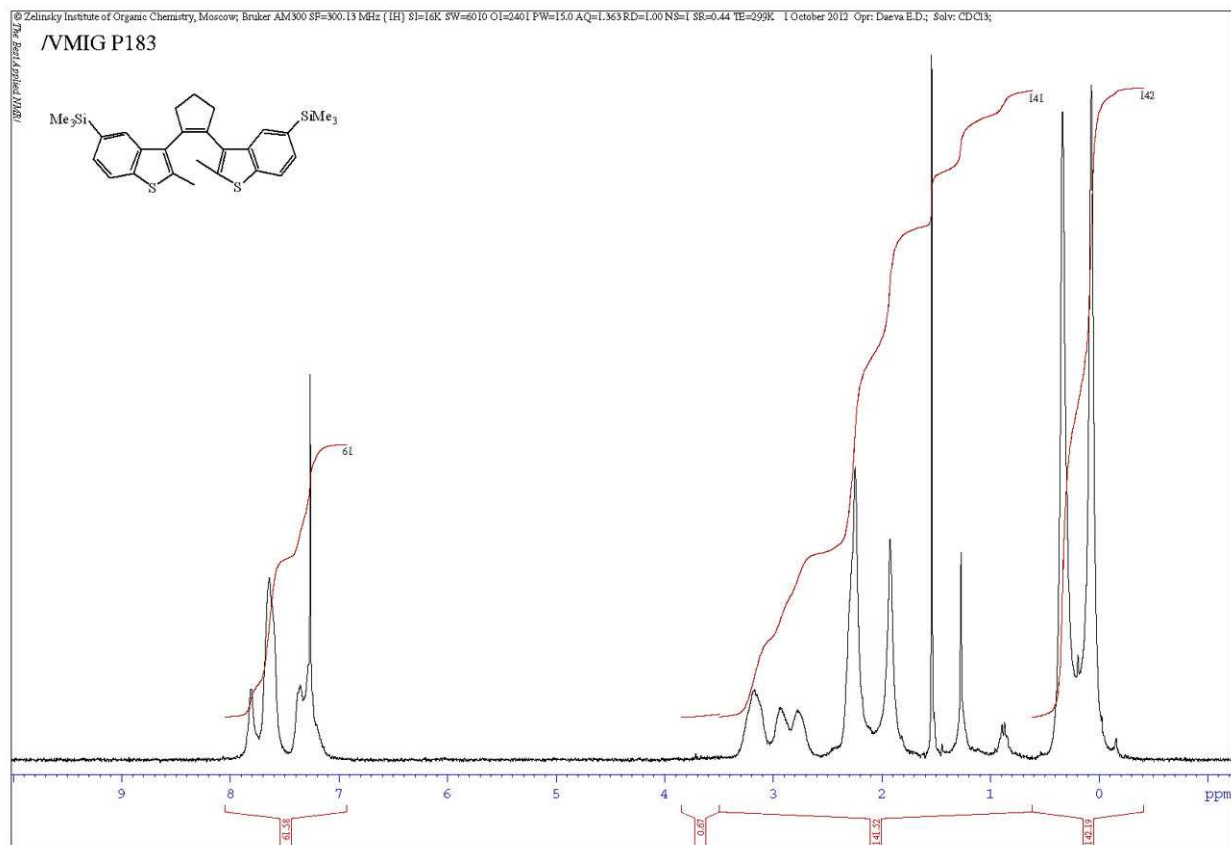


FIGURE S107. ^1H NMR spectrum of dibenzothiophene **10** in CDCl_3 .

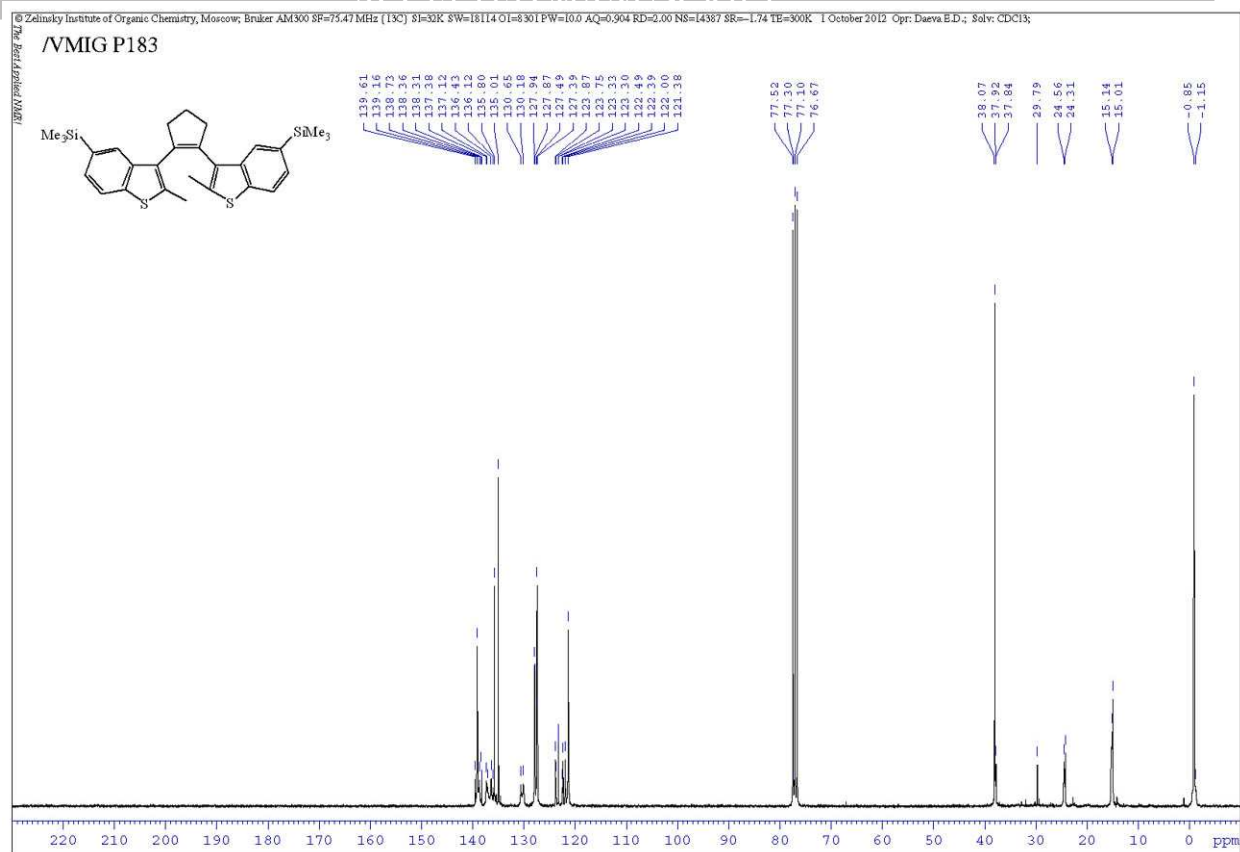


FIGURE S108. ^{13}C NMR spectrum of dibenzothiophene **10** in CDCl_3 .

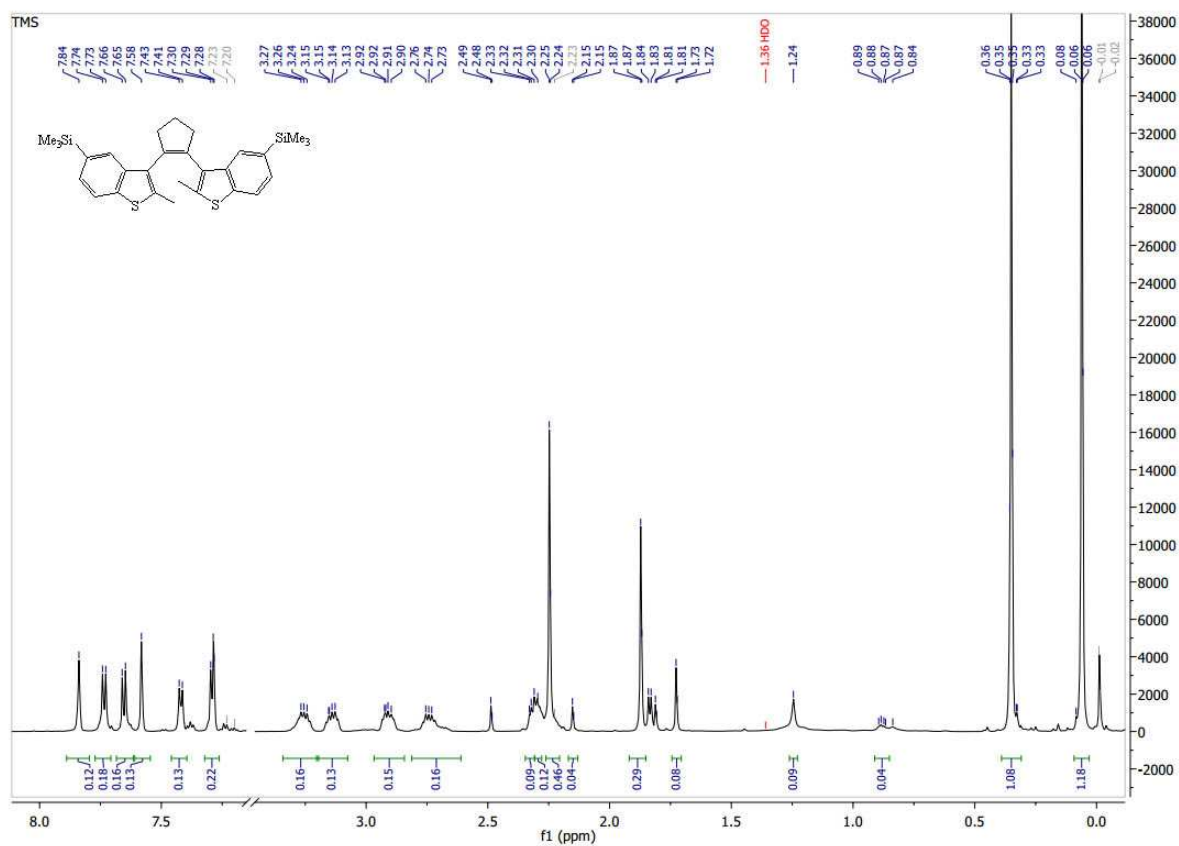


FIGURE S109. ^1H NMR spectrum of dibenzothiophene **10** at 600 MHz in CDCl_3 at 235 K.

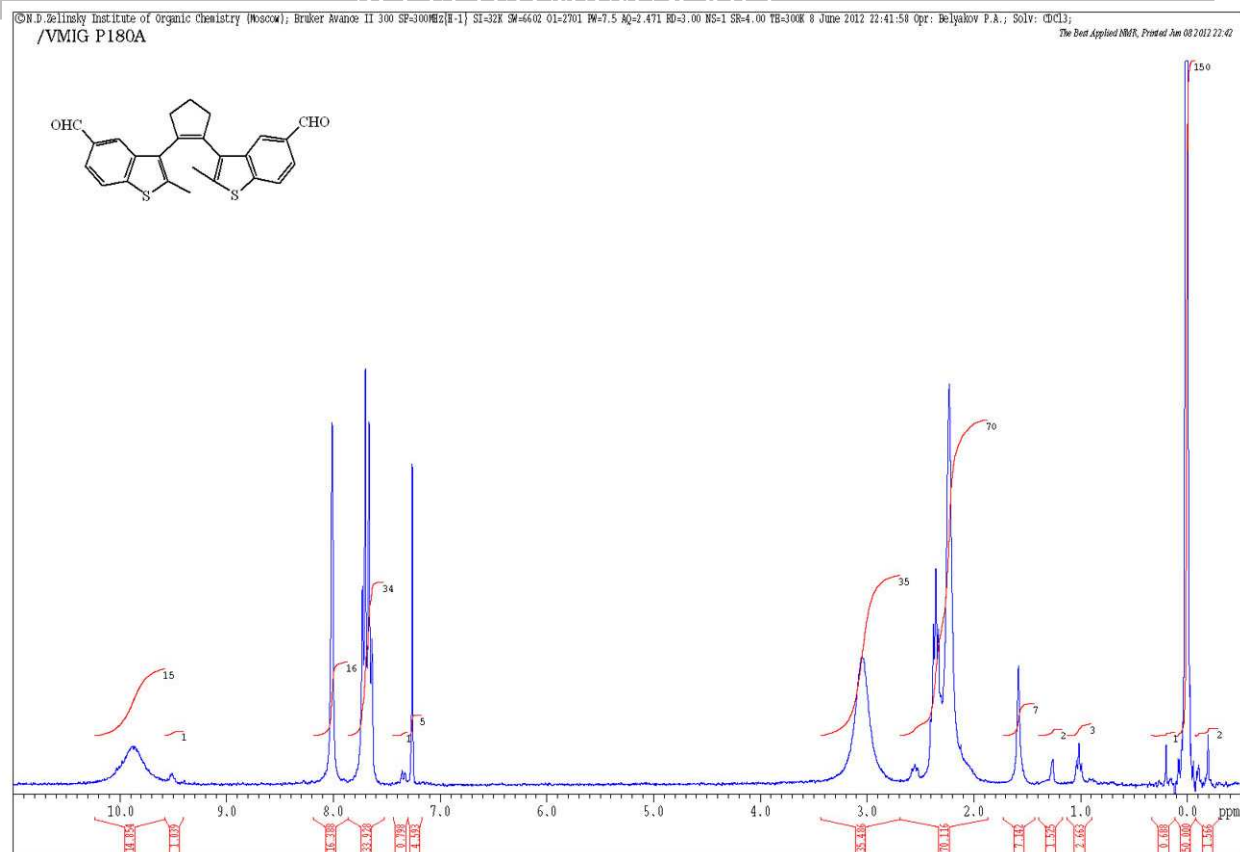


FIGURE S110. ¹H NMR spectrum of dibenzothienylethene **11** in CDCl₃.

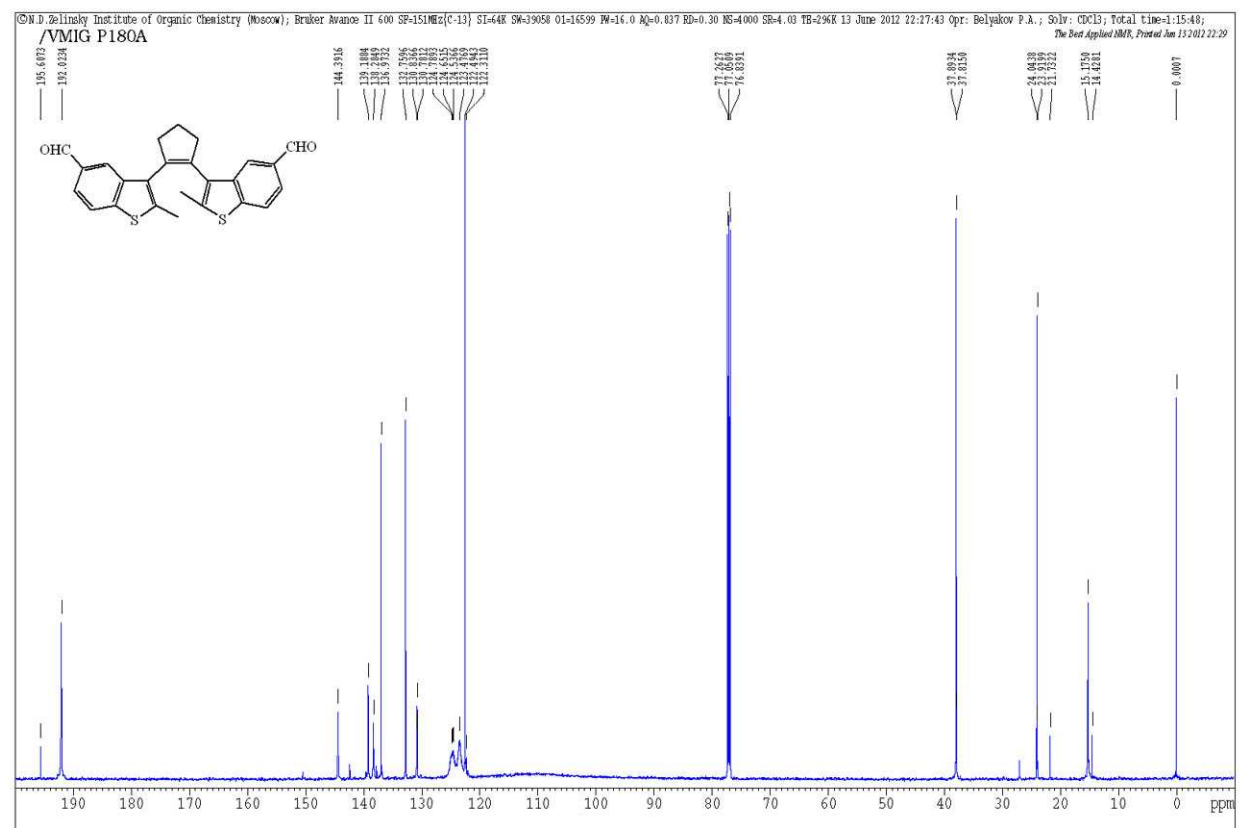


FIGURE S111. ¹³C NMR spectrum of dibenzothienylethene **11** in CDCl₃.

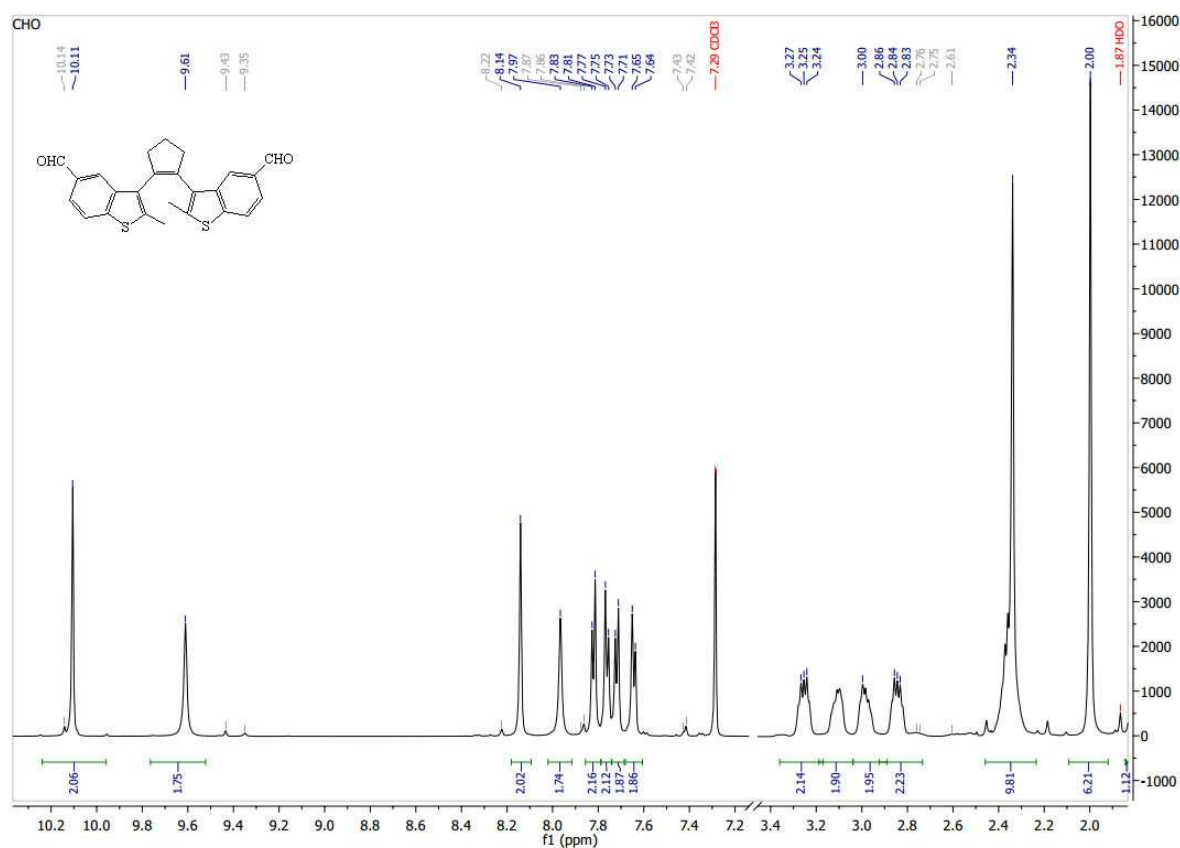


FIGURE S112. ^1H NMR spectrum of dibenzothiophene **11** at 600 MHz in CDCl_3 at 235 K.

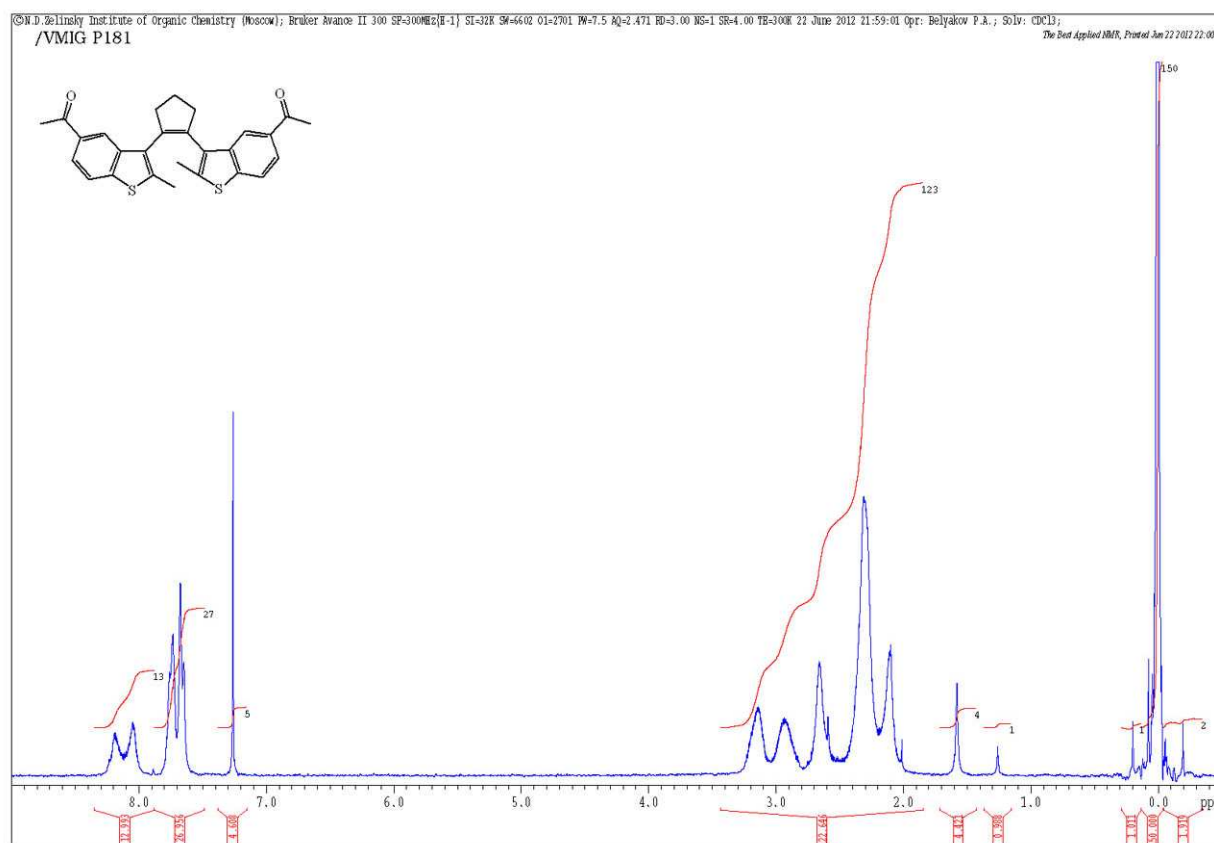


FIGURE S113. ^1H NMR spectrum of dibenzothiophene **12** in CDCl_3 .

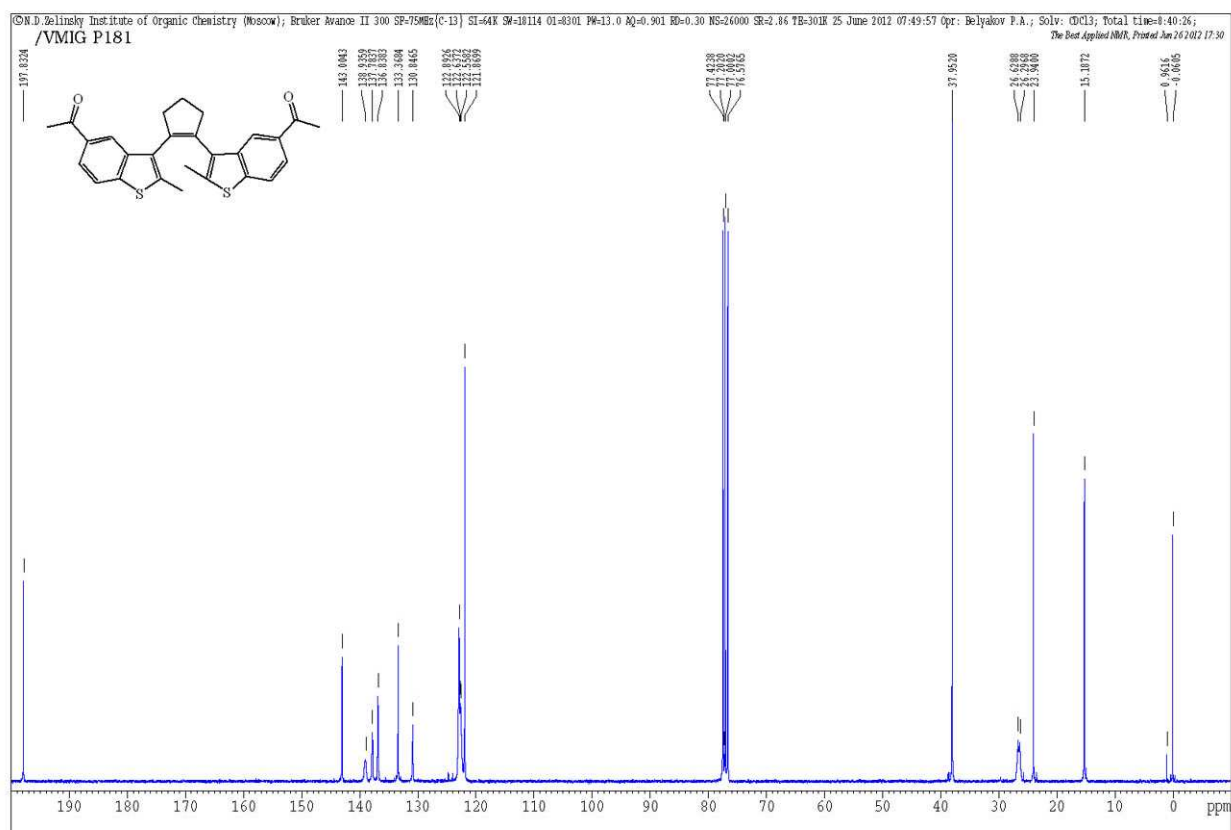


FIGURE S114. ^{13}C NMR spectrum of dibenzothiophene **12** in CDCl_3 .

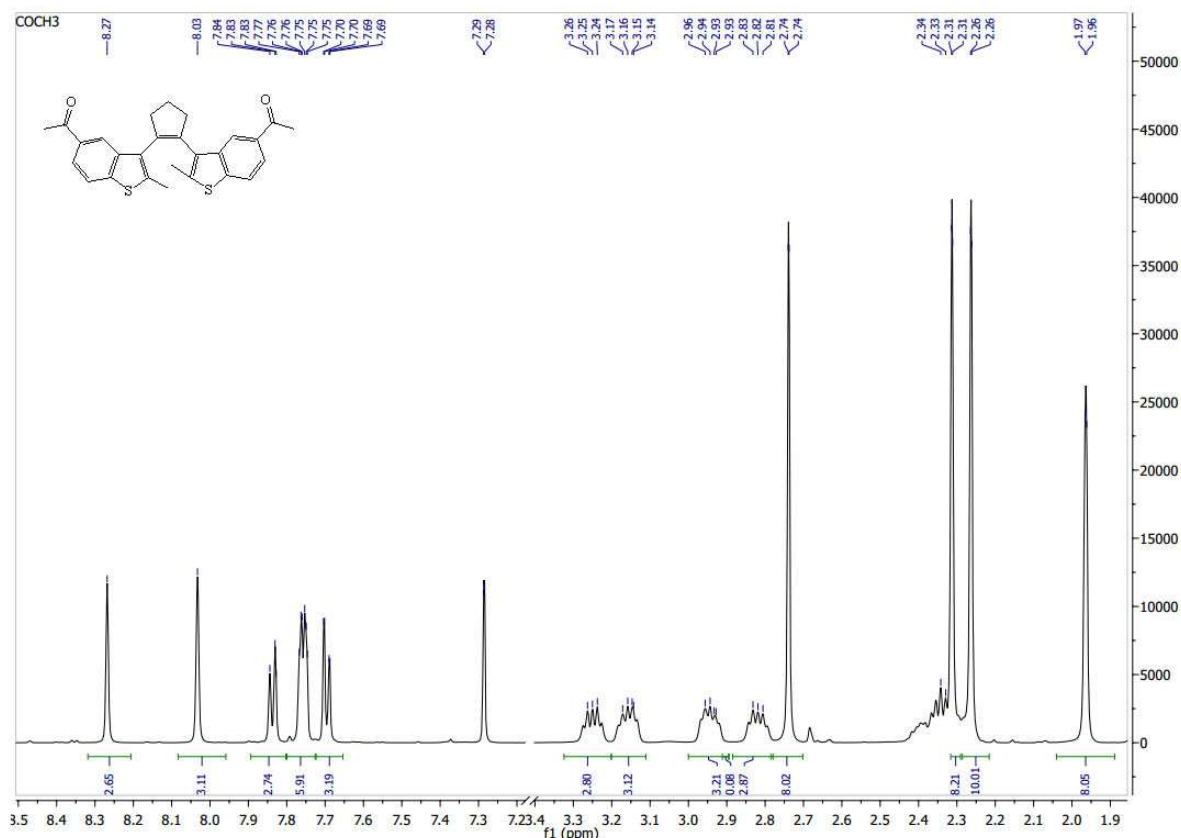


FIGURE S115. ^1H NMR spectrum of dibenzothiophene **12** at 600 MHz in CDCl_3 at 235 K.

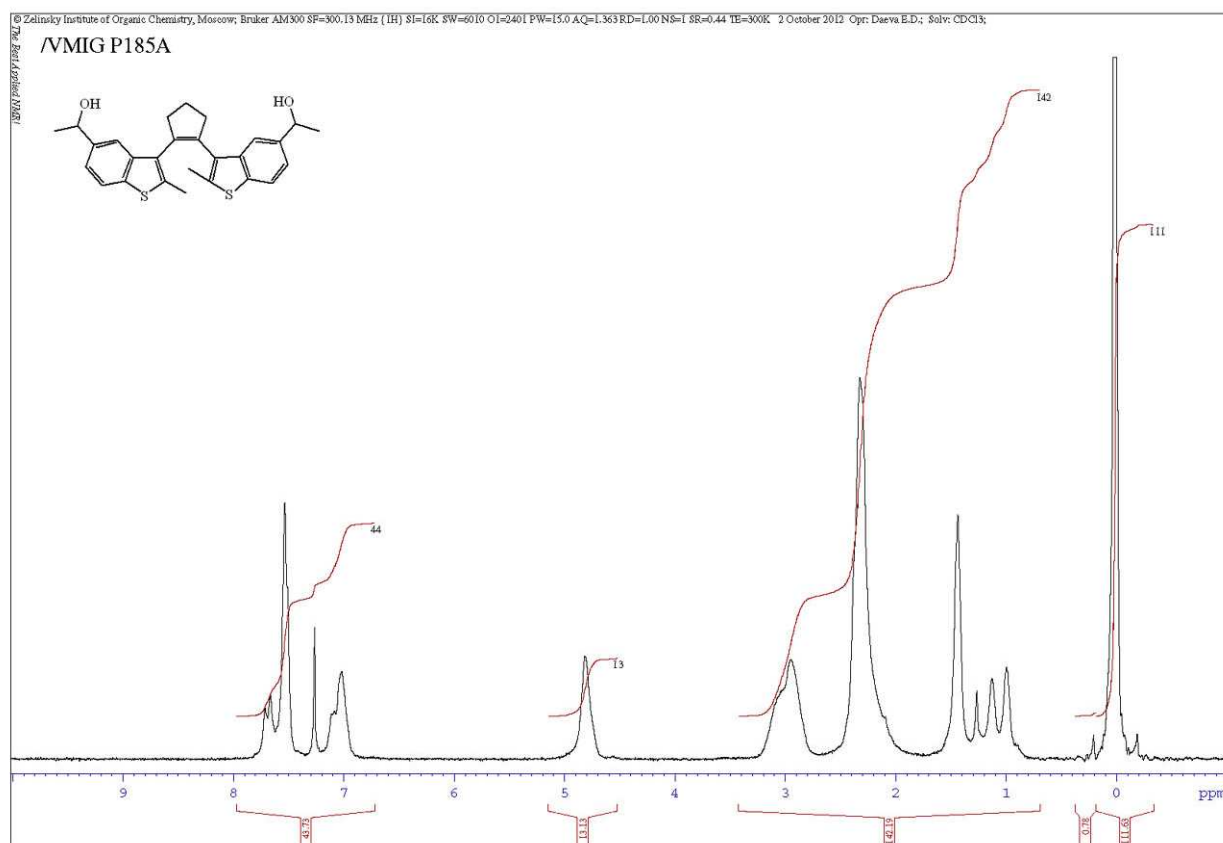


FIGURE S116. ^1H NMR spectrum of dibenzothienylethene **13** in CDCl_3 .

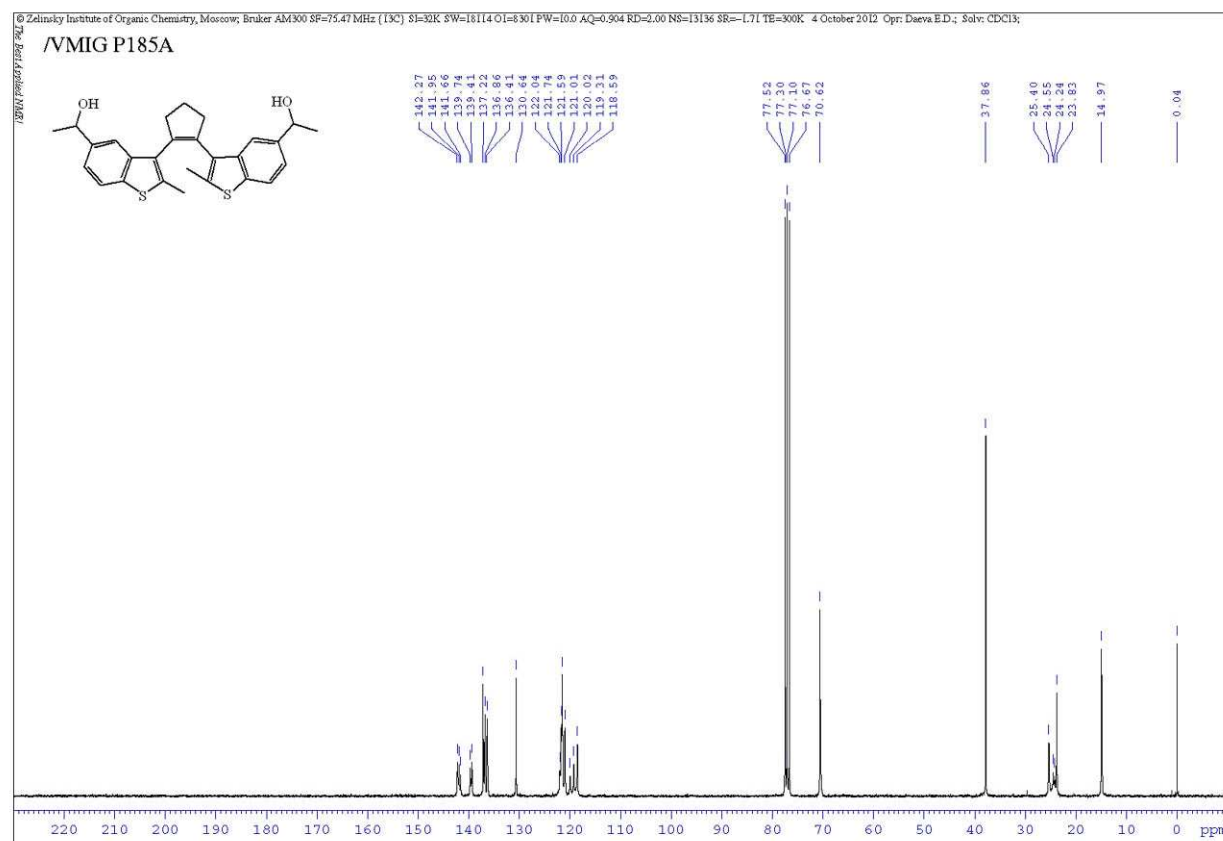


FIGURE S117. ^{13}C NMR spectrum of dibenzothienylethene **13** in CDCl_3 .

© N.D. Zelinsky Institute of Organic Chemistry (Moscow); Bruker Avance II 300 SP-300MHz[^2H -1] SI-32K SM-6402 01-2701 PW-7.5 RQ-2.471 RD-3.00 NS-1 SR-4.00 TB-300K 9 December 2011 22:43:49 Opt: Belyakov P.A.; Solv: CDCl_3 ;
/VMIG P168

The Best Applied NMR, Printed Dec 09 2011 22:44

N#Cc1ccc2c(c1)c3ccccc3c2-c4cc5c(cc4)sc(C)cc5C#N

150

79

1

2

3

14.4

ppm

S46

Chemical structure of compound 10 is shown in the top left corner. The structure is a dicyanide derivative of a fluorene-like system, specifically 1,1'-bis(cyano)-2,2'-bis(methylene)-5,5'-bibenzofuran.

¹H NMR spectrum (CDCl₃) of compound 10. The x-axis represents the chemical shift in ppm (f1), ranging from 1.9 to 8.1. The y-axis represents intensity, ranging from 0 to 110,000. The spectrum shows several peaks, with integration values provided below the baseline: 3.13, 3.12, 1.83, 3.11, 0.98, 1.05, 3.10, 1.91, 3.10, 6.79, and 8.87. A chemical structure of compound 10 is shown in the top left corner.

S47

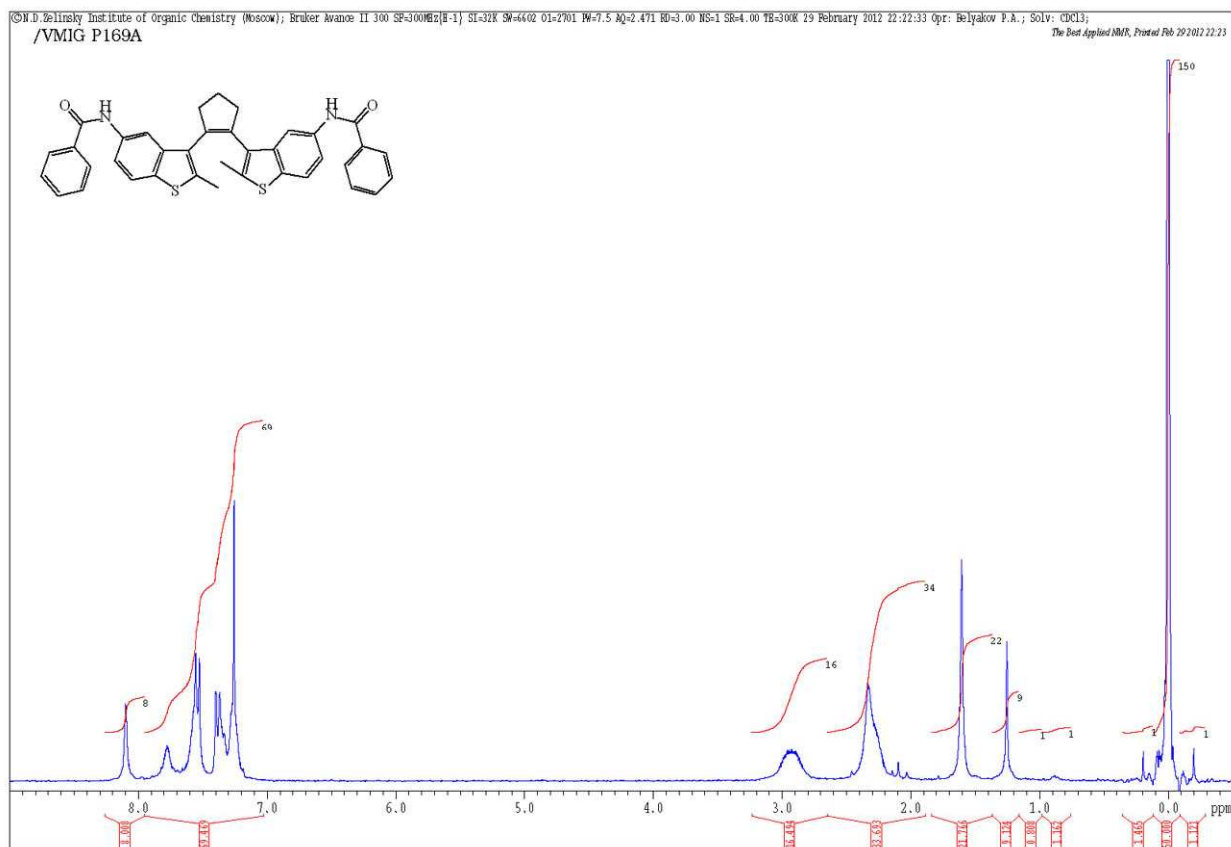


FIGURE S122. ¹H NMR spectrum of dibenzothienylethene **15** in CDCl₃.

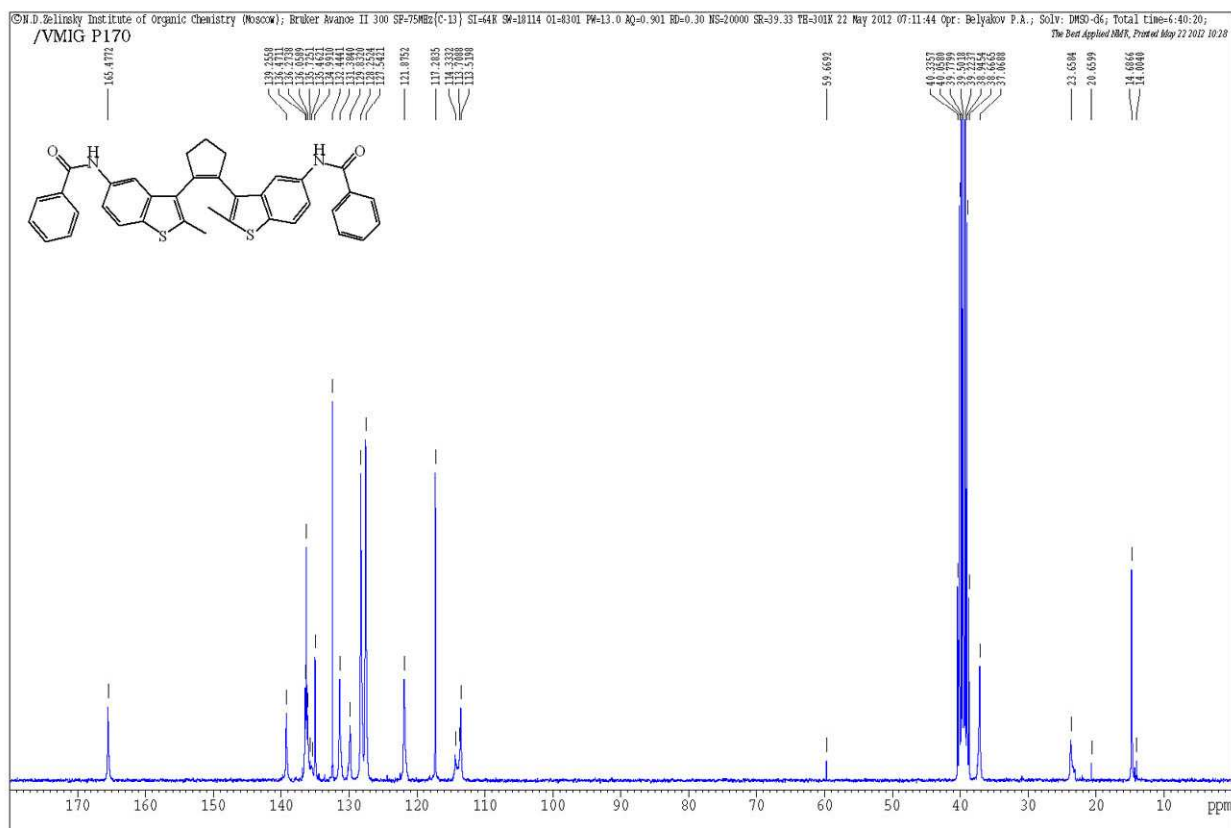


FIGURE S123. ¹³C NMR spectrum of dibenzothienylethene **15** in DMSO-*d*₆.

© Zelinsky Institute of Organic Chemistry, Moscow; Bruker AM300 SF=300.13 MHz (1H) S1=16K SW=6010 O1=2401 PW=15.0 AQ=L363 RD=L00 NS=1 SR=0.44 TE=299K 1 October 2012 Opr: Daeva E.D.; Solv: CDCl3;

VMIG P179

c1ccc(Oc2ccc3c(c2)sc(C4C(CCC4)c5ccc6c(c5)sc(C7C(CCC7)c8ccc(Oc9ccccc89)cc6)cc3)c

105

82

142

1.0

3.4

4.6

5.6

8.72

0.33

100.16

ppm

S49

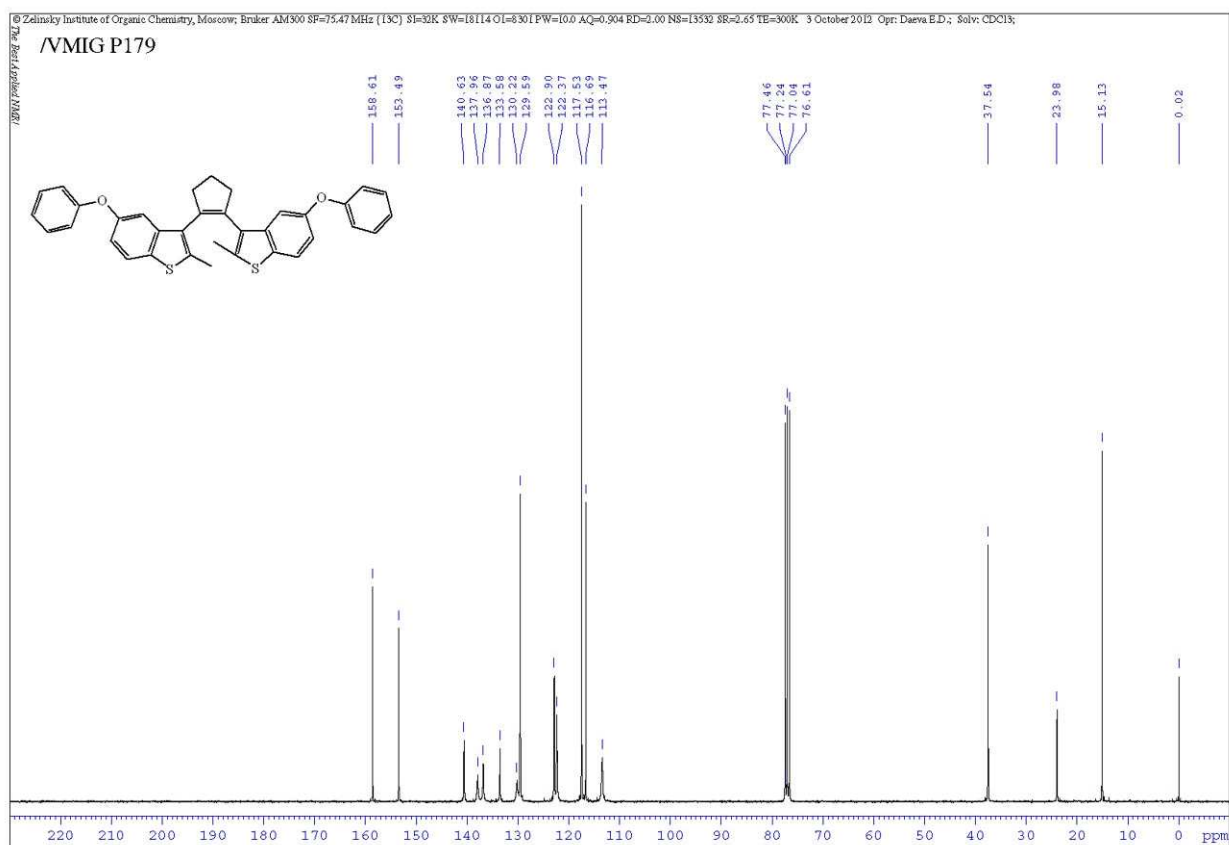


FIGURE S126. ^{13}C NMR spectrum of dibenzothiophene **16** in CDCl_3 .

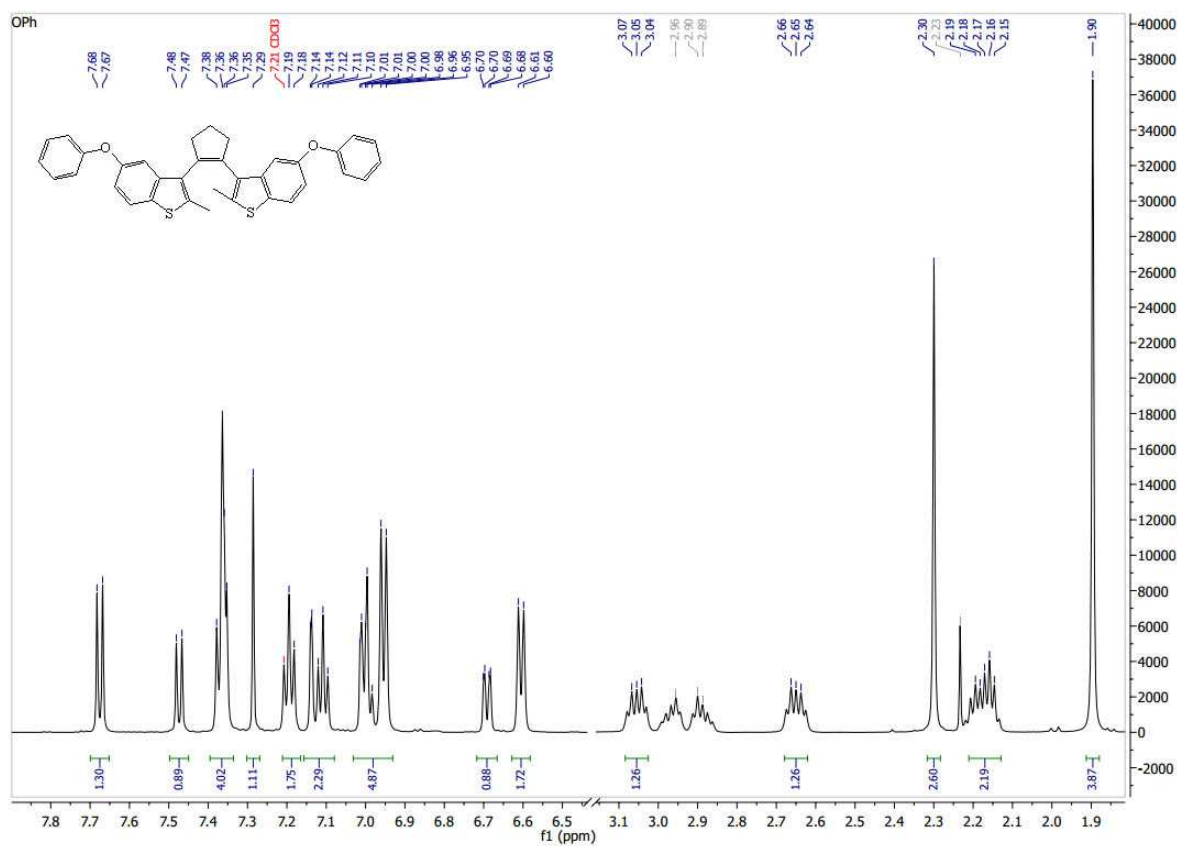


FIGURE S127. ^1H NMR spectrum of dibenzothiophene **16** at 600 MHz in CDCl_3 at 235 K.

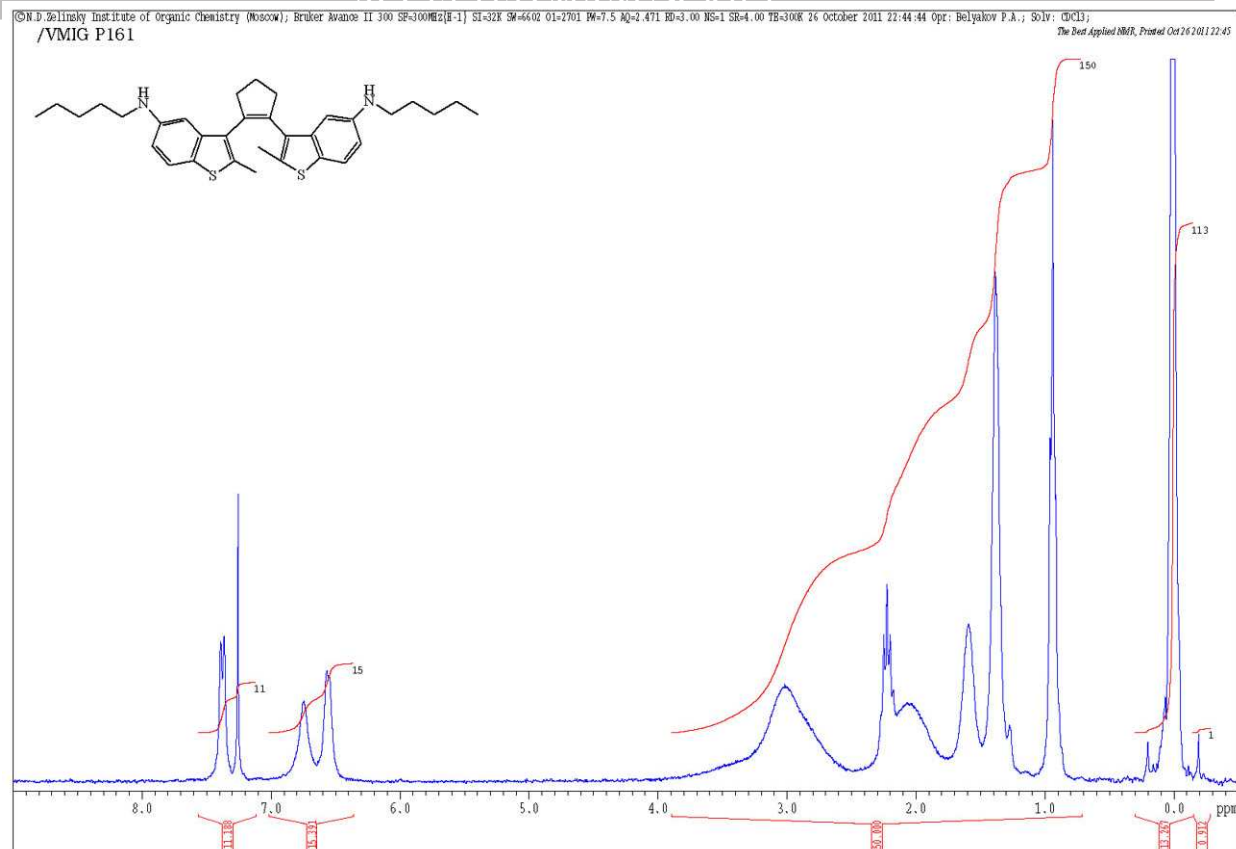


FIGURE S128. ^1H NMR spectrum of dibenzothienylethene **17** in CDCl_3 .

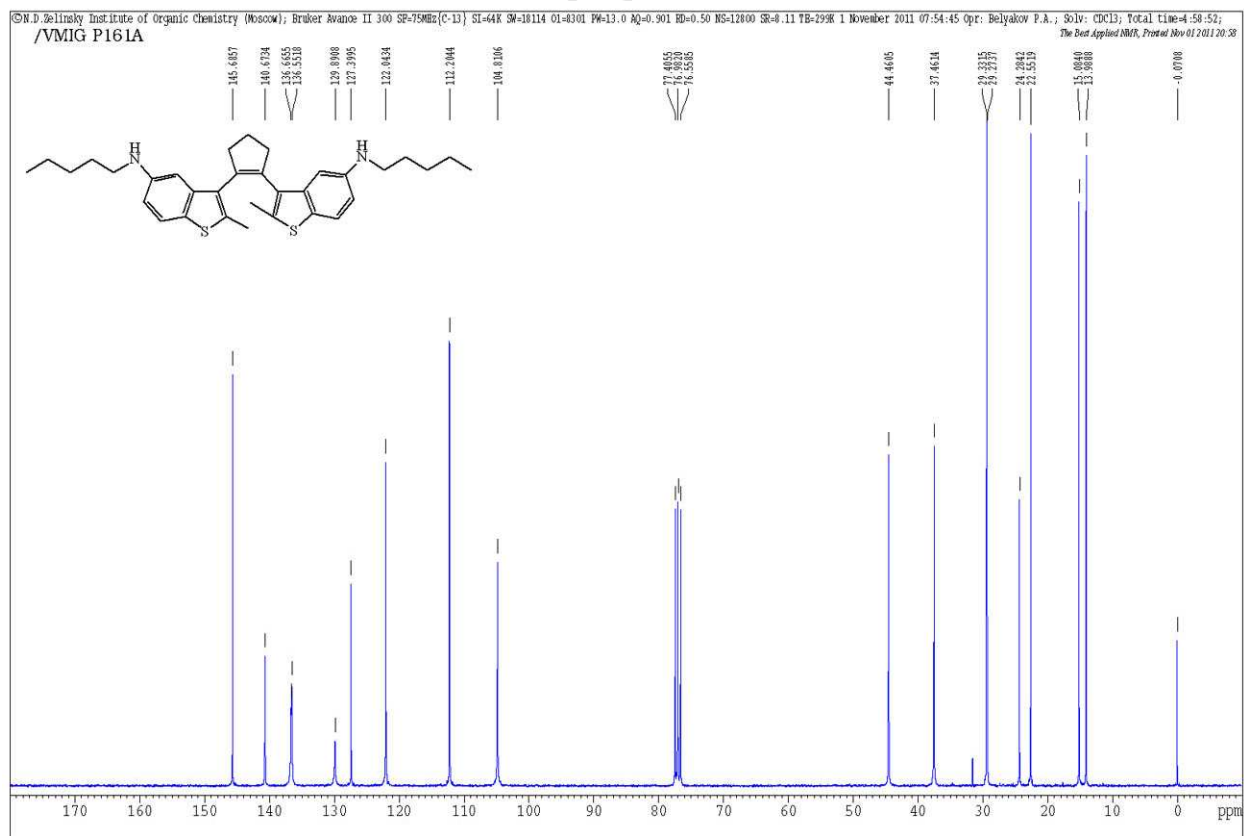


FIGURE S129. ^{13}C NMR spectrum of dibenzothienylethene **17** in CDCl_3 .

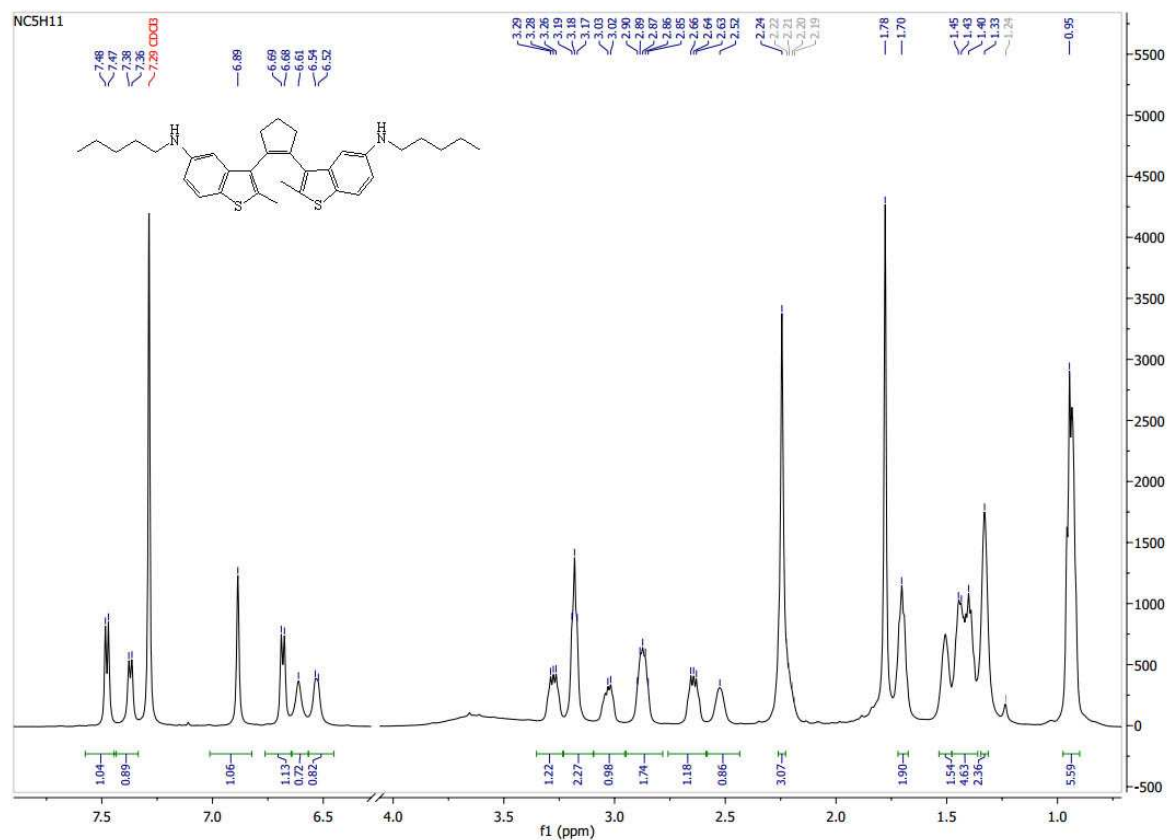


FIGURE S130. ^1H NMR spectrum of dibenzothienylethene **17** at 600 MHz in CDCl_3 at 235 K.

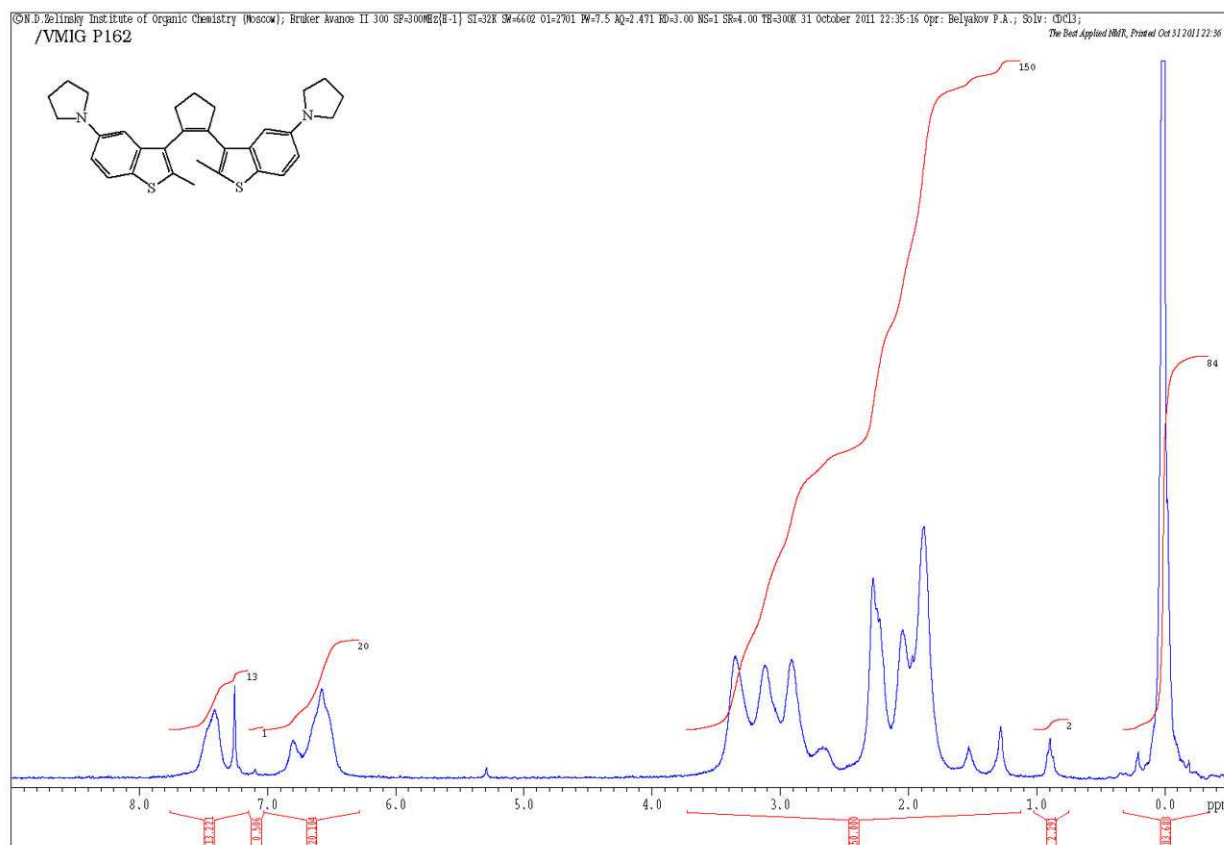


FIGURE S131. ^1H NMR spectrum of dibenzothienylethene **18** in CDCl_3 .

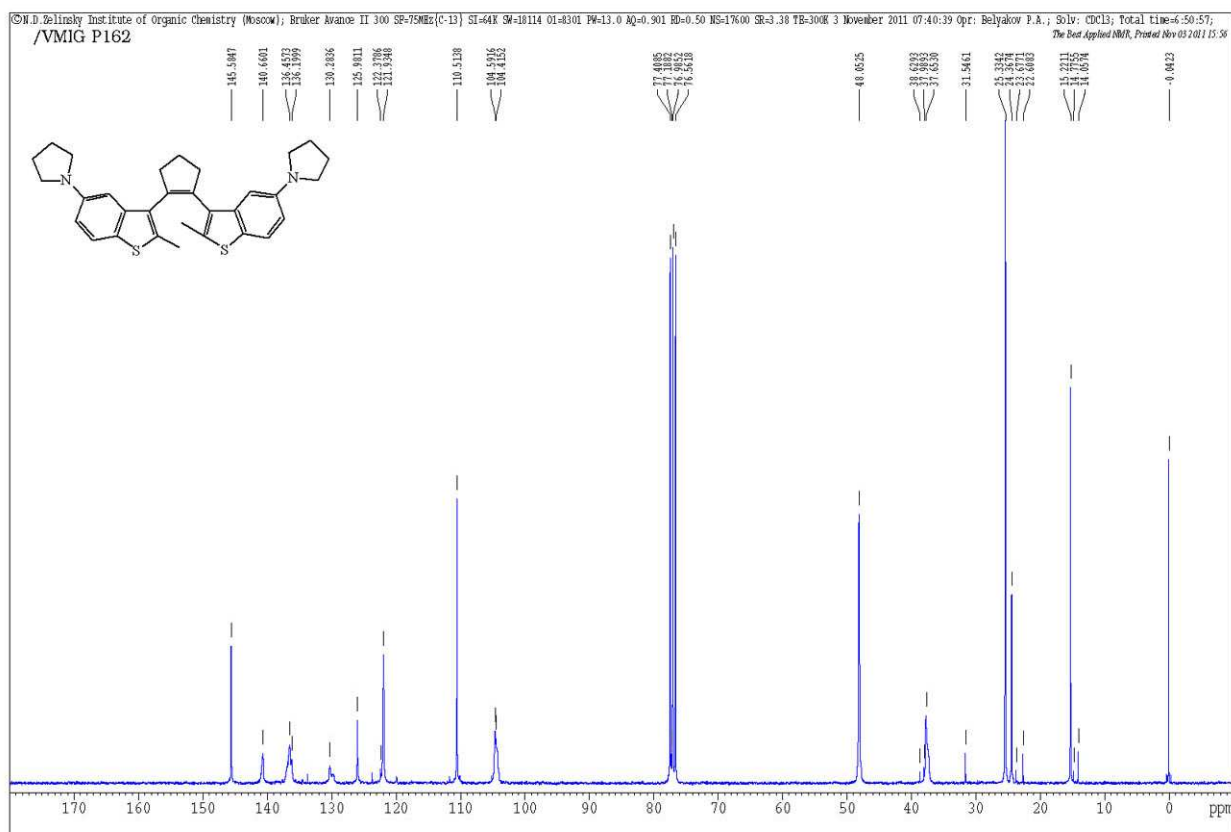


FIGURE S132. ¹³C NMR spectrum of dibenzothienylethene **18** in CDCl₃.

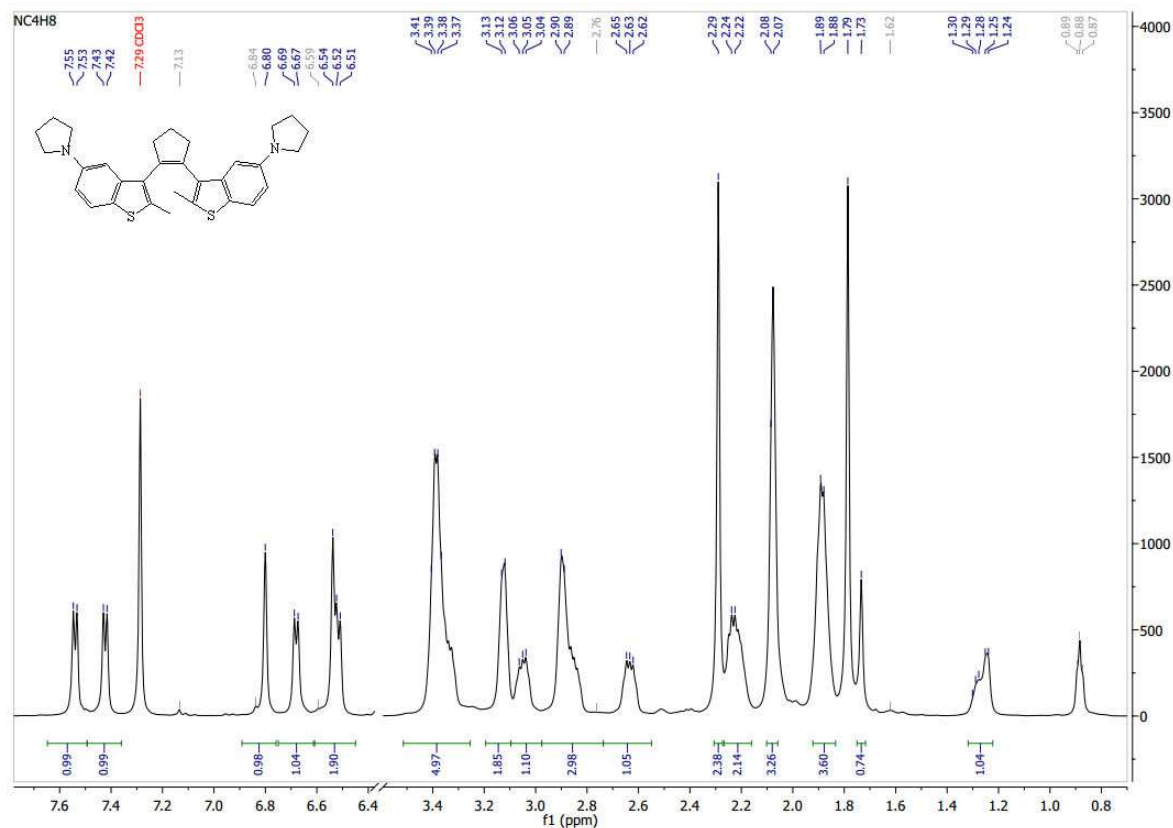


FIGURE S133. ¹H NMR spectrum of dibenzothienylethene **18** at 600 MHz in CDCl₃ at 235 K.

6. X-ray crystallography and computational data.

X-ray diffraction data were collected on a APEX II DUO CCD diffractometer using molybdenum radiation [$\lambda(\text{MoK}\alpha) = 0.71072 \text{ \AA}$, ω -scans] for **3**, **4**, **6**, **9**, **11**, **12**, **14**, **15**, **16** and using copper radiation [$\lambda(\text{CuK}\alpha) = 1.54178 \text{ \AA}$, ω -scans] for **18** at 100K. The substantial redundancy in data allowed empirical absorption correction to be applied with SADABS by multiple measurements of equivalent reflections. The structures were solved by direct methods and refined by the full-matrix least-squares technique against F^2 in the anisotropic-isotropic approximation. In **4**, **6**, **11** and **14**, the local C_2 symmetry led to a significant anisotropy of displacement parameters of the atom C(3C), which in case of **11** resulted in its disorder by two positions with equal occupancies. In **11**, the analysis of the Fourier maps has also revealed a disorder of the oxygen atom of the C=O group by two positions with the occupancies 0.630(2) and 0.370(2); the positional and anisotropic displacement parameters of these two components were refined with the constraints on the C=O bond length (DFIX) and anisotropic displacement parameters (EADP). Hydrogen atoms in all structures were placed in calculated positions and refined within the riding model. All calculations were performed with the SHELXTL software package.^{S1} Crystal data and structure refinement parameters are listed in Table 10. Crystallographic data (excluding structure factors) for the structures reported in this paper have been deposited to the Cambridge Crystallographic Data Centre as supplementary no.: CCDC-997775 (for **3**), CCDC-997776 (for **4**), CCDC-997777 (for **6**), CCDC-997778 (for **9**), CCDC-997779 (for **11**), CCDC-997780 (for **12**), CCDC-997781 (for **14**), CCDC-997782 (for **15**), CCDC-997783 (for **16**), CCDC-997784 (for **18**) These data can be obtained free of charge from The Cambridge Crystallographic Data via www.ccdc.cam.ac.uk/data_request/cif.

Dibenzothiénylcyclopentenenes

	3 (H)	4 (Cl)	6 (Br)	9 (I)	11 (CHO)
Formula	C ₂₃ H ₂₀ S ₂	C ₂₃ H ₁₇ Cl ₂ S ₂	C ₂₃ H ₁₇ Br ₂ S ₂	C ₂₃ H ₁₈ I ₂ S ₂	C ₂₅ H ₂₀ O ₂ S ₂
M	360.51	428.39	517.31	612.29	416.53
T, K	100	100	100	100	100
Crystal system	Orthorhombic	Orthorhombic	Orthorhombic	Monoclinic	Monoclinic
Space group	P2 ₁ 2 ₁ 2 ₁	Ccc2	Ccc2	P2 ₁ /c	C2/c
Z	4	4	4	4	4
a, Å	8.9614(4)	15.6594(11)	15.5976(13)	9.2763(3)	13.9038(12)
b, Å	11.7359(6)	15.6349(11)	16.0800(14)	19.9271(6)	7.5904(6)
c, Å	17.1964(8)	8.2392(6)	8.2883(7)	12.4670(4)	19.1707(16)
α, °	90.00	90.00	90.00	90.00	90.00
β, °	90.00	90.00	90.00	109.6888(14)	104.911(2)
γ, °	90.00	90.00	90.00	90.00	90.00
V, Å ³	1808.55(15)	2017.2(2)	2078.8(3)	2169.79(12)	1955.1(3)
D _{calc} , g·cm ⁻³	1.324	1.411	1.653	1.874	1.415
μ, cm ⁻¹	2.97	5.34	41.06	30.97	2.92
F(000)	760	884	1028	1176	872
2θ _{max} , °	58	57	57	62	55
Reflections measured	22084	11765	7178	43052	6942
Independent reflections (R _{int})	4805 (0.0256)	2665 (0.0214)	2723 (0.0254)	6923 (0.0323)	2284 (0.0295)
Observed reflections [I > 2σ(I)]	4617	2551	2464	6284	1951
Number of refined parameters	226	123	125	246	151
R1	0.0284	0.0243	0.0272	0.0203	0.0350
wR2	0.0799	0.0706	0.0670	0.0461	0.0980
GOF	1.058	1.016	1.002	1.062	0.972
Δρ _{max} , Δρ _{min} (e Å ⁻³)	0.318/-0.310	0.270/-0.174	0.733/-0.552	0.897/-0.462	0.615/-0.190

	12 (COMe)	14 (CN)	15 (NHCOPh)	16 (OPh)	18 (NC ₄ H ₈)
Formula	C ₂₇ H ₂₄ O ₂ S ₂	C ₂₅ H ₁₇ N ₂ S ₂	C ₃₇ H ₃₀ N ₂ O ₂ S ₂	C ₃₅ H ₂₈ O ₂ S ₂	C ₃₁ H ₃₄ N ₂ S ₂
M	444.58	409.53	598.75	544.69	498.72
T, K	100	100	100	100	100
Crystal system	Monoclinic	Orthorhombic	Orthorhombic	Triclinic	Monoclinic
Space group	P2 ₁ /n	Ccc2	P2 ₁ 2 ₁ 2 ₁	P-1	P2 ₁ /n
Z	4	4	4	2	4
a, Å	16.067(11)	15.5295(17)	9.2685(4)	11.0040(2)	12.058(3)
b, Å	8.288(6)	16.4148(18)	13.3989(6)	11.3396(2)	17.000(4)
c, Å	16.624(12)	8.1914(9)	24.3430(11)	13.1450(2)	12.473(3)
α, °	90.00	90.00	90.00	69.1450(8)	90.00
β, °	100.454(18)	90.00	90.00	76.3654(8)	93.288(4)
γ, °	90.00	90.00	90.00	62.5117(8)	90.00
V, Å ³	2177(3)	2088.1(4)	3023.1(2)	1354.69(4)	2552.7(9)
D _{calc} , g·cm ⁻³	1.356	1.303	1.316	1.335	1.298
μ, cm ⁻¹	2.67	2.68	2.13	2.29	20.52
F(000)	936	852	1256	572	1064
2θ _{max} , °	60	60	57	100	119
Reflections measured	27777	13203	37257	218785	31182
Independent reflections (Rint)	6359 (0.0283)	3049 (0.0564)	8044 (0.0312)	28154 (0.0302)	3723 (0.1134)
Observed reflections [I > 2σ(I)]	5475	2466	7593	22805	2673
Number of refined parameters	284	132	393	356	318
R1	0.0345	0.0422	0.0308	0.0443	0.0506
wR2	0.1037	0.1105	0.0875	0.1181	0.1473
GOF	1.026	1.065	1.039	0.998	1.030
Δρ _{max} , Δρ _{min} (e Å ⁻³)	0.512/-0.207	0.361/-0.231	0.282/-0.249	1.266/-0.590	0.392/-0.281

Multipole refinement for **16** was performed within the Hansen–Coppens formalism,^{S2} with a total pseudostatic charge density distribution $\rho(\mathbf{r})$ calculated as a sum of pseudoatomic charge densities. The refinement in this study was done with XD2006 software.^{S3} The multipole

expansion was truncated at the hexadecapole level ($l = 4$) for heavy atoms and at the octupole level ($l = 3$) for C and O atoms. For hydrogen atoms, only the populations of monopoles and D_{10} harmonics were refined. In each case, we used low-angle reflections with $\sin \theta/\lambda \leq 0.904 \text{ \AA}^{-1}$ to refine multipole parameters and high angle reflections with $\sin \theta/\lambda \geq 0.504 \text{ \AA}^{-1}$ to refine positions and anisotropic displacement parameters of heavy atoms. Multipole and monopole populations and corresponding κ coefficients in **16** were refined separately in the first steps of the refinement and together in the last steps. The overall quality of the experiment and the refinement was supported by analysis of differences of mean-squares displacement amplitudes (DMSDA) along interatomic vectors in molecule; those values did not exceed $9 \times 10^{-4} \text{ \AA}^{-2}$. Electron density residuals were randomly distributed in the unit cell of **16** and didn't exceed 0.36 e\AA^{-3} . The refinement for **16** was carried out against F and converged to $R = 0.0305$, $R_w = 0.0248$ and $GOF = 1.52$ (for 22613 merged reflections with $I > 3\sigma(I)$). The estimation of the kinetic energy $g(\mathbf{r})$ was based on the Kirzhnits's approximation^{S4} relating it to the values of the $\rho(\mathbf{r})$ and its derivatives: $g(\mathbf{r}) = (3/10)(3\pi^2)^{2/3}[\rho(\mathbf{r})]^{5/3} + (1/72)|\nabla\rho(\mathbf{r})|^2/\rho(\mathbf{r}) + 1/6\nabla^2\rho(\mathbf{r})$. The use of this relation in conjunction with the virial theorem ($2g(\mathbf{r}) + v(\mathbf{r}) = 1/4\nabla^2\rho(\mathbf{r})$) provided the value of the potential energy density $v(\mathbf{r})$ in a critical points from experimental diffraction data. For the critical point search in intermolecular areas, we have used the following procedure: 1) each atom has been surrounded by the cluster with the radii 6 \AA and each contact with distance up to 4 \AA has been analysed; 2) for all the critical points found, we have calculated bond paths to verify for what particular pair of atoms the interaction occurred. By means of this procedures, we have checked all interatomic interactions, and thus obtained the molecular graph for supramolecular organization. The topological analysis of the experimental $\rho(\mathbf{r})$ distribution and data visualization were performed with WinXPRO program suite.^{S5}

Topological analysis of the theoretical $\rho(\mathbf{r})$ distribution, as well as integration of $\rho(\mathbf{r})$ and its derivatives over atomic basis, was performed with AIMAll^{S6} and AIM2002^{S7} software packages.

TABLE S2. Selected bond lengths and angles in the crystal structures for dibenzothiénylcyclopentenenes with the parallel orientation of the benzothiophene rings according to XRD and DFT data.

Parameters	3 (H)		12 (COMe)		15 (NHCOPh)		18 (NC₄H₈)	
	XRD	DFT	XRD	DFT	XRD	DFT	XRD	DFT
C(1C)-C(5C), Å	1.347(2)	1.348	1.343(2)	1.346	1.338	1.344	1.354(5)	1.35
C(1C)-C(2), Å	1.478(2)	1.471	1.477(2)	1.472	1.475	1.464	1.471(5)	1.471
C(5C)-C(2'), Å	1.476(2)	1.467	1.477(2)	1.47	1.475	1.472	1.474(5)	1.467
C(1')C(2')C(5C)C(1C)	-62	-56.2	-60.8	60.8	61.7	63.8	-54.5	-54.6
C(1)C(2)C(5C)C(1C), °	129.5	126.7	115.5	120.8	124.9	119.6	130	127.6
C(2)C(1)C(1')C(2') °	17.4	21.3	11.1	14.2	13.9	17.1	22.7	24.9
Ω , °	70.7	65.8	69.5	69.6	73.4	70.9	64.2	63.9

Ω , ° - the dihedral angle between the benzothiophene rings

TABLE S3. Geometry parameters for the parallel orientation in the isolated state for dibenzothiénylcyclopentenenes **4** (Cl), **14** (CN), and **16** (OPh) according to DFT calculations (for comparison).

Parameters	4 (Cl)	14 (CN)	16 (OPh)
	DFT	DFT	DFT
C(1C)-C(5C), Å	1.348	1.349	1.348
C(1C)-C(2), Å	1.471	1.468	1.468
C(5C)-C(2'), Å	1.467	1.471	1.471
C(1')C(2')C(5C)C(1C)	56.5	56.2	55.5
C(1)C(2)C(5C)C(1C), °	126.3	127.1	125.4
C(2)C(1)C(1')C(2') °	21.5	22.1	20.6
Ω , °	64.4	62.6	65.7

Ω , ° - the dihedral angle between the benzothiophene rings

TABLE S4. Selected bond lengths and angles in the crystal structures for dibenzothiénylcyclopentenenes with the antiparallel orientation of the benzothiophene rings according to XRD and DFT data.

Parameters	4 (Cl)		6 (Br)		9 (I)	
	XRD	DFT	XRD	DFT	XRD	DFT
C(1C)-C(5C), Å	1.342(3)	1.348	1.334(5)	1.348	1.348(2)	1.348

C(1C)-C(2), Å	1.481(2)	1.468	1.481(4)	1.468	1.474(2)	1.468
C(5C)-C(2'), Å		1.469		1.469	1.481(2)	1.469
C(1')C(2')C(5C)C(1C)		55.2		55.4	62.9	55.4
C(1)C(2)C(5C)C(1C), °	127.9		130.3		125	
C(2)C(1)C(1')C(2') °	122.2	81.4	124.5	81.6	126.9	81.7
Ω , °	66.4	65.8	64.7	64.7	64	65.4
C(1)...C(1')	5.364(2)	3.659	5.401(4)	3.665	6.496	3.661

Parameters	11 (CHO)		14 (CN)		16 (OPh)	
	XRD	DFT	XRD	DFT	XRD	DFT
C(1C)-C(5C), Å	1.343(2)	1.347	1.339(4)	1.348	1.3541(7)	1.349
C(1C)-C(2), Å	1.477(2)	1.469	1.478(3)	1.468	1.4732(7)	1.468
C(5C)-C(2'), Å		1.470		1.469	1.4718(7)	1.468
C(1')C(2')C(5C)C(1C)	66	55.4		56.4	58.8	54.9
C(1)C(2)C(5C)C(1C), °		54.7	128.1		49.9	54.6
C(2)C(1)C(1')C(2') °	92.8	81.6	121.3	81.8	80.5	81.1
Ω , °	85.8	65.3	65.4	64.6	59.7	65.7
C(1)...C(1')	4.162	3.655	5.360(3)	3.671	3.570(1)	3.641

Ω , ° - the dihedral angle between the benzothiophene rings

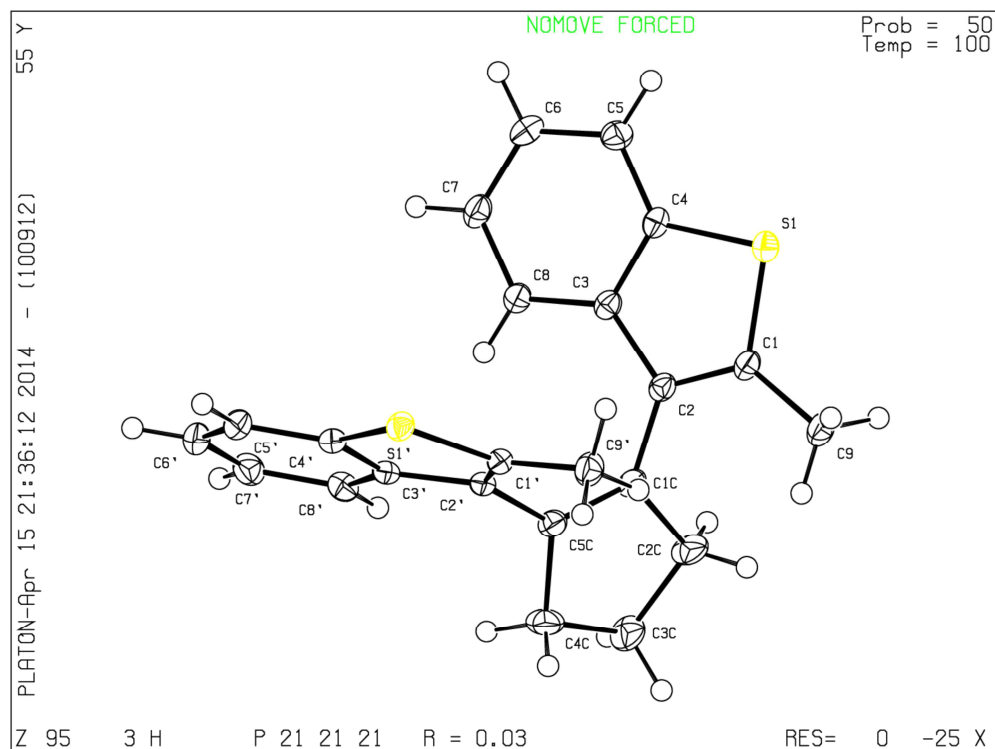


FIGURE 134. Ellipsoid plot for dibenzothiophene 3 (H).

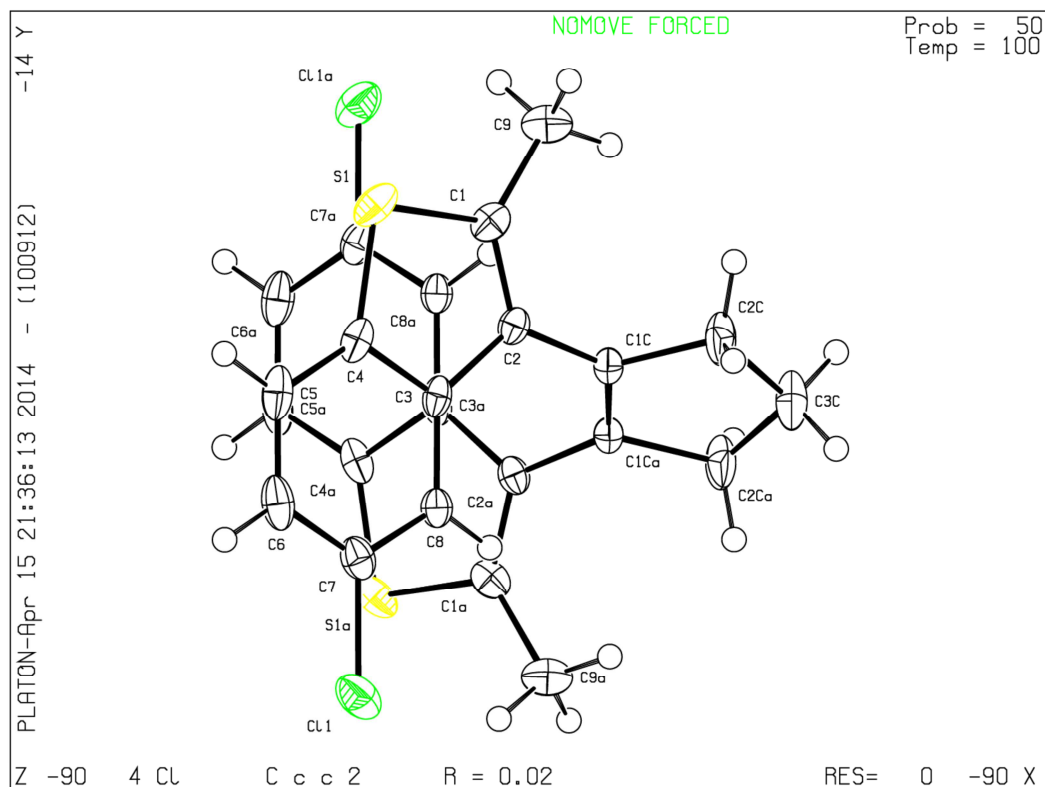


FIGURE 135. Ellipsoid plot for dibenzothienylethene **4** (Cl).

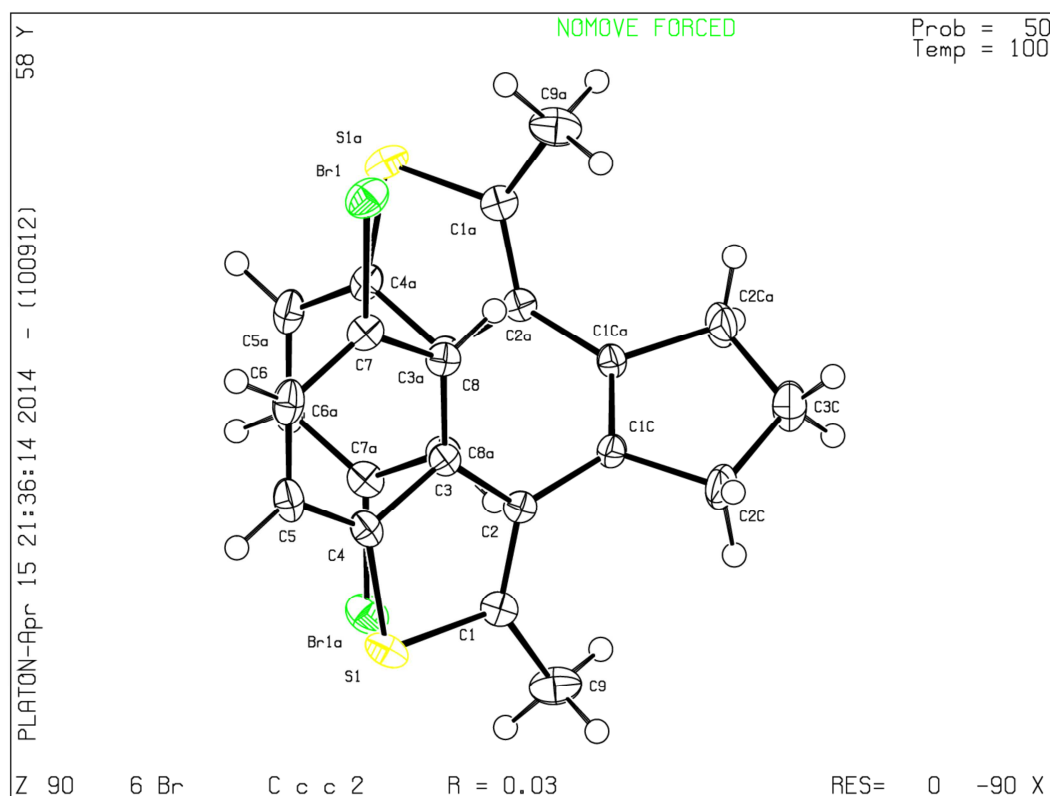


FIGURE 136. Ellipsoid plot for dibenzothienylethene **6** (Br).

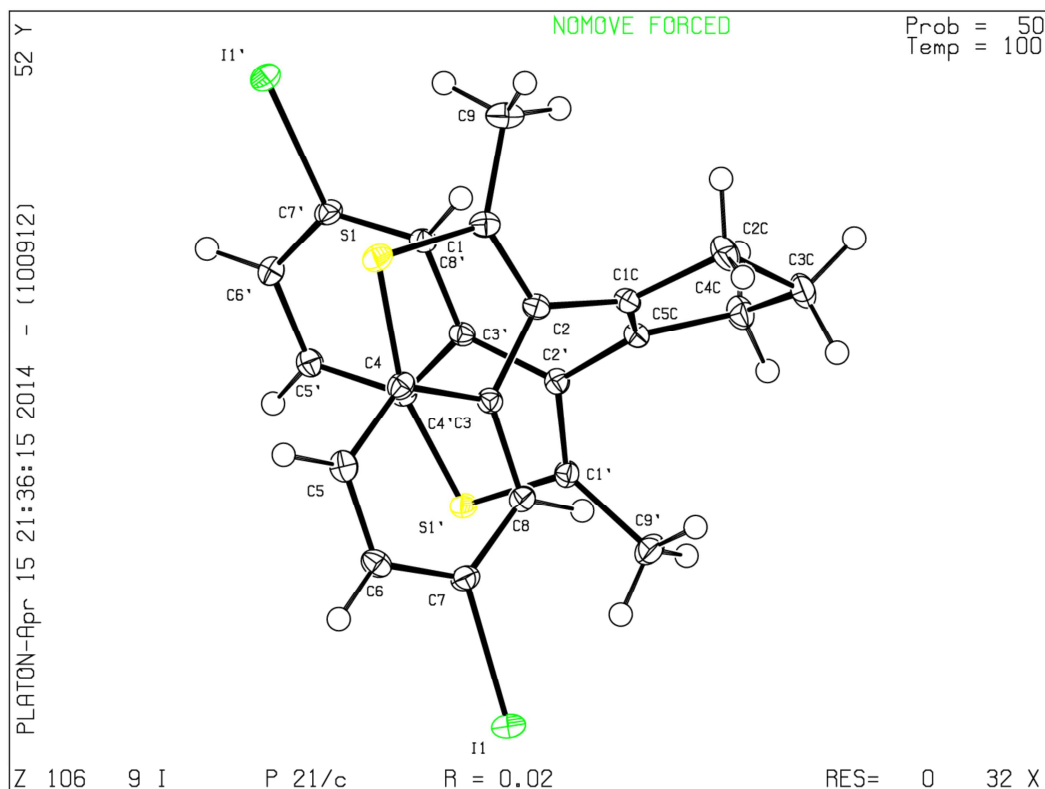


FIGURE 137. Ellipsoid plot for dibenzothiophene **9** (I).

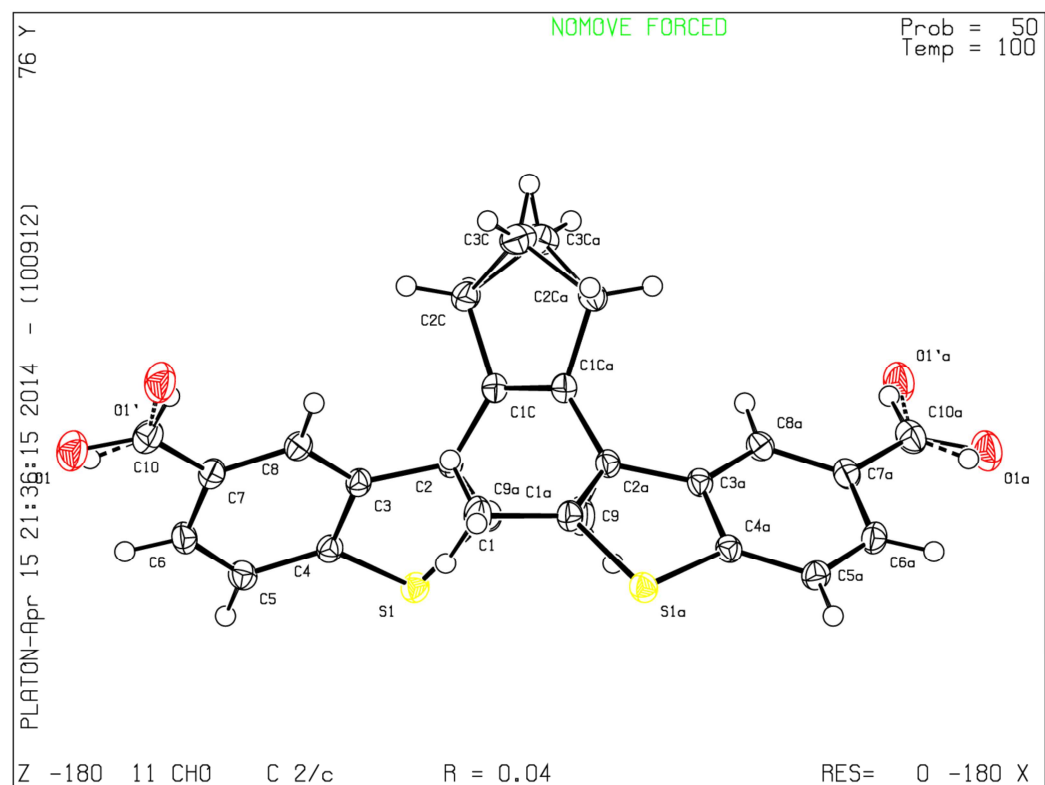


FIGURE 138. Ellipsoid plot for dibenzothiophene **11** (CHO).

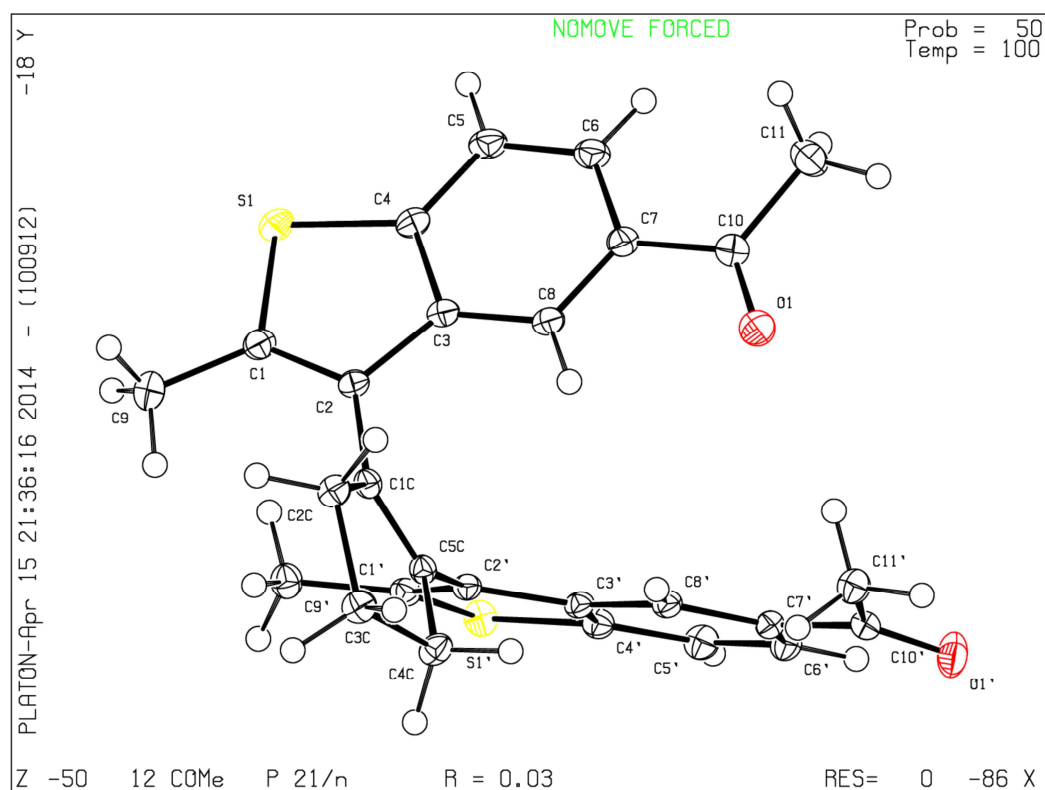


FIGURE 139. Ellipsoid plot for dibenzothiophene **12** (COMe).

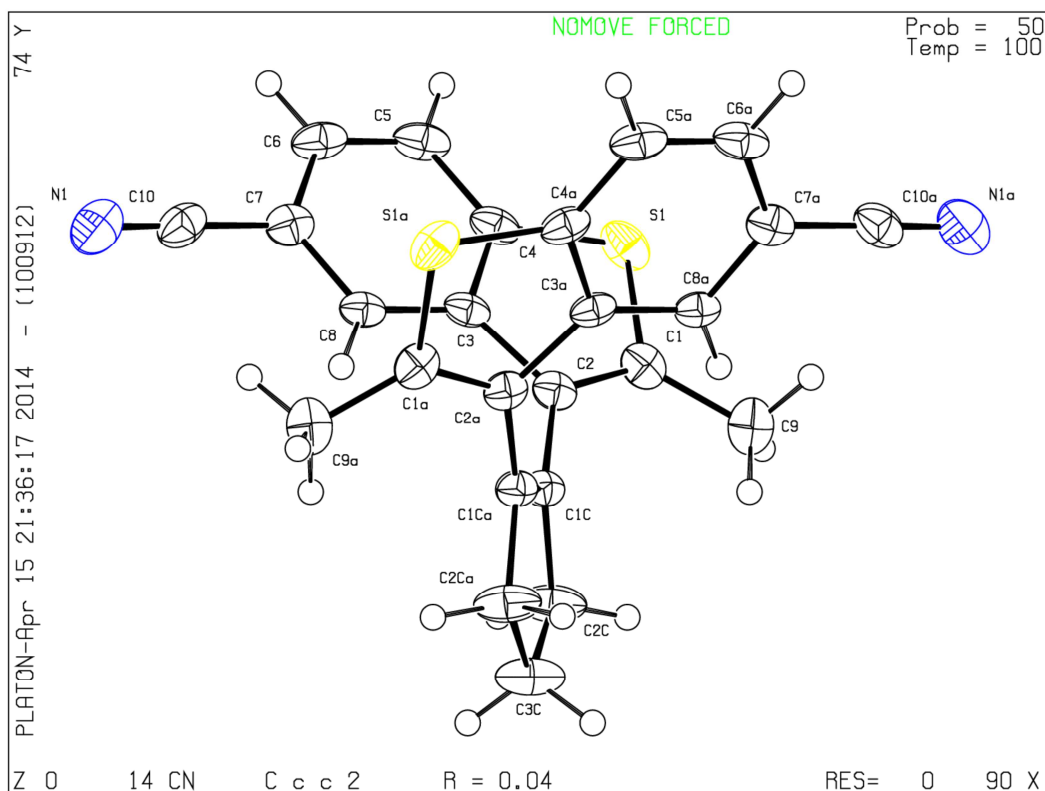


FIGURE 140. Ellipsoid plot for dibenzothiophene **14** (CN).

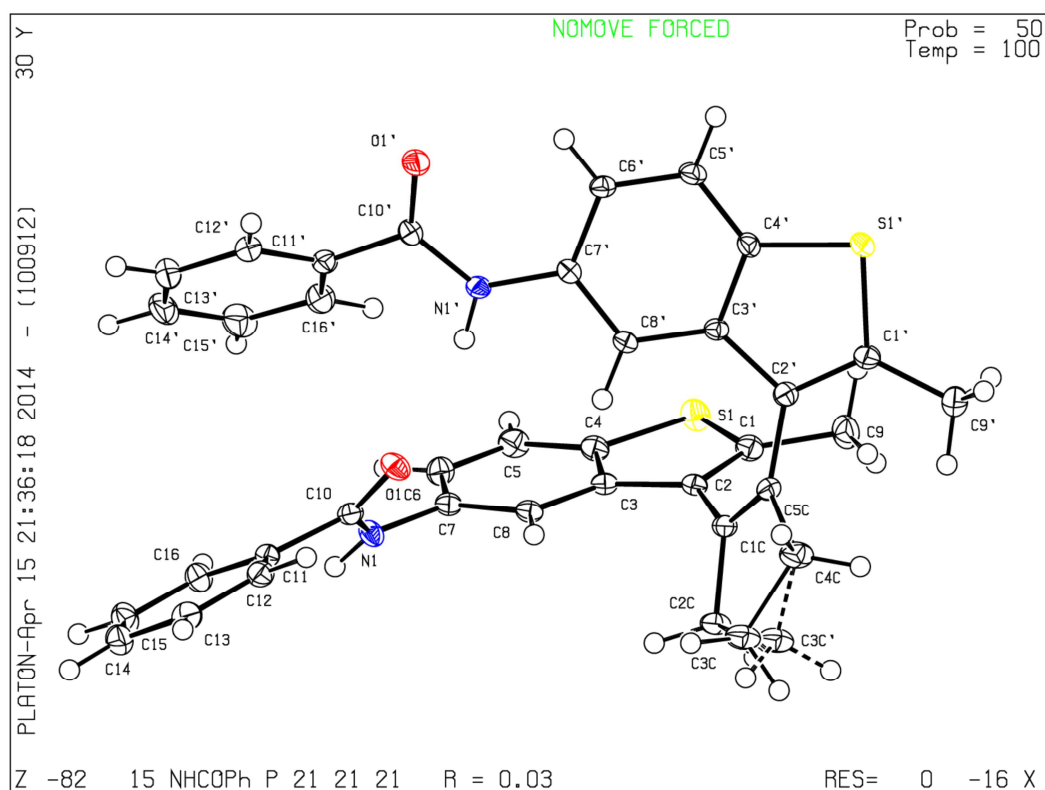


FIGURE 141. Ellipsoid plot for dibenzothienylethene **15** (NHCOPh).

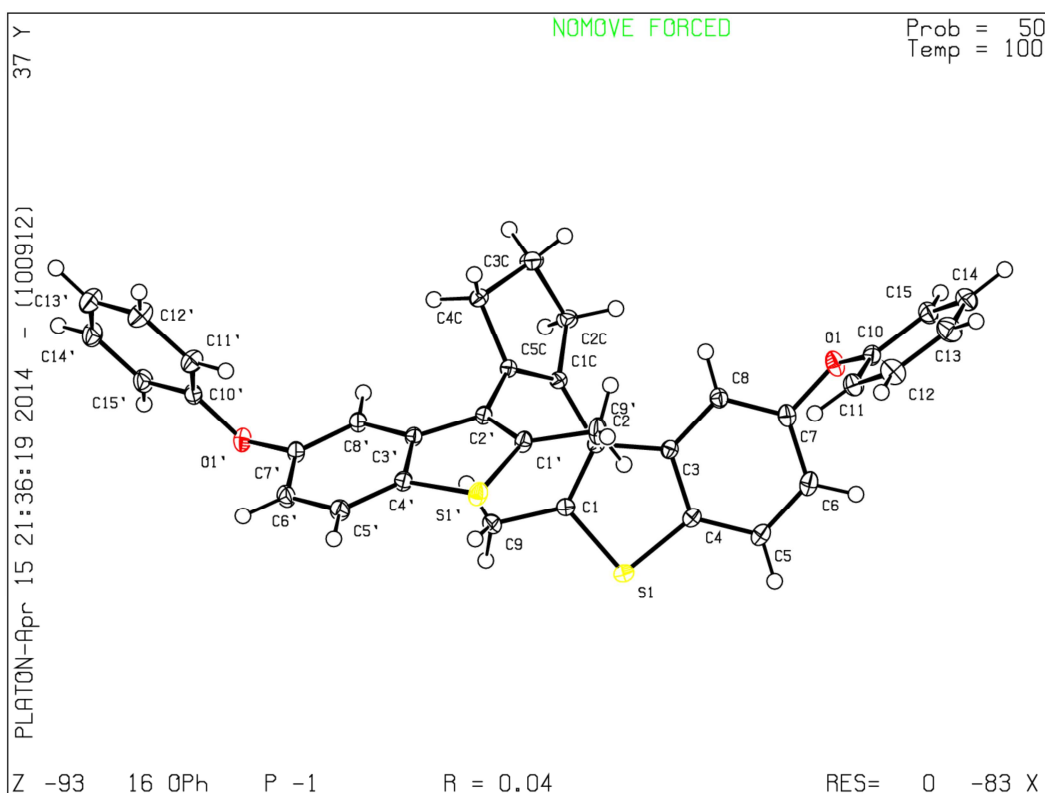


FIGURE 142. Ellipsoid plot for dibenzothienylethene **16** (OPh).

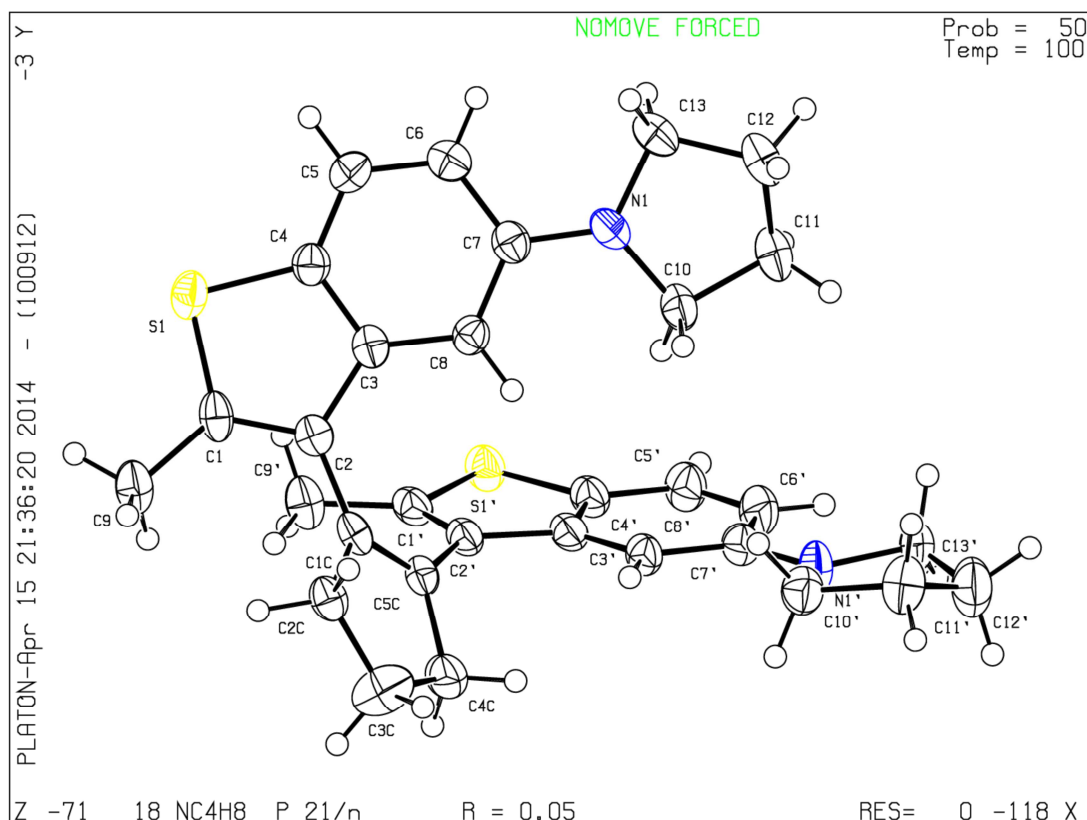


FIGURE 143. Ellipsoid plot for dibenzothienylethene **18** (NC₄H₈).

7. References.

- S1. G. M. Sheldrick, *Acta. Cryst.* **2008**, A64, 112-122.
- S2. N. K. Hansen, P. Coppens, *Acta Cryst.* **1978**, A34, 909-921.
- S3. A. Volkov, P. Macchi, L. J. Farrugia, C. Gatti, P. Mallinson, T. Richter, T. Koritsanszky, *XD2006 – A Computer Program Package for Multipole Refinement, Topological Analysis of Charge Densities and Evaluation of Intermolecular Energies from Experimental and Theoretical Structure Factors*, **2006**.
- S4. D. A. Kirzhnits, *Sov. Phys. JETP* **1957**, 5, 64-71.
- S5. A. Stash V. J. Tsirelson, *Appl. Cryst.* **2002**, 35, 371-373.
- S6. T. A. Keith, *AIMAll, Version 13.05.06*, **2013**.
- S7. F. Biegler-Konig, J. Schonbohm, D. Bayles, *J. Comput. Chem.* **2001**, 22, 545-559.

checkCIF/PLATON report

You have not supplied any structure factors. As a result the full set of tests cannot be run.

THIS REPORT IS FOR GUIDANCE ONLY. IF USED AS PART OF A REVIEW PROCEDURE FOR PUBLICATION, IT SHOULD NOT REPLACE THE EXPERTISE OF AN EXPERIENCED CRYSTALLOGRAPHIC REFEREE.

No syntax errors found. CIF dictionary Interpreting this report

Datablock: 3_H

Bond precision:	C-C = 0.0020 Å	Wavelength=0.71073	
Cell:	a=8.9614(4)	b=11.7359(6)	c=17.1964(8)
	alpha=90	beta=90	gamma=90
Temperature:	100 K		

	Calculated	Reported
Volume	1808.55(15)	1808.55(15)
Space group	P 21 21 21	P 21 21 21
Hall group	P 2ac 2ab	P 2ac 2ab
Moiety formula	C23 H20 S2	C23 H20 S2
Sum formula	C23 H20 S2	C23 H20 S2
Mr	360.53	360.51
Dx, g cm ⁻³	1.324	1.324
Z	4	4
Mu (mm ⁻¹)	0.297	0.297
F000	760.0	760.0
F000'	761.22	
h,k,lmax	12,16,23	12,16,23
Nref	4808[2729]	4805
Tmin,Tmax	0.928,0.942	0.916,0.943
Tmin'	0.915	

Correction method= MULTI-SCAN

Data completeness= 1.76/1.00	Theta(max)= 29.000
------------------------------	--------------------

R(reflections)= 0.0284(4617)	wR2(reflections)= 0.0799(4805)
-------------------------------	---------------------------------

S = 1.058	Npar= Npar = 226
-----------	------------------

The following ALERTS were generated. Each ALERT has the format
test-name_ALERT_alert-type_alert-level.
Click on the hyperlinks for more details of the test.

● **Alert level G**

PLAT005_ALERT_5_G	No _iucr_refine_instructions_details in the CIF	Please Do !
PLAT066_ALERT_1_G	Predicted and Reported Tmin&Tmax Range Identical	? Check
PLAT380_ALERT_4_G	Incorrectly? Oriented X(sp2)-Methyl Moiety	C9 Check
PLAT380_ALERT_4_G	Incorrectly? Oriented X(sp2)-Methyl Moiety	C9' Check
PLAT720_ALERT_4_G	Number of Unusual/Non-Standard Labels	13 Note

0 **ALERT level A** = Most likely a serious problem - resolve or explain
 0 **ALERT level B** = A potentially serious problem, consider carefully
 0 **ALERT level C** = Check. Ensure it is not caused by an omission or oversight
 5 **ALERT level G** = General information/check it is not something unexpected

1 ALERT type 1 CIF construction/syntax error, inconsistent or missing data
 0 ALERT type 2 Indicator that the structure model may be wrong or deficient
 0 ALERT type 3 Indicator that the structure quality may be low
 3 ALERT type 4 Improvement, methodology, query or suggestion
 1 ALERT type 5 Informative message, check

Datablock: 4_Cl

Bond precision:	C-C = 0.0019 A	Wavelength=0.71073
Cell:	a=15.6594(11) alpha=90	b=15.6349(11) beta=90
Temperature:	100 K	c=8.2392(6) gamma=90
	Calculated	Reported
Volume	2017.2(2)	2017.2(2)
Space group	C c c 2	C c c 2
Hall group	C 2 -2c	C 2 -2c
Moiety formula	C23 H17 Cl2 S2	C23 H17 Cl2 S2
Sum formula	C23 H17 Cl2 S2	C23 H17 Cl2 S2
Mr	428.41	428.39
Dx,g cm-3	1.411	1.411
Z	4	4
Mu (mm-1)	0.534	0.534
F000	884.0	884.0
F000'	886.42	
h,k,lmax	21,21,11	21,21,11
Nref	2669[1429]	2665
Tmin,Tmax	0.914,0.943	0.856,0.944
Tmin'	0.852	

Correction method= MULTI-SCAN

Data completeness= 1.86/1.00 Theta(max)= 28.990

R(reflections)= 0.0243(2551) wR2(reflections)= 0.0706(2665)

S = 1.016

Npar= Npar = 123

The following ALERTS were generated. Each ALERT has the format

test-name_ALERT_alert-type_alert-level.

Click on the hyperlinks for more details of the test.

● Alert level G

PLAT005_ALERT_5_G No _iucr_refine_instructions_details in the CIF Please Do !
 PLAT066_ALERT_1_G Predicted and Reported Tmin&Tmax Range Identical ? Check
 PLAT380_ALERT_4_G Incorrectly? Oriented X(sp2)-Methyl Moiety C9 Check
 PLAT720_ALERT_4_G Number of Unusual/Non-Standard Labels 3 Note

- 0 **ALERT level A** = Most likely a serious problem - resolve or explain
 0 **ALERT level B** = A potentially serious problem, consider carefully
 0 **ALERT level C** = Check. Ensure it is not caused by an omission or oversight
 4 **ALERT level G** = General information/check it is not something unexpected
- 1 ALERT type 1 CIF construction/syntax error, inconsistent or missing data
 0 ALERT type 2 Indicator that the structure model may be wrong or deficient
 0 ALERT type 3 Indicator that the structure quality may be low
 2 ALERT type 4 Improvement, methodology, query or suggestion
 1 ALERT type 5 Informative message, check

Datablock: 6_Br

Bond precision: C-C = 0.0038 Å

Wavelength=0.71073

Cell: a=15.5976(13) b=16.0800(14) c=8.2883(7)
 alpha=90 beta=90 gamma=90
 Temperature: 100 K

	Calculated	Reported
Volume	2078.8(3)	2078.8(3)
Space group	C c c 2	C c c 2
Hall group	C 2 -2c	C 2 -2c
Moiety formula	C23 H17 Br2 S2	C23 H17 Br2 S2
Sum formula	C23 H17 Br2 S2	C23 H17 Br2 S2
Mr	517.31	517.31
Dx, g cm ⁻³	1.653	1.653
Z	4	4
Mu (mm ⁻¹)	4.106	4.106
F000	1028.0	1028.0
F000'	1027.06	
h,k,lmax	21,21,11	21,21,11
Nref	2762[1478]	2723
Tmin,Tmax	0.335,0.389	0.260,0.452
Tmin'	0.152	

Correction method= MULTI-SCAN

Data completeness= 1.84/0.99 Theta(max)= 28.990

R(reflections)= 0.0272(2464) wR2(reflections)= 0.0670(2723)

S = 1.002 Npar= Npar = 125

The following ALERTS were generated. Each ALERT has the format

test-name_ALERT_alert-type_alert-level.

Click on the hyperlinks for more details of the test.

● Alert level G

PLAT005_ALERT_5_G No _iucr_refine_instructions_details in the CIF Please Do !
 PLAT720_ALERT_4_G Number of Unusual/Non-Standard Labels 3 Note

- 0 **ALERT level A** = Most likely a serious problem - resolve or explain
- 0 **ALERT level B** = A potentially serious problem, consider carefully
- 0 **ALERT level C** = Check. Ensure it is not caused by an omission or oversight
- 2 **ALERT level G** = General information/check it is not something unexpected

- 0 ALERT type 1 CIF construction/syntax error, inconsistent or missing data
- 0 ALERT type 2 Indicator that the structure model may be wrong or deficient
- 0 ALERT type 3 Indicator that the structure quality may be low
- 1 ALERT type 4 Improvement, methodology, query or suggestion
- 1 ALERT type 5 Informative message, check

Datablock: 9_I

Bond precision: C-C = 0.0020 Å

Wavelength=0.71073

Cell: a=9.2763(3) b=19.9271(6) c=12.4670(4)

 alpha=90 beta=109.6888(14) gamma=90

Temperature: 100 K

	Calculated	Reported
Volume	2169.79(12)	2169.79(12)
Space group	P 21/c	P 21/c
Hall group	-P 2ybc	-P 2ybc
Moiety formula	C23 H18 I2 S2	C23 H18 I2 S2
Sum formula	C23 H18 I2 S2	C23 H18 I2 S2
Mr	612.31	612.29
Dx,g cm-3	1.874	1.874
Z	4	4
Mu (mm-1)	3.097	3.097
F000	1176.0	1176.0
F000'	1173.54	
h,k,lmax	13,28,18	13,28,18
Nref	6923	6923
Tmin,Tmax	0.446,0.591	0.363,0.621
Tmin'	0.278	

Correction method= MULTI-SCAN

Data completeness= 1.000

Theta(max)= 31.000

R(reflections)= 0.0203(6284)

wR2(reflections)= 0.0461(6923)

S = 1.062

Npar= Npar = 246

The following ALERTS were generated. Each ALERT has the format

test-name_ALERT_alert-type_alert-level.

Click on the hyperlinks for more details of the test.



Alert level G

PLAT005_ALERT_5_G No _iucr_refine_instructions_details in the CIF Please Do !
 PLAT720_ALERT_4_G Number of Unusual/Non-Standard Labels 12 Note

- 0 **ALERT level A** = Most likely a serious problem - resolve or explain
 - 0 **ALERT level B** = A potentially serious problem, consider carefully
 - 0 **ALERT level C** = Check. Ensure it is not caused by an omission or oversight
 - 2 **ALERT level G** = General information/check it is not something unexpected
-
- 0 ALERT type 1 CIF construction/syntax error, inconsistent or missing data
 - 0 ALERT type 2 Indicator that the structure model may be wrong or deficient
 - 0 ALERT type 3 Indicator that the structure quality may be low
 - 1 ALERT type 4 Improvement, methodology, query or suggestion
 - 1 ALERT type 5 Informative message, check

Datablock: 11_CHO

Bond precision: C-C = 0.0020 Å

Wavelength=0.71073

Cell: a=13.9038(12) b=7.5904(6) c=19.1707(16)
 alpha=90 beta=104.911(2) gamma=90
 Temperature: 100 K

	Calculated	Reported
Volume	1955.1(3)	1955.1(3)
Space group	C 2/c	C 2/c
Hall group	-C 2yc	-C 2yc
Moiety formula	C25 H20 O2 S2	C25 H20 O2 S2
Sum formula	C25 H20 O2 S2	C25 H20 O2 S2
Mr	416.55	416.53
Dx,g cm-3	1.415	1.415
Z	4	4
Mu (mm-1)	0.292	0.292
F000	872.0	872.0
F000'	873.32	
h,k,lmax	18,9,25	18,9,25
Nref	2297	2284
Tmin,Tmax	0.936,0.957	0.915,0.958
Tmin'	0.913	

Correction method= MULTI-SCAN

Data completeness= 0.994

Theta(max)= 27.730

R(reflections)= 0.0350(1951)

wR2(reflections)= 0.0980(2284)

S = 0.972

Npar= Npar = 151

The following ALERTS were generated. Each ALERT has the format

test-name_ALERT_alert-type_alert-level.

Click on the hyperlinks for more details of the test.

Alert level B

PLAT390_ALERT_3_B Deviating Methyl C3C X-C-H Bond Angle 119 Degree

Alert level C

PLAT094_ALERT_2_C Ratio of Maximum / Minimum Residual Density 3.24 Why ?
 PLAT390_ALERT_3_C Deviating Methyl C3C X-C-H Bond Angle 117 Degree

Alert level G

PLAT005_ALERT_5_G No _iucr_refine_instructions_details in the CIF Please Do !
 PLAT066_ALERT_1_G Predicted and Reported Tmin&Tmax Range Identical ? Check
 PLAT301_ALERT_3_G Main Residue Disorder Percentage = 10 Note
 PLAT720_ALERT_4_G Number of Unusual/Non-Standard Labels 4 Note

0 **ALERT level A** = Most likely a serious problem - resolve or explain

1 **ALERT level B** = A potentially serious problem, consider carefully

- 2 **ALERT level C** = Check. Ensure it is not caused by an omission or oversight
 4 **ALERT level G** = General information/check it is not something unexpected
- 1 ALERT type 1 CIF construction/syntax error, inconsistent or missing data
 1 ALERT type 2 Indicator that the structure model may be wrong or deficient
 3 ALERT type 3 Indicator that the structure quality may be low
 1 ALERT type 4 Improvement, methodology, query or suggestion
 1 ALERT type 5 Informative message, check

Datablock: 12_COMe

Bond precision: C-C = 0.0019 Å Wavelength=0.71073

Cell: a=16.067(11) b=8.288(6) c=16.624(12)
 alpha=90 beta=100.454(18) gamma=90

Temperature: 100 K

	Calculated	Reported
Volume	2177(3)	2177(3)
Space group	P 21/n	P 21/n
Hall group	-P 2yn	-P 2yn
Moiety formula	C27 H24 O2 S2	C27 H24 O2 S2
Sum formula	C27 H24 O2 S2	C27 H24 O2 S2
Mr	444.60	444.58
Dx,g cm-3	1.357	1.356
Z	4	4
Mu (mm-1)	0.267	0.267
F000	936.0	936.0
F000'	937.34	
h,k,lmax	22,11,23	22,11,23
Nref	6359	6359
Tmin,Tmax	0.935,0.963	0.919,0.964
Tmin'	0.918	

Correction method= MULTI-SCAN

Data completeness= 1.000 Theta(max)= 30.000

R(reflections)= 0.0345(5475) wR2(reflections)= 0.1037(6359)

S = 1.026 Npar= Npar = 284

The following ALERTS were generated. Each ALERT has the format
test-name_ALERT_alert-type_alert-level.
 Click on the hyperlinks for more details of the test.



Alert level C

PLAT094_ALERT_2_C Ratio of Maximum / Minimum Residual Density 2.47 Why ?

Alert level G

PLAT005_ALERT_5_G No _iucr_refine_instructions_details in the CIF Please Do !
 PLAT066_ALERT_1_G Predicted and Reported Tmin&Tmax Range Identical ? Check
 PLAT720_ALERT_4_G Number of Unusual/Non-Standard Labels 12 Note

0 **ALERT level A** = Most likely a serious problem - resolve or explain
 0 **ALERT level B** = A potentially serious problem, consider carefully
 1 **ALERT level C** = Check. Ensure it is not caused by an omission or oversight
 3 **ALERT level G** = General information/check it is not something unexpected

1 ALERT type 1 CIF construction/syntax error, inconsistent or missing data
 1 ALERT type 2 Indicator that the structure model may be wrong or deficient
 0 ALERT type 3 Indicator that the structure quality may be low
 1 ALERT type 4 Improvement, methodology, query or suggestion
 1 ALERT type 5 Informative message, check

Datablock: 14_CN

Bond precision: C-C = 0.0029 Å Wavelength=0.71073

Cell: a=15.5295(17) b=16.4148(18) c=8.1914(9)
 alpha=90 beta=90 gamma=90

Temperature: 100 K

	Calculated	Reported
Volume	2088.1(4)	2088.1(4)
Space group	C c c 2	C c c 2
Hall group	C 2 -2c	C 2 -2c
Moiety formula	C25 H17 N2 S2	C25 H17 N2 S2
Sum formula	C25 H17 N2 S2	C25 H17 N2 S2
Mr	409.55	409.53
Dx, g cm ⁻³	1.303	1.303
Z	4	4
Mu (mm ⁻¹)	0.268	0.268
F000	852.0	852.0
F000'	853.25	
h,k,lmax	21,23,11	21,23,11
Nref	3055[1631]	3049
Tmin,Tmax	0.935,0.961	0.919,0.961
Tmin'	0.918	

Correction method= MULTI-SCAN

Data completeness= 1.87/1.00 Theta(max)= 30.080

R(reflections)= 0.0422(2466) wR2(reflections)= 0.1105(3049)

S = 1.065

Npar= Npar = 132

The following ALERTS were generated. Each ALERT has the format

test-name_ALERT_alert-type_alert-level.

Click on the hyperlinks for more details of the test.

● Alert level G

```
PLAT005_ALERT_5_G No _iucr_refine_instructions_details in the CIF Please Do !
PLAT066_ALERT_1_G Predicted and Reported Tmin&Tmax Range Identical ? Check
PLAT380_ALERT_4_G Incorrectly? Oriented X(sp2)-Methyl Moiety ..... C9 Check
PLAT710_ALERT_4_G Delete 1-2-3 or 2-3-4 Linear Torsion Angle ... # 33 Do !
      C8 -C7 -C10 -N1      13.00 14.00  1.555  1.555  1.555  1.555
PLAT710_ALERT_4_G Delete 1-2-3 or 2-3-4 Linear Torsion Angle ... # 34 Do !
      C6 -C7 -C10 -N1      17.00  0.00  1.555  1.555  1.555  1.555
PLAT720_ALERT_4_G Number of Unusual/Non-Standard Labels ..... 3 Note
```

```
0 ALERT level A = Most likely a serious problem - resolve or explain
0 ALERT level B = A potentially serious problem, consider carefully
0 ALERT level C = Check. Ensure it is not caused by an omission or oversight
6 ALERT level G = General information/check it is not something unexpected

1 ALERT type 1 CIF construction/syntax error, inconsistent or missing data
0 ALERT type 2 Indicator that the structure model may be wrong or deficient
0 ALERT type 3 Indicator that the structure quality may be low
4 ALERT type 4 Improvement, methodology, query or suggestion
1 ALERT type 5 Informative message, check
```

Datablock: 15_NHCOPh

```
Bond precision:  C-C = 0.0019 A      Wavelength=0.71073

Cell:            a=9.2685(4)      b=13.3989(6)      c=24.3430(11)
                  alpha=90        beta=90            gamma=90
Temperature:     100 K
```

	Calculated	Reported
Volume	3023.1(2)	3023.1(2)
Space group	P 21 21 21	P 21 21 21
Hall group	P 2ac 2ab	P 2ac 2ab
Moiety formula	C37 H30 N2 O2 S2	C37 H30 N2 O2 S2
Sum formula	C37 H30 N2 O2 S2	C37 H30 N2 O2 S2
Mr	598.77	598.75
Dx,g cm-3	1.316	1.316
Z	4	4
Mu (mm-1)	0.213	0.213
F000	1256.0	1256.0
F000'	1257.45	
h,k,lmax	12,18,33	12,18,33
Nref	8041[4500]	8044
Tmin,Tmax	0.929,0.944	0.916,0.945
Tmin'	0.914	

Correction method= MULTI-SCAN

Data completeness= 1.79/1.00 Theta(max)= 28.990

R(reflections)= 0.0308(7593) wR2(reflections)= 0.0875(8044)

S = 1.039 Npar= Npar = 393

The following ALERTS were generated. Each ALERT has the format

test-name_ALERT_alert-type_alert-level.

Click on the hyperlinks for more details of the test.

Alert level B

PLAT410_ALERT_2_B Short Intra H...H Contact H4CB .. H3CD .. 1.84 Ang.

Alert level C

PLAT410_ALERT_2_C Short Intra H...H Contact H2CB .. H3CD .. 1.98 Ang.

Alert level G

PLAT005_ALERT_5_G No _iucr_refine_instructions_details in the CIF	Please Do !
PLAT007_ALERT_5_G Number of Unrefined Donor-H Atoms	2 Why ?
PLAT066_ALERT_1_G Predicted and Reported Tmin&Tmax Range Identical	? Check
PLAT301_ALERT_3_G Main Residue Disorder Percentage =	2 Note
PLAT380_ALERT_4_G Incorrectly? Oriented X(sp2)-Methyl Moiety	C9 Check
PLAT380_ALERT_4_G Incorrectly? Oriented X(sp2)-Methyl Moiety	C9' Check
PLAT720_ALERT_4_G Number of Unusual/Non-Standard Labels	16 Note
PLAT779_ALERT_4_G Suspect or Irrelevant (Bond) Angle in CIF #	25 Check
C3C -C2C -C3C' 1.555 1.555 1.555	20.30 Deg.
PLAT779_ALERT_4_G Suspect or Irrelevant (Bond) Angle in CIF #	59 Check
C3C' -C4C -C3C 1.555 1.555 1.555	20.60 Deg.

0 **ALERT level A** = Most likely a serious problem - resolve or explain

- 1 **ALERT level B** = A potentially serious problem, consider carefully
 1 **ALERT level C** = Check. Ensure it is not caused by an omission or oversight
 9 **ALERT level G** = General information/check it is not something unexpected
- 1 ALERT type 1 CIF construction/syntax error, inconsistent or missing data
 2 ALERT type 2 Indicator that the structure model may be wrong or deficient
 1 ALERT type 3 Indicator that the structure quality may be low
 5 ALERT type 4 Improvement, methodology, query or suggestion
 2 ALERT type 5 Informative message, check

Datablock: 16_OPh

Bond precision: C-C = 0.0009 Å Wavelength=0.71073

Cell: a=11.0040(2) b=11.3396(2) c=13.1450(2)
 alpha=69.1450(8) beta=76.3654(8) gamma=62.5117(8)

Temperature: 100 K

	Calculated	Reported
Volume	1354.69(4)	1354.69(4)
Space group	P -1	P -1
Hall group	-P 1	-P 1
Moiety formula	C35 H28 O2 S2	C35 H28 O2 S2
Sum formula	C35 H28 O2 S2	C35 H28 O2 S2
Mr	544.71	544.69
Dx, g cm ⁻³	1.335	1.335
Z	2	2
Mu (mm ⁻¹)	0.229	0.229
F000	572.0	572.0
F000'	572.71	
h,k,lmax	23,24,28	23,24,28
Nref	28420	28154
Tmin,Tmax	0.941,0.951	0.906,0.951
Tmin'	0.904	


Correction method= MULTI-SCAN

Data completeness= 0.991 Theta(max)= 50.000

R(reflections)= 0.0443(22805) wR2(reflections)= 0.1181(28154)

S = 0.998 Npar= Npar = 356

The following ALERTS were generated. Each ALERT has the format
test-name_ALERT_alert-type_alert-level.
 Click on the hyperlinks for more details of the test.

 **Alert level C**

DIFMX01_ALERT_2_C The maximum difference density is > 0.1*ZMAX*0.75
 _refine_diff_density_max given = 1.266
 Test value = 1.200
 DIFMX02_ALERT_1_C The maximum difference density is > 0.1*ZMAX*0.75
 The relevant atom site should be identified.
 PLAT094_ALERT_2_C Ratio of Maximum / Minimum Residual Density 2.15 Why ?
 PLAT097_ALERT_2_C Large Reported Max. (Positive) Residual Density 1.27 eA-3

**Alert level G**

PLAT005_ALERT_5_G No _iucr_refine_instructions_details in the CIF Please Do !
 PLAT066_ALERT_1_G Predicted and Reported Tmin&Tmax Range Identical ? Check
 PLAT154_ALERT_1_G The su's on the Cell Angles are Equal 0.00080 Degree
 PLAT180_ALERT_4_G Check Cell Rounding: # of Values Ending with 0 = 3
 PLAT720_ALERT_4_G Number of Unusual/Non-Standard Labels 12 Note

- 0 **ALERT level A** = Most likely a serious problem - resolve or explain
 0 **ALERT level B** = A potentially serious problem, consider carefully
 4 **ALERT level C** = Check. Ensure it is not caused by an omission or oversight
 5 **ALERT level G** = General information/check it is not something unexpected
- 3 ALERT type 1 CIF construction/syntax error, inconsistent or missing data
 3 ALERT type 2 Indicator that the structure model may be wrong or deficient
 0 ALERT type 3 Indicator that the structure quality may be low
 2 ALERT type 4 Improvement, methodology, query or suggestion
 1 ALERT type 5 Informative message, check

Datablock: 18_NC4H8

Bond precision: C-C = 0.0052 Å Wavelength=1.54178

Cell: a=12.058(3) b=17.000(4) c=12.473(3)
 alpha=90 beta=93.288(4) gamma=90
 Temperature: 100 K

	Calculated	Reported
Volume	2552.6(11)	2552.7(9)
Space group	P 21/n	P 21/n
Hall group	-P 2yn	-P 2yn
Moiety formula	C31 H34 N2 S2	C31 H34 N2 S2
Sum formula	C31 H34 N2 S2	C31 H34 N2 S2
Mr	498.74	498.72
Dx, g cm-3	1.298	1.298
Z	4	4
Mu (mm-1)	2.052	2.052
F000	1064.0	1064.0
F000'	1069.02	
h,k,lmax	13,19,14	13,19,14
Nref	3785	3723
Tmin,Tmax	0.821,0.921	0.791,0.922
Tmin'	0.782	

Correction method= MULTI-SCAN

Data completeness= 0.984

Theta(max)= 59.990

R(reflections)= 0.0506(2673)

wR2(reflections)= 0.1473(3723)

S = 1.030

Npar= Npar = 318

The following ALERTS were generated. Each ALERT has the format

test-name_ALERT_alert-type_alert-level.

Click on the hyperlinks for more details of the test.



Alert level B

THETM01_ALERT_3_B The value of $\sin(\theta_{\max})/\lambda$ is less than 0.575

Calculated $\sin(\theta_{\max})/\lambda = 0.5616$



Alert level C

PLAT241_ALERT_2_C High	Ueq as Compared to Neighbors for	C3C Check
PLAT340_ALERT_3_C Low Bond Precision on	C-C Bonds	0.0052 Ang.



Alert level G

PLAT005_ALERT_5_G No _iucr_refine_instructions_details	in the CIF	Please Do !
PLAT066_ALERT_1_G Predicted and Reported Tmin&Tmax Range	Identical	? Check
PLAT152_ALERT_1_G The Supplied and Calc. Volume s.u. Differ by ...		2 Units
PLAT720_ALERT_4_G Number of Unusual/Non-Standard Labels		12 Note

- 0 **ALERT level A** = Most likely a serious problem - resolve or explain
 1 **ALERT level B** = A potentially serious problem, consider carefully
 2 **ALERT level C** = Check. Ensure it is not caused by an omission or oversight
 4 **ALERT level G** = General information/check it is not something unexpected
- 2 ALERT type 1 CIF construction/syntax error, inconsistent or missing data
 1 ALERT type 2 Indicator that the structure model may be wrong or deficient
 2 ALERT type 3 Indicator that the structure quality may be low
 1 ALERT type 4 Improvement, methodology, query or suggestion
 1 ALERT type 5 Informative message, check

It is advisable to attempt to resolve as many as possible of the alerts in all categories. Often the minor alerts point to easily fixed oversights, errors and omissions in your CIF or refinement strategy, so attention to these fine details can be worthwhile. In order to resolve some of the more serious problems it may be necessary to carry out additional measurements or structure refinements. However, the purpose of your study may justify the reported deviations and the more serious of these should normally be commented upon in the discussion or experimental section of a paper or in the "special_details" fields of the CIF. checkCIF was carefully designed to identify outliers and unusual parameters, but every test has its limitations and alerts that are not important in a particular case may appear. Conversely, the absence of alerts does not guarantee there are no aspects of the results needing attention. It is up to the individual to critically assess their own results and, if necessary, seek expert advice.

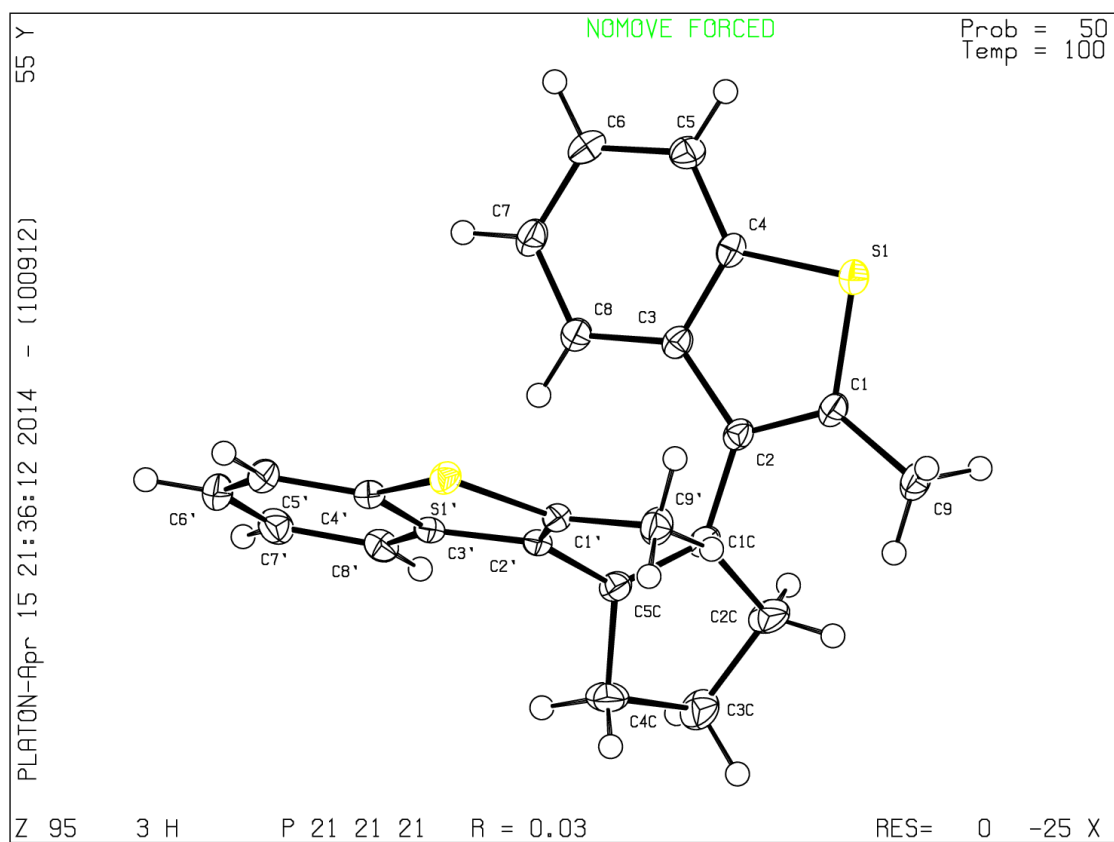
Publication of your CIF in IUCr journals

A basic structural check has been run on your CIF. These basic checks will be run on all CIFs submitted for publication in IUCr journals (*Acta Crystallographica*, *Journal of Applied Crystallography*, *Journal of Synchrotron Radiation*); however, if you intend to submit to *Acta Crystallographica Section C* or *E*, you should make sure that full publication checks are run on the final version of your CIF prior to submission.

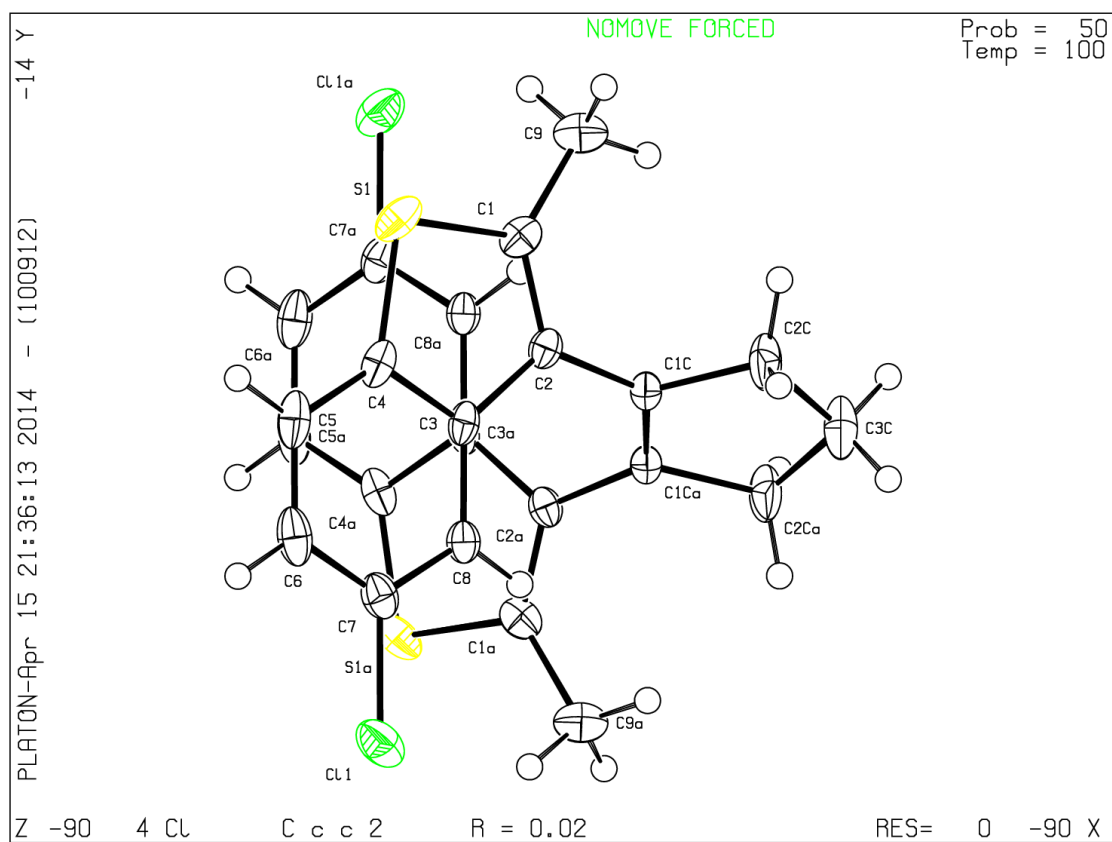
Publication of your CIF in other journals

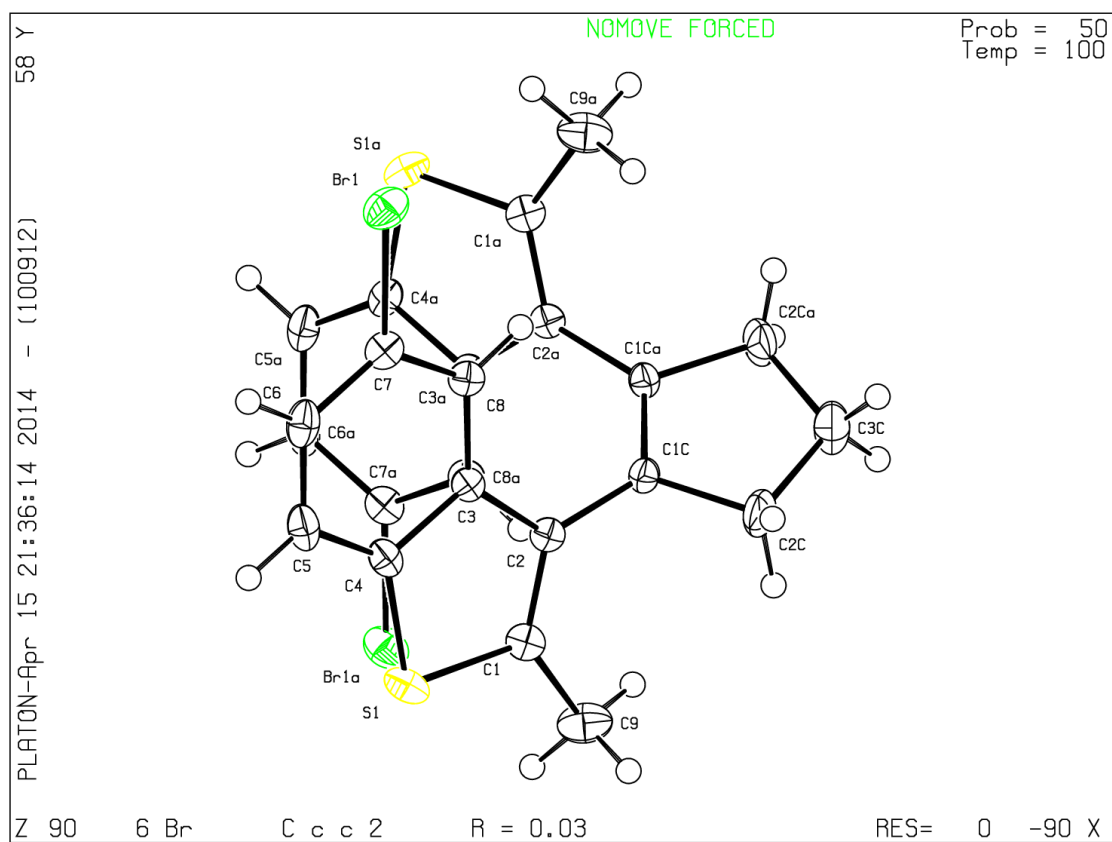
Please refer to the *Notes for Authors* of the relevant journal for any special instructions relating to CIF submission.

PLATON version of 05/02/2014; check.def file version of 05/02/2014

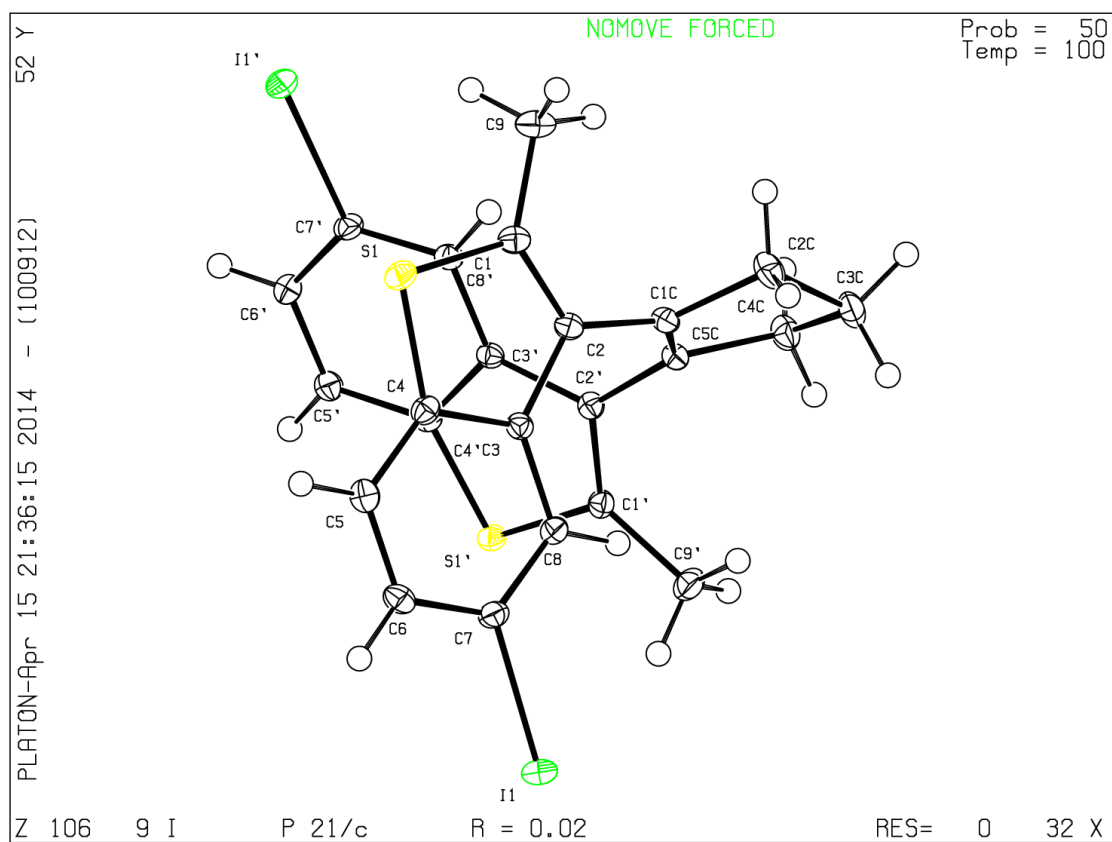


Datablock 4_Cl - ellipsoid plot

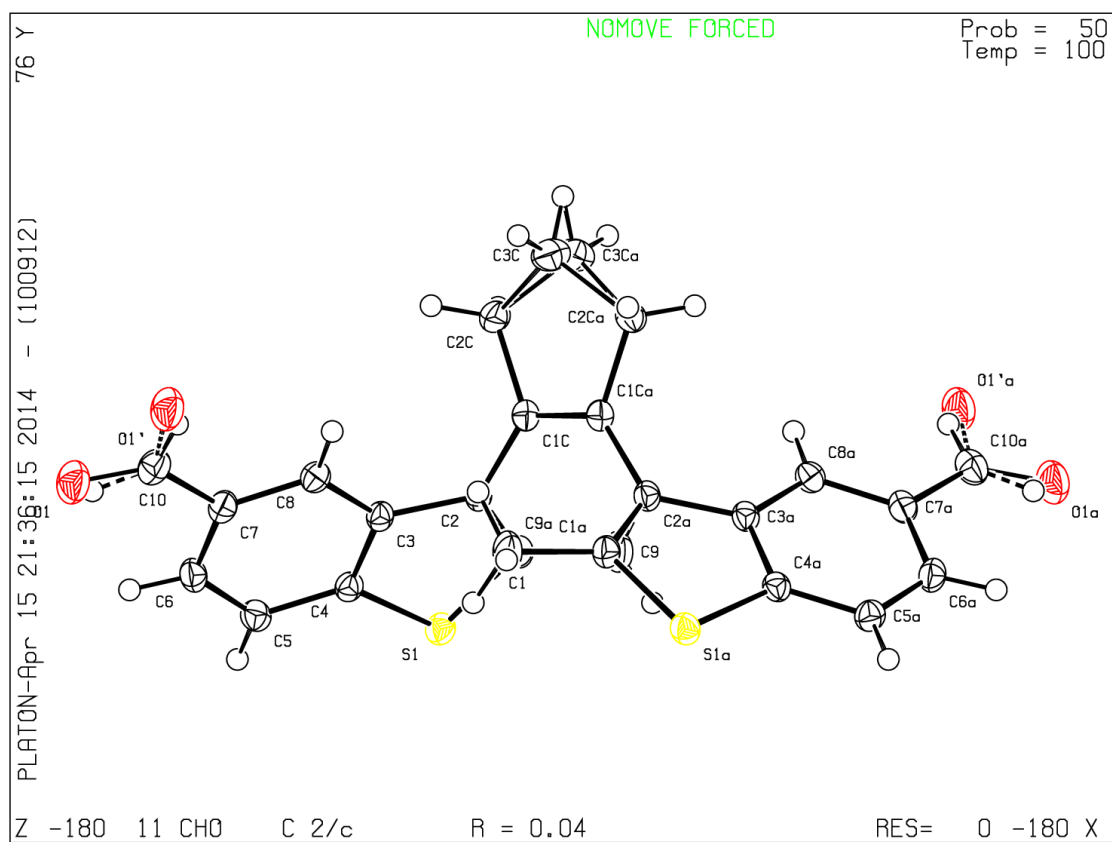




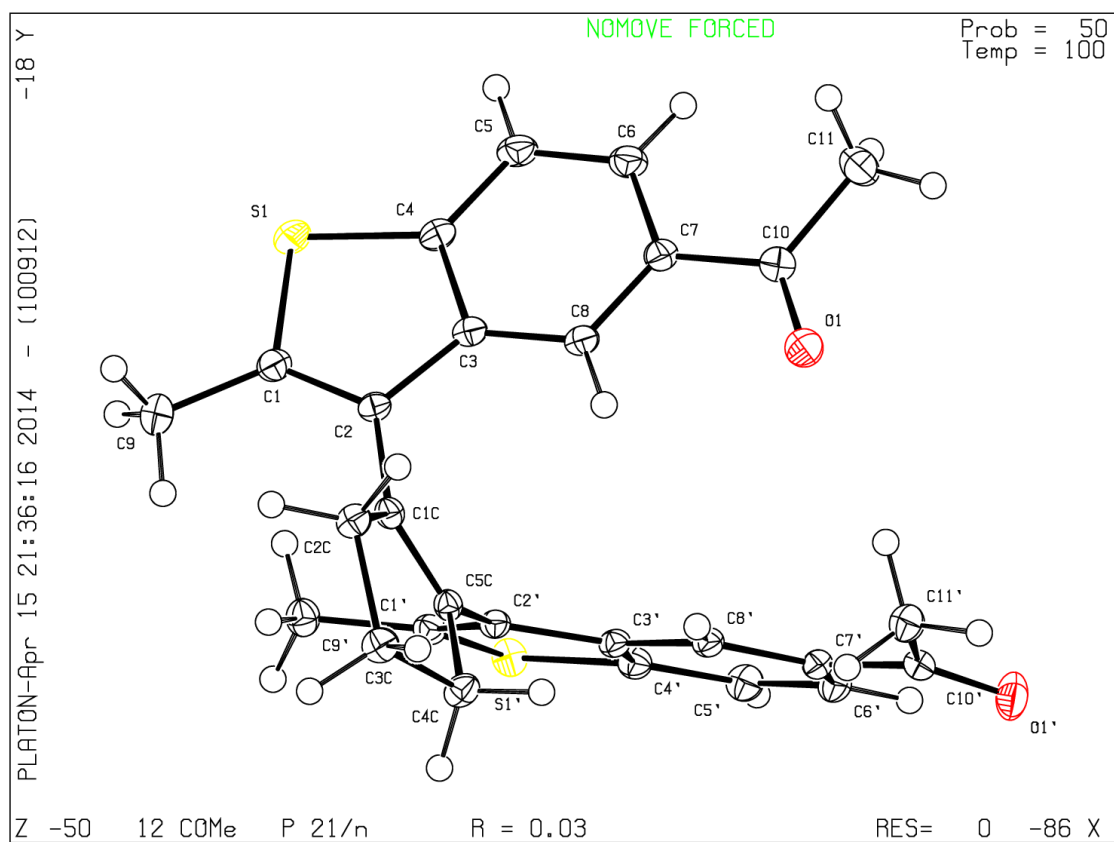
Datablock 9_I - ellipsoid plot



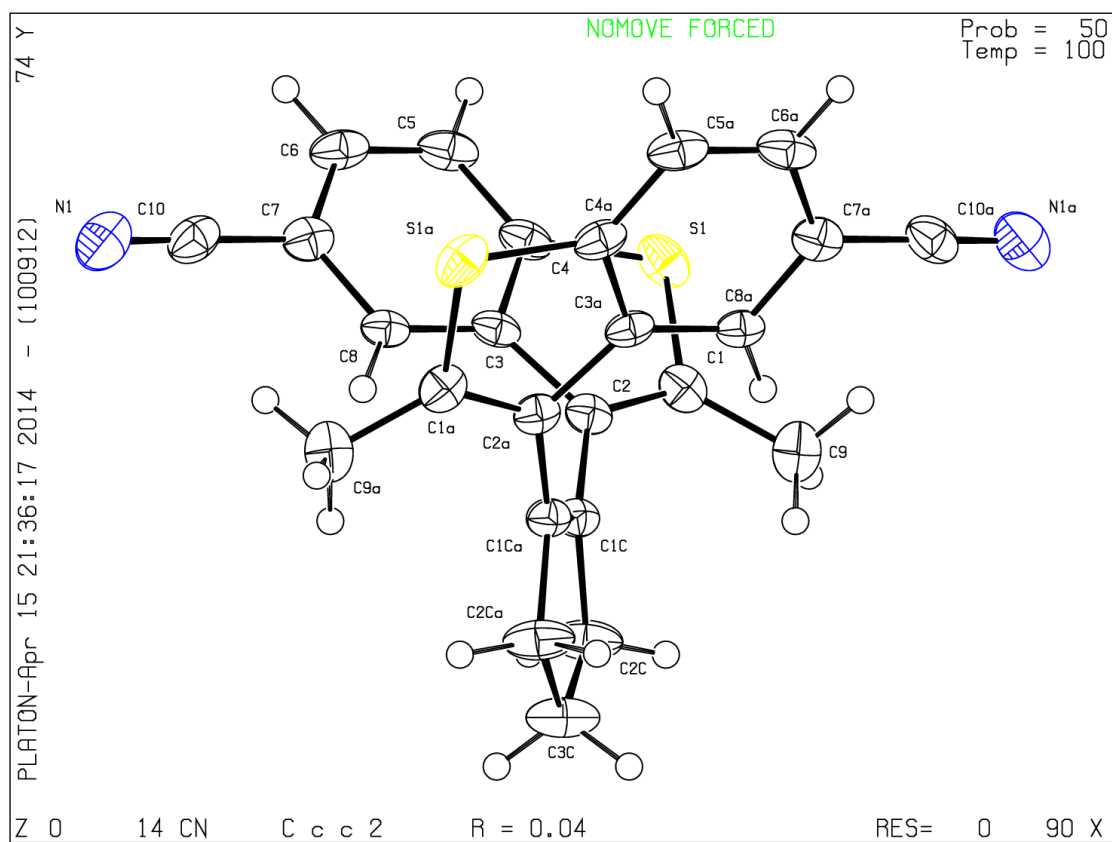
Datablock 11_CHO - ellipsoid plot

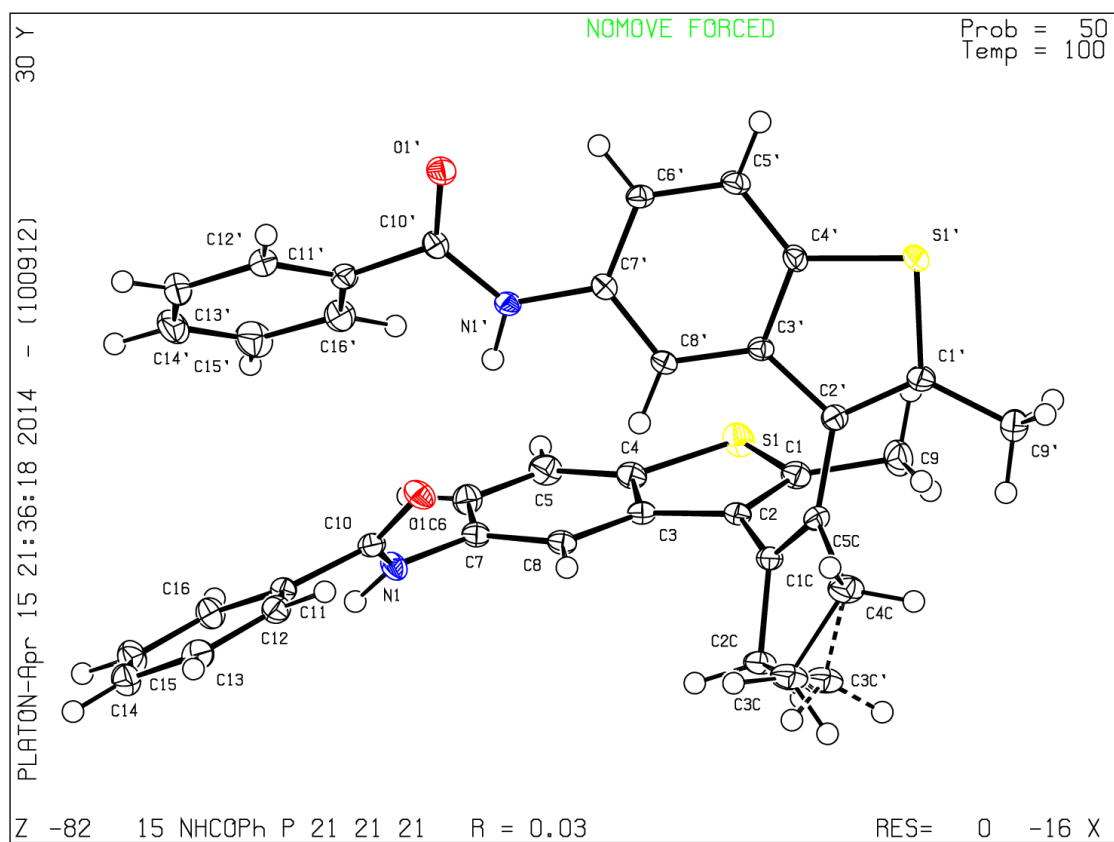


Datablock 12_COMe - ellipsoid plot

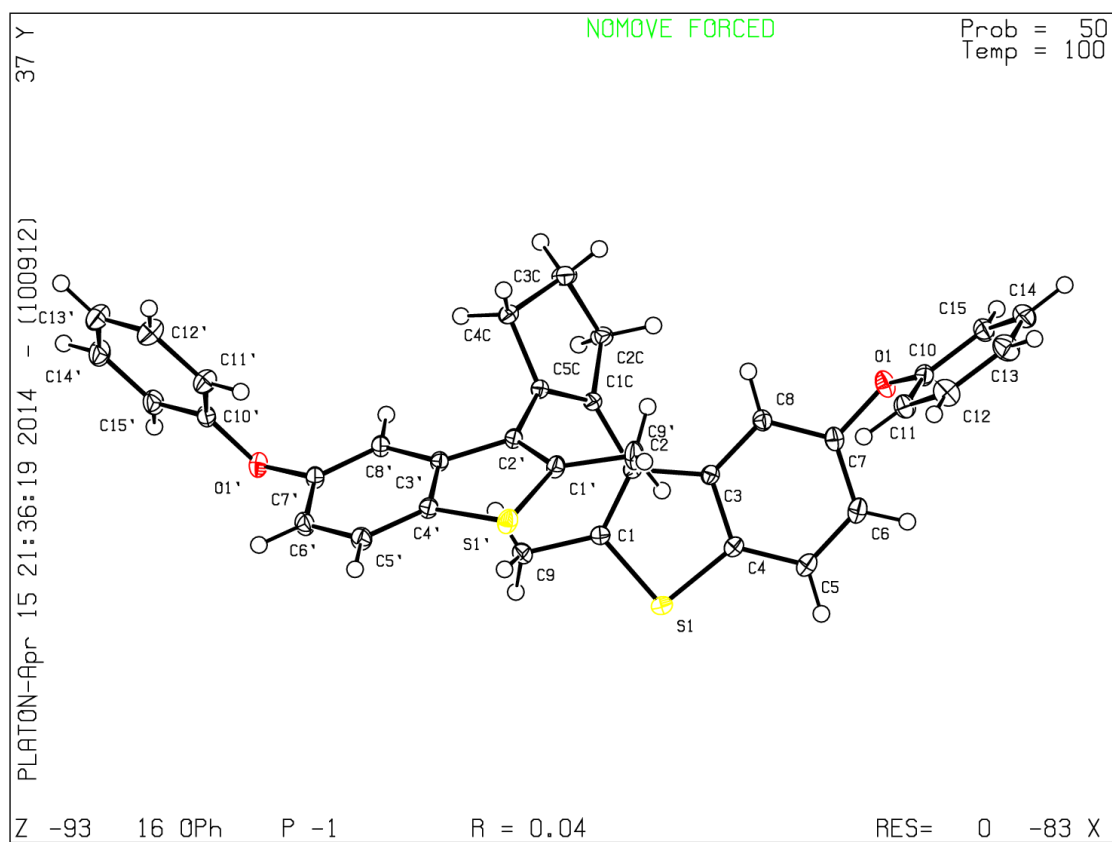


Datablock 14_CN - ellipsoid plot





Datablock 16_OPh - ellipsoid plot



Datablock 18_NC4H8 - ellipsoid plot

